2014-08-29

PDC Drill Bit Redesign and Simulation for Optimized Performance

Sivagnanam, Mohan

UNIVERSITY OF CALGARY

PDC Drill Bit Redesign and Simulation for Optimized Performance

by

Mohan Sivagnanam

A THESIS

SUBMITTED TO THE FACULTY OF GRADUATE STUDIES

IN PARTIAL FULFILMENT OF THE REQUIREMENTS FOR THE

DEGREE OF MASTER OF SCIENCE

DEPARTMENT OF MECHANICAL AND MANUFACTURING ENGINEERING

CALGARY, ALBERTA

AUGUST, 2014

Abstract

Polycrystalline diamond compact (PDC) drill bit design influences the bit hydraulics and hence the drilling performance. To improve the hydraulics, the fluid flow pattern across the drill bit should be optimized for low pressure drop, low recirculation flow and high velocity. Design of Experiments (DOE) was used to study the effect of various design parameters. Computational Fluid Dynamics (CFD) was used to simulate the fluid flow in the complex geometry of the drill bit. Response Surface Methodology was applied to optimize the design parameters for improved bit hydraulics.

Preliminary simulations were conducted by increasing the complexity to meet the real time operation. Simulations based on fractional factorial experiment were used to identify the significant factors from the 15 design parameters. The optimum limits of the most significant five factors were identified from simulations based on central composite design (CCD). The optimization procedure was assessed by comparing the optimum design with the original design for Newtonian and Non-Newtonian conditions.

Acknowledgements

I would like to thank Dr. Geir Hareland for providing the original motivation for this project. My sincere gratitude extends to my supervisor, Dr. Robert Martinuzzi for his unconditional motivation, constructive discussions, invaluable supervision and patience that helped me throughout the course of my project.

I would like to acknowledge the benefits of WESTGRID computational facilities which played the key role in my project.

I am grateful to my parents for their love and support which helped me to concentrate on my research. I have to thank my dearest wife, Ranjani for her constant support, encouragement and patience which helped me in the process of completing this research work. The love and happiness bestowed by my son, Bharath provided the emotional support and motivation for the completion of my thesis.

I am thankful to all my friends in the Drilling Research Team at the University of Calgary who have been very supportive and encouraging throughout the course of my project.

To my parents

Table of Contents

List of Tables

List of Figures and Illustrations

List of Symbols, Abbreviations and Nomenclature

Latin Symbols

A_t	Total nozzle area
Abr	Formation abrasiveness
A_w	Wear flat area underneath the PDC cutter
ΔBG	Cumulative bit wear function
C_c	Bit wear coefficient
d	Nozzle diameter
D	Bit diameter
D_c	PDC cutter diameter
$\vec{F}$	External body force
f	Friction Coefficient between cutter and rock
$\vec{g}$	Gravitational acceleration
G_B	Geometric function
G_k	Production of turbulence kinetic energy
G_ω	Generation of ω
h_t	Hydraulic factor
I	Identity unit tensor
k	Turbulence kinetic energy
$\dot{m}$	Mass flow rate
N	Number of nozzle
N_c	Number of face cutters of PDC bit
p	Static pressure
q	Drilling fluid flowrate
Re	Flow Reynolds number
$Re_t = k^2/\nu\varepsilon = k/\nu\omega$	Turbulence Reynolds number
S_k *and* S_ω	User-defined source terms
T	Temperature

t	Time
t_c	PDC layer thickness
$u^* = \sqrt{\tau_\omega/\rho}$	Friction velocity at the nearest wall
u^+_{turb}	Friction velocity in the logarithmic region near the wall
u, v, w	Velocity magnitude
$\vec{v}$	Overall velocity vector
v	Velocity at nozzle
W_f	Wear function
y	Distance to the nearest wall
$y^+ = yu^*/\nu$	Non-dimensional wall distance
Y_k *and* Y_ω	Dissipation of k and ω

Greek Symbols

α	PDC cutter side-rake angle
θ	Half the wedge angle of the cutter
θ'	PDC cutter backrake angle
μ	Dynamic viscosity
μ_t	Turbulent viscosity
ν	Kinematic viscosity
ρ	Density
σ	Confined compressive strength
ε	Dissipation rate
Ψ	Depth from the bottom-hole surface
ω	Specific dissipation rate
$\bar{\bar{\tau}}$	Stress tensor
τ_ω	Wall shear stress
Γ_k *and* Γ_ω	Effective diffusivity of k and ω
σ_k *and* σ_ω	Turbulent Prandtl numbers for k and ω

Abbreviations

ANOVA	Analysis of variance
CAD	Computer-aided design
CCD	Central composite design
CCF	Face-centered central composite
CCS	Confined compressive strength
CFD	Computational fluid dynamics
DHM	Down hole motor
DOE	Design of Experiments
HSI	Hydraulic horse power per unit area
JSA	Junk slot area
PDC	Polycrystalline diamond compacts
PRESTO	Pressure staggering option
ROP	Drilling rate of penetration
RPM	Rotary speed of the drill bit
RSM	Response surface methodology
VOF	Volume of fluid
WOB	Weight on bit

Chapter One: Introduction

One of the most important concerns in the oil and gas industry is the time and cost associated with drilling wells. The focus of the drilling industry is to minimize the overall drilling cost without compromising the safety and environmental standards. The efficiency of drilling, measured in terms of the Rate of Penetration (ROP), is the most important criteria in the drilling economics as it directly influences the time taken for drilling a well. Based on the relationship between drilling cost and ROP, it had been shown that maximizing the ROP will result in minimizing the drilling cost (Bourgoyne et al., 1991). The rate of penetration or the drilling performance depends on the lithological characteristics of the formations being drilled, drilling fluid properties, the downward force acting on the drill bit or Weight on Bit (WOB), rotation of the drill bit (RPM) or the combined rotation of drill string and the downhole motor (DHM), and bit hydraulics. Among the above parameters, drill bit hydraulics has been recognized as the major factor influencing the drilling performance (Akin et al., 1997; Hariharan & Azar, 1996; Lim & Chukwu, 1996; Moslemi & Ahmadi, 2014).

The purpose of proper hydraulic design of drill bits is to have appropriate conditions of drilling fluid flow rate and bit pressure drop to facilitate the removal of cuttings generated during drilling. Bit hydraulics plays an important role in this process, especially during drilling in sticky or soft formations such as shale plays. Poor hydraulic design causes improper bottomhole cleaning, which may result in balling (the accumulation of cuttings on the bit face) that decreases the ROP, or may halt drilling in severe cases. Drill bit design influences the bit hydraulics in terms of the drilling fluid flow rate and pressure drop across the bit which affects the removal of

generated drill cuttings; bottomhole cleaning; reduced chip hold-down pressure and bit cooling as well as power consumption. Some typical problems due to ineffective bit hydraulics are bit balling and pre-mature bit wear due to regrinding of chips. These problems will reflect on the drilling performance and hence increase the drilling cost. Increasing the hydraulic power at the mud pump improved the drilling performance of jet bits (Speer, 1959). Effective cleaning was achieved beneath the bit by maximizing the bit horsepower or nozzle-jet impact force (Guo & Liu, 2011).

On the other hand, bit hydraulics is also influenced by the local design criteria of drill bits. Modifying the drill bit design parameters like cutters profile (arrangement of cutters' placement) and distribution, nozzle size and orientation and bit body could lead to effective utilization of the hydraulic effect at the bottomhole and hence aid in maximizing the drilling performance. Physical bit design parameters such as junk slot area and face volume (blade proximity and junk slot shape) were investigated to minimize bit balling and improve bit hydraulics (Wells et al., 2008).

Experimental methods to develop bit design are expensive due to complexity in reproduction of well condition. In order to achieve maximum drilling performance along with low cost and time, real-time data evaluation should be coupled with selection and optimization of drill bit and drilling parameters. To facilitate the improvement in drilling hydraulics, the fluid flow pattern should be optimized in terms of the pressure distribution and the velocity profile beneath the drill bit. With the help of computational methods, the influence of bit design factors can be understood and utilized for improving the bit hydraulics. An effective approach to improve flow patterns is to optimize the position and orientation of the injection jet nozzles on the drill bit. Computational Fluid Dynamics (CFD) is one of the computational tools, efficient to

simulate the fluid flow phenomena in complex geometry of drill bit design with the incorporation of the bit rotation and multi-phase condition at the downhole of the well. The use of CFD in optimizing drill bit design will provide inexpensive and reliable results to improve the drilling performance.

A major challenge in the optimization of a drill bit design is the large number of design parameters that need to be considered. Efficient optimization thus requires a strategy for identifying the significance of different design parameters and a suitable test matrix for optimization. To this end, statistical approaches used in planning and designing experiments, and analysis of the experimental results for the selection and optimization of the influencing factors, are also well suited to the design process. Fractional factorial design is one of the experimental designs in statistics that allows for the selection of the parameters having significant influence on a particular output (Myers, 1971; Simpson et al., 2001). The optimum limits for the selected parameters could be obtained by the application of central composite design and response surface methodology (Onwubolu & Kumar, 2006).

1.1 Objective and Layout of the Thesis

The main objective of this research is to conduct simulation studies to achieve improvement in the bit hydraulics through an optimization process that includes recommending optimum design criteria along with the corresponding operational parameters. After a thorough literature review, the following hypothesis was tested to achieve the above mentioned objective. Utilization of the statistical approach of experimental design (DOE) on the design parameters of the PDC drill bit may lead to identification of design limits of the significant parameters with the aid of CFD simulation and analysis for optimum performance of the drill bit. The objective

function for optimization is set through simulation results for the actual drill bit design. The focus of the objective function is to determine the point closest to the peak of each of the desired characteristics under the constraint of the given operating conditions. The simulations using the original drill bit design serve as the bench mark for comparing the simulation results of the optimized design.

This thesis consists of six chapters. More specifically, chapter **One** provides an introduction to the topics of this thesis. Chapter **Two** includes a detailed literature review on PDC drill bit design, bit hydraulics and performance, application of CFD for simulating drill bit conditions, and experimental design and response surface methodology for selection and optimization of influencing parameters. Chapter **Three** explains the methodology for CFD implementation for PDC drill bit and statistical approach for design optimization. Chapter **Four** provides information on numerical model set up of a PDC drill bit for a computational domain. The results and discussions are provided in Chapter **Five**. It includes the selection of the most influencing parameters and optimization of selected parameters by statistical approach. Finally, the conclusions from this study and recommendations for the future work are provided in Chapter **Six**.

Chapter Two: Literature Review

In this section, the design of a current bit parameters influencing PDC drill bit performance is discussed and the important design parameters identified. The PDC drill bit chosen for the study is an 8 ¾ inch (222 mm) diameter PDC drill bit consisting of seven nozzles and five blades with 65 cutters. The design parameters of PDC drill bit are reviewed with respect to their influence on the drilling performance. The geometric modeling methods and the use of Computational fluid dynamics for the flow simulation are discussed. The application of Design of Experiments (DOE) as a design optimization tool on the context of identifying the significant parameters and their design limits for optimum drilling performance is discussed.

2.1 Parameters important for a PDC Drill Bit

Drill bits are the essential tools for the process of drilling to recover oil and gas from underground reserves. There are mainly two classifications of drill bits: drag bit and rolling cutter bit. Roller-cone bit which belongs to the rolling cutter bit category has conical cutters or cones that have spiked teeth around them. Polycrystalline diamond compacts (PDC) drill bit belong to the category of drag bits, which consists of fixed cutter blades integrated with the body of the bit and rotate as a single unit along with drill string. A schematic view of a PDC drill bit and its major components is shown in Figure 2-1.

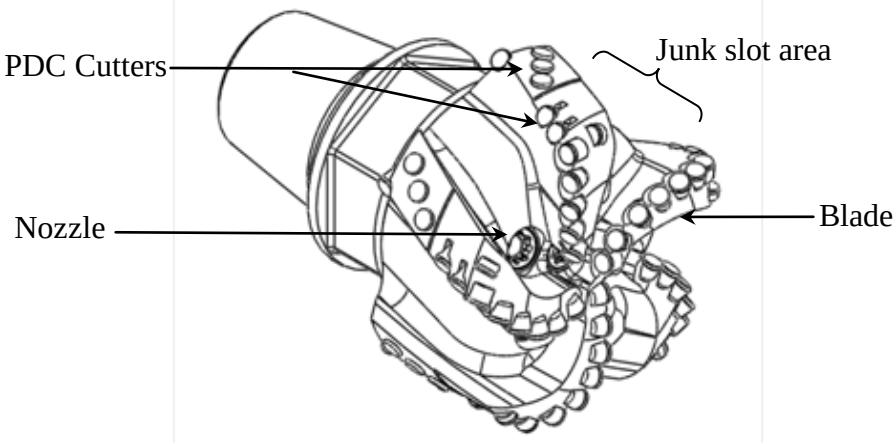

Figure 2-1. Isometric view of PDC drill bit

The PDC drill bits were introduced in 1973 with cutting elements made of polycrystalline diamond compacts. These drill bits have been used for the soft to medium-hard formations of clays and shale with appropriate design features (Balkenbush & Onisko, 1985; Cerkovnik, 1982). The drilling industry is constantly looking for innovative drill bit designs which can improve drilling performance and lower the associated cost (Moslemi & Ahmadi, 2014; Offenbacher et al., 1983). A 100% increase in drilling rate or bit life may reduce drilling cost by 50% or 11%, respectively (Striegler, 1979). Consequently, modification of any parameter that may improve drilling performance reduces drilling cost.

The factors affecting drilling rate and bit life are the weight on bit (WOB), rotary speed and bit hydraulics (Akin et al., 1997). Bit hydraulics has the greatest impact on the effective use of PDC drill bits (Keller & Crow, 1983; Prooyen et al., 1982). Increased hydraulic horsepower has been shown to improve drilling performance in terms of increased Rate of Penetration (ROP) and reduced bit balling (Balkenbush & Onisko, 1985; Cerkovnik, 1982; Kendall & Goins Jr, 1960). Bit balling is the phenomena of sticky shale getting trapped in the face of the drill bit flow path, which in turn causes serious drag on the bit and obstructs the fluid flow in the flow path (Figure 2-2). Drilling fluid flow rate and bit pressure drop are governed by bit hydraulics. Proper

bit hydraulics are understood to mean that the drilling fluid flow rate and bit pressure drop result in efficient removal of bottomhole rock cuttings, reduction of chip hold-down pressure, bit and bottomhole cleaning and bit cooling (Cerkovnik, 1982; Garcia-Gavito & Azar, 1994; Guo & Liu, 2011). Hydraulic horsepower at the bit is maximized by using all the available pressure for the bit excluding system losses, and hence achieve optimum drilling by ensuring that the maximum available hydraulic horsepower is being expended at the bit (Kerr, 1988).

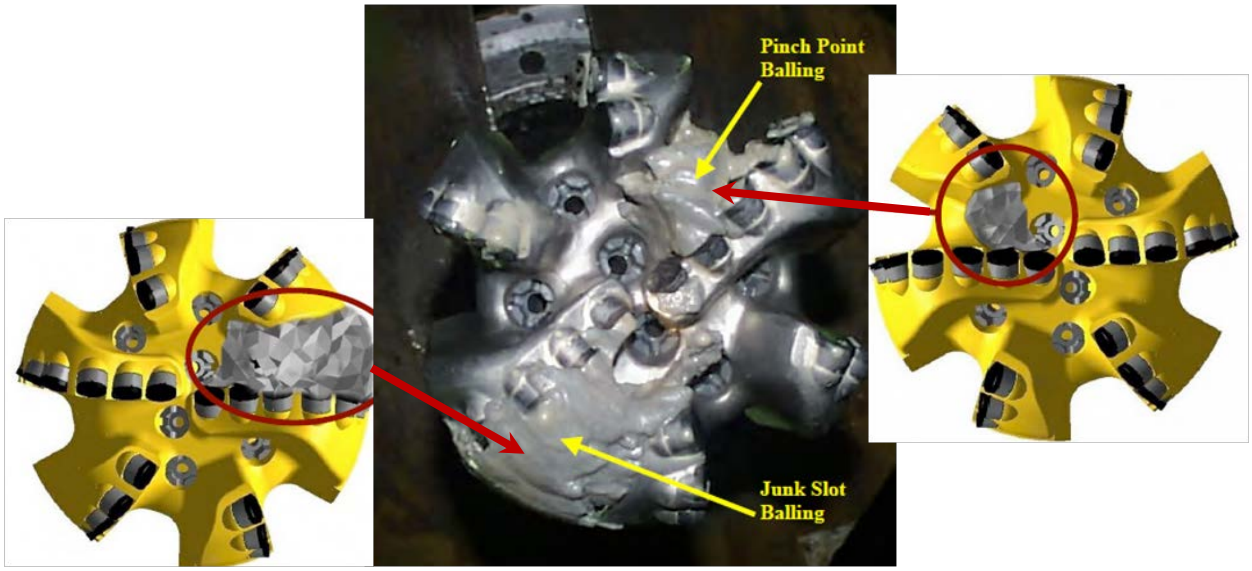

Figure 2-2. Bit balling in PDC drill bit (Wells et al., 2008)

The hydraulic parameters associated with bit hydraulic design are nozzle fluid velocity, hydraulic horsepower, impact force, and pressure. Garcia-Gavito and Azar (1994) studied the ROP effect of fluid-flow behavior as a function of flow rate, number of nozzles, nozzle sizes, and bit design and reported as follows: smaller nozzle sizes yield higher pressure gradients that lead to higher crossflow fluid velocities and thus improve hole cleaning; better bottomhole cleaning is achieved when the nozzle fluid velocity is increased, either by reducing the nozzle

size or by increasing the overall flow rate; Nozzle location has an important effect on bottomhole cleaning and thus on drilling rate; the drilling rate was higher when the center nozzles were open and the outer nozzles blanked; the effect of bit hydraulics on drilling rate depends not only on the bit hydraulic level used but also on fluid-flow geometry at the hole bottom, which is governed by bit mechanical and hydraulic designs.

It is known that maximizing the bit-face volume and the junk-slot area between the blades of the bit improves the bit performance and reduces the balling effects (Figure 2-2). However, using bit-face volume and junk-slot area alone is insufficient to predict drilling performance and bit balling (Wells et al., 2008). Chip generation is also affected by the cutter orientation which in turn describes the back rake, side rake and cutter exposure (Cerkovnik, 1982).

Bottomhole cleaning is also influenced by the crown shape of the drill bit. The crown shape of the bit as shown in Figure 2-3 is associated with the cutting structure as well as hydraulic structure and processing technology (Ju et al., 2013). The flow path profile of the drill bit, which defines the number and size of cutters, is another factor that affects the bit hydraulics and bit balling. Warren and Armagost (1988) have reported that flat profiles lead to more bit balling compared to that of bladed profiles. Drill bits with parabolic profile and bladed hydraulic design was shown to result in less balling compared to that of flat profile and open-faced bit hydraulic design (Hariharan & Azar, 1996).

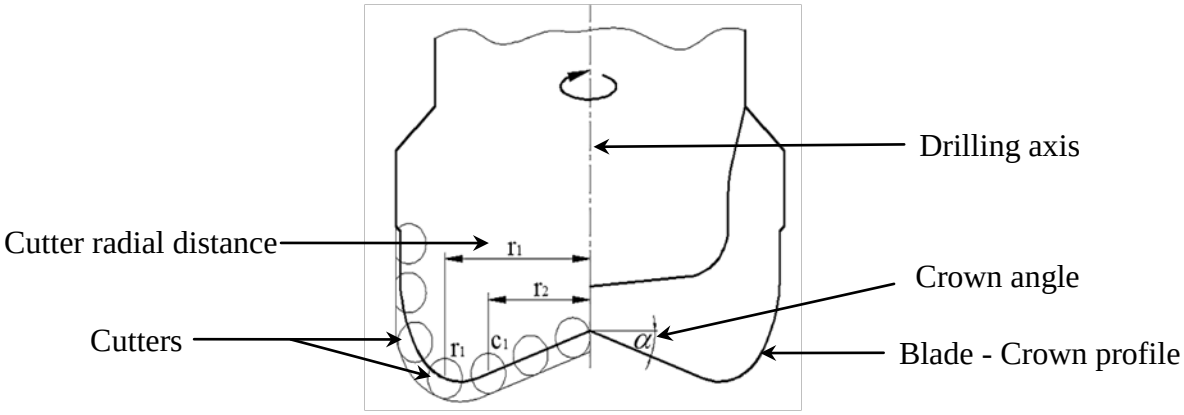

Figure 2-3. PDC drill bit crown cutting unit (Ju et al., 2013)

The effect of two- and three- nozzle bits on bottomhole cleaning were compared by Lim and Chukwu (1996). The asymmetrical flow generated beneath the two-nozzle bit in conjunction with smaller sized nozzles showed a higher cutting-transport ratio than the three-nozzle bit. Improved cleaning has been reported in drill bit with nozzles of uniform total flow area when the number of nozzles has been increased (Mensa-Wilmot & Fear, 2002). This has been attributed to more-uniform fluid flow distribution underneath the bit. Glowka (1983) has shown that higher bottomhole crossflow velocities and cutter cooling rates can be obtained with smaller nozzles located near the center of the bit. The flow pattern around the PDC bit is highly influenced by the nozzle orientation and the flow deflection by the cutter geometry (Watson et al., 1997).

King et al. (1990), have reported an insignificant effect of drill bit rotation rate on fluid flow for the case of turbulent flow conditions around a three-cutter PDC drill bit. The ROP of a drill bit is influenced by the rotary speed of the drill bit (Bourgoyne et al., 1991). At low values of rotation rate, ROP increases linearly with rotation rate. At high rotary speeds, the effect on ROP is very low due to the less efficient bottomhole cleaning. Hence, the effect of drill bit rotation rate should be considered in order to improve the performance of the drill bit. According

to Wu et al. (2011), the HSI level (hydraulic horse power per square inch) at the bit significantly influences the drilling performance. The mathematical model should consider the effect of HSI on ROP in order to optimize the hydraulic parameters such as flow rate and nozzle sizes. PDC bits have been shown to be less responsive to the change in the HSI level at the bit than the rollercone bits.

Thus, the above reports emphasize the influence of design parameters on the drilling performance. Modification of the flow distribution underneath the bit will result in improving the drilling efficiency using the available pressure drop in the downhole. In addition, achieving the optimum flow regime across the bit would ensure the proper cuttings removal and bottomhole cleaning. The major design parameters of PDC drill bit are: the nozzle size that is associated with the bottom-hole cross-flow velocities and pressure drop across bit; the nozzle placement that influences the bit cooling, mitigation of cutter balling and enhancing bottomhole cleaning; nozzle inclination influences the flow pattern around the PDC drill bit. This research will significantly contribute to an in-depth understanding of the drilling performance and the influence of the combined effect of the associated design parameters.

2.2 Mathematical Modeling of drilling performance

Drilling performance of PDC drill bits was analyzed based on cutter-rock interaction. The ability of the PDC bits to drill different formations with excellent efficiency was demonstrated by Millheim (1986). Several authors have made great attempts to develop mathematical model for PDC bits in order to estimate the penetration rate using drilling variables.

2.2.1 Rate of Penetration Models for PDC drill bit

The drilling forces in a single PDC cutter model were related to the parameters such as cutter force, cutter temperature and cutter wear (Warren & Sinor, 1986). The model was developed based on geometrical relationships, which was tested and verified using different sets of laboratory data. The results showed that the measured values were 50% higher than the model predicted values of drilling forces such as bit torque and WOB for certain drilling rate and rotational speed ranges. Kuru and Wojtanowsicz (1988), had applied single cutter force analysis to study the performance of the bit. The effect of friction between the PDC cutters and the rock was included in the model to predict the ROP, bit torque as well as the bit life. Rampersad et al. (1994) developed a model to predict the formation drillability of drag bits. From this model, the drilling rate can be estimated according to:

$$ROP = \frac{14.4 * WOB * RPM * \cos\alpha}{\sigma * D * \tan\theta} * \frac{a}{RPM^b * WOB^c} \quad \text{...(2-1)}$$

where:

ROP	Drilling rate (ft/hr)
WOB	Weight on the bit (klbf)
RPM	Rotary speed
α	PDC cutter side-rake angle (degree)
a, b, c	Bit Design Constants
σ	Confined compressive strength (psi)
D	Bit diameter (inch)
θ	Half the wedge angle of the cutter (degree)

This model was based on the conservation of mass where rate of cutting removal in front of the cutter is equivalent to rate of penetration. The effect of the operational parameters (WOB, RPM) was integrated on the rate of penetration (ROP) with proper consideration of geometrical relationship (D, α & θ) and rock failure criteria (σ) as shown above. A comprehensive drilling rate model based on rock-cutter interaction and the effect of drilling operation and bit design parameters was developed recently (Motahhari et al., 2010). This model considered the back rake angle and wear flat area. Back rake angle is the angle between the leading edge of a cutting tool and a perpendicular to the surface being cut; it controls the chip flow, and thrust force of the cut and the strength of the cutting edges. The wear flat area is the area formed under the cutter due to friction between the cutting edge and the surface being cut. Based on this model, one obtains:

$$\text{ROP} = W_f \frac{14.4 * \text{WOB} * \text{RPM}^b * cos\,\alpha}{\sigma * D * (tan\,\theta + \mu)} \quad \text{...(2-2)}$$

$$W_f = a * \frac{\text{WOB}^c}{{N_c}^d \sigma^e {A_w}^f} (1 + \frac{\mu}{tan\,\theta'}) \quad \text{...(2-3)}$$

$$A_w = \frac{{D_c}^2}{4\,sin\,\theta'} * arccos\left(1 - \frac{\Delta BG}{4}\right) - \frac{{D_c}^2(4 - \Delta BG)}{64 * sin\theta'} \sqrt{8 * \Delta BG * \Delta BG^2} \quad \text{...(2-4)}$$

where:

W_f Wear function

μ Viscosity (cp)

f Friction Coefficient between cutter and rock

N_c Number of face cutters of PDC bit

D Bit diameter (inch)

θ' PDC cutter backrake angle (degree)

D_c PDC cutter diameter (inch)

ΔBG Cumulative bit wear function

A_w Wear flat area underneath the PDC cutter (inch^2)

However this model does not account for the effect of cumulative cutters wear on ROP. Wu et al. (2011) integrated the effect of cumulative cutters wear on the ROP of PDC drill bits resulting in:

$$G_B = \frac{t_c . N_c}{\cos \alpha} . \sqrt{\frac{\Delta BG . {D_c}^2}{2 . \cos^3 \theta} (1 - \frac{\Delta BG}{8 . \cos \theta})} \quad \text{...(2-5)}$$

$$\Delta BG = \frac{C_c}{G_B} * \sum_{i=1}^{n} \mathrm{WOB}_i * \mathrm{RPM}_i * \mathrm{CCS}_i * Abr_i \quad \text{...(2-6)}$$

where:

G_B Geometric function

t_c PDC layer thickness (m)

C_c Bit wear coefficient

CCS	Confined compressive strength (Mpa)
Abr	Formation abrasiveness
RPM	Rotary speed of the bit
WOB	Weight on the bit (Tonne)

In this model, the cumulative bit wear was shown to be a function of the geometry and orientation of the cutter. Removing the cutting underneath the drill bit is the main function of drilling fluids which is the primary factor in maintaining appropriate downhole condition and enhancing drilling efficiency. Impact of bit hydraulic effect on rate of penetration of drill bit has been extensively investigated but uncertainty still exists over the hydraulic parameters to be optimized. Fluid velocity, flow rate, jet nozzle geometry and drilling fluid properties can significantly affect the penetration rate of bit. Steady state cleaning or perfect cleaning is the situation which requires the rate of cutting removal from underneath the bit to be equal to the rate at which the new chips are formed.

2.2.2 Integration of the Hydraulic Effect on the Rate of Penetration Models

A model developed by Kendall and Goins Jr (1960) incorporated pump horse power and the standpipe pressure as constraints for maximizing the hydraulic horse power, jet velocity and jet impact force at the bit. Pump flow rate corresponding to minimum annular velocity and proper bit nozzle size corresponding to maximum jet nozzle velocity have been found to clean the bit and carry the cutting to surface with highest fluid velocity at bit. The maximum cross flow velocity at the bit has been shown to be coincident with the maximum impact force required for the optimum hydraulic level (McLean, 1964). Based on the laboratory analysis of micro bits,

drilling rate was increased with the increase in the Reynolds number at the bottomhole or near bit nozzle (Eckel, 1968).

The hydraulic effect on drilling rate has been quantified based on the major hydraulic parameters: jet impact force, hydraulic horse power and jet velocity (Doiron & Deane, 1982). It has been reported that the rate of penetration (ROP) varies exponentially with respect to the hydraulic horse power concentration (HP per surface area) at the bit if the other parameters are held constant (Warren & Winters, 1984). Increase in hydraulic energy at the bit face increases the drilling rate as a result of better hole cleaning (Warren, 1987). The new hydraulic model was developed Wu et al. (2011) as seen from:

$$\mathrm{ROP}_{actual} = \mathrm{ROP}_{clean} * h_t \quad \text{...(2-7)}$$

$$h_t = R_1 . \frac{(\mathrm{HSI} . \left(\frac{\mathrm{JSA}}{20}\right))^{R_2}}{ROP_{clean}{}^{R_3}} \quad \text{...(2-8)}$$

where:

ROP	Rate of penetration (m/hr)
h_t	Hydraulic factor
JSA	Junk slot area (inch^2)
HSI	Hydraulic horse power per unit area
R_1, R_2, R_3	Constants

Based on the mathematical models discussed in the section 2.2.1, the analysis of drilling performance is mainly dependent on the operational parameters and few design parameters such

as PDC layer thickness, bit wear coefficient, size and number of nozzles. The placement and the orientation of the nozzle were not considered in the calculation in the mathematical models due to the complexity involved in quantifying their effect on drilling rate. Therefore, it is essential to develop a system that incorporates the effect of drill bit design parameters on the flow pattern and hence drilling hydraulics. A computational approach would be best suited to consider the influence of drill bit design parameters on drilling performance, since this allows exploration of a large number of parameters at minimal cost when compared to prototype production, turn-around time and experimental complexity in reproducing actual conditions in a laboratory.

2.3 Computational methods for drill bit design

Computational Fluid Dynamics (CFD) is one method used in the hydraulic design and manufacturing of drill bits. CFD simulations were used to assess drill bit performance for various conditions of hydraulic design parameters to determine the optimum set of parameters for improved flow distribution across the PDC drill bit and the results were validated using laser velocimetry experiments (King et al., 1990). Asymmetric nozzles with special interior transitional surfaces was shown to improve the ROP of PDC drill bit compared to that of traditional circular nozzles with the aid of CFD (Akin et al., 1997). The angle of the nozzles and the deflection of the flow by the cutters were found to have significant impact on the flow pattern around the PDC drill bit based on CFD simulation (Watson et al., 1997).

2.3.1 Need for numerical simulation on drilling application

Laboratory drilling experiments have been used to investigate the performance of bit hydraulics. Flow field characteristics were measured in terms of flow tracer tracking and cutter heat transfer coefficient across the face of a stud-mounted PDC bit in a test facility of Sandia

Laboratories (Glowka, 1983). The effect of downhole pressure on PDC drill bit performance was studied in a laboratory drilling system under simulated downhole pressure conditions (Andersen & Azar, 1993). Increasing the confining pressure resulted in reducing the PDC-bit performance.

However, experimental methods to develop bit design are expensive due to complexity in reproduction of well condition. In addition, the availability of drilling data at the drill bit is insufficient to carry out in-lab experiments to replicate the downhole condition. Laboratory testing methods are very difficult for performing optimization studies, in which various parameters need to be modified and the fluid flow across the bit geometry should be accessed. With the experiments, it is not possible to observe the flow field across the drill bit and hence the influence of geometry is assessed indirectly in terms of other factors such as ROP. CFD would allow, if accurate, a direct look at how nozzle size, nozzle placement, etc. affects the flow field and how this flow field affects performance. With the advancements in the computational methods, numerical simulations of complex drill bit conditions are made easy and flexible. These methods allow easier modification of the system at a lower cost and time.

2.3.2 CFD application on PDC drill bit

CFD tools have been successfully used to study the cutting transport in Wellbores, which is a complex phenomenon being influenced by mud density, cutting size and density, rate of penetration and mud circulation rate (Bilgesu et al., 2002). Studies using CFD revealed that the maximum balling ROP of a PDC drill bit increases with increased fluid velocity across the cutting structure (Wells et al., 2008). 3D CAD modeling and analytical studies in association with CFD analysis facilitated the introduction of innovative cutter technology into the PDC drill bit, which resulted in 120% ROP increase (Mortimer, 2010). Application of CFD modeling of

flow distribution by modification of PDC drill bit profile, shape, cone angles, back rake angles and cutters allowed the design of PDC drill bits that were best suited for hard/abrasive formation (Henry et al., 2011).

2.3.3 Flow-field model and governing equations

CFD studies use the solution for the full non-linear three dimensional Navier-Stokes equations coupled with appropriately chosen turbulence model for the given flow domain. A commercial CFD model was used to predict the cutting transport in wellbores (Bilgesu et al., 2002). A power law model was used to represent the rheology of the drilling fluid and Newtonian model for water. It was reported that the annular velocity was critical in hole cleaning. Simulation results for two different turbulence models were compared. The first model uses a constant amount of viscosity and in this the eddy viscosity was assumed constant. The second simulation were done with a *k-ε* model, where the eddy viscosity changes locally as,

$$v_t = C_\mu \, k^2/\varepsilon \qquad \text{...(2-9)}$$

where C_μ is constant, k is kinetic energy of the fluctuations and ε is dissipation rate. Comparison of simulation of these two turbulence models resulted in the conclusion that both models exhibited similar fluid behavior in PDC drill bit (King et al., 1990). The rationale for this result given by the authors is that the Reynolds number defining the turbulence, Re_t, was not sufficiently high, such that the additional modelling sophistication using the *k-ε* model did not appear warranted. However, it is noted here that the grid used was rather coarse and that the near-wall conditions (important for the transport of mud) were not adequately resolved, such that

the turbulence field may not have been adequately resolved. For a study on hydraulic performance of PDC drill bit and annulus based on particle tracking method, Moslemi and Ahmadi (2014) used realizable k-ε turbulent model with near-wall treatment of scalable wall functions for solving the fluid flow field and pressure-based coupled algorithm was used for solving the momentum and continuity equations. The simulation results show that the cuttings transport ratio increased with increase in nozzle jet velocity and HSI. Though the k-ε model in combination with wall functions has been applied to many industrial CFD simulations, the k-ω model is more accurate and robust for boundary layer applications (Menter, 2011). The k-ε equation has a lack of sensitivity to adverse pressure gradients and therefore may under-predict separation. On the other hand, the standard k-ω model shows superior performance for wall-bounded boundary layer, free shear, and low Reynolds number flows and it is suitable for complex boundary layer flows under adverse pressure gradient and separation (Menter, 1993). The actual drill bit model has complex geometry with narrow flow paths and cross flows across the flow paths, which in turn lead to wall shear and adverse pressure gradients. Hence, the k-ω model would be the best choice for predicting the flow behavior across the PDC drill bit surface.

There are few reports on computational simulations of PDC drill bit flow behavior considering multiphase flow (solid/liquid). The cutting transport in wellbores was studied using a commercially available CFD model for an incompressible two-phase flow (drilling fluid/granular particles) with different drilling fluid densities and particle sizes. Low flow rates are favorable for high cutting transport efficiency, whereas at high circulation rates, this efficiency decreases for all mud densities (Bilgesu et al., 2002). Using a particle tracking methodology, the hydraulic performance of PDC drill bit was evaluated for a two-phase model which included a solid phase dispersed in a fluid phase (Moslemi & Ahmadi, 2014). The cutting trajectory was assessed by

discrete phase model considering that only the fluid impacts particles and not vice versa. Based on the correlation of cutting transport ratio with ROP, it is reported that the cutting transport ratio can be used an indicator of cleaning efficiency.

A numerical method used in CFD simulation to study the fluid-fluid interface is the volume of fluid (VOF) method. The VOF model is simple, flexible and efficient for studying the complex free boundaries. Fluid-fluid interface between two or more fluids can be modelled by VOF method by using momentum equations and tracking the volume fraction of each of the fluids throughout the flow domain (Hirt & Nichols, 1981). Simulation of bifurcation of pendant drops based on VOF method was validated with experimental results in terms of surface tension effects (Gueyffier et al., 1999).

Based on literature, both the realizable k-ε and standard k-ω models can be used to represent the turbulence in the flow domain. As the k-ω model is suitable for low turbulence Reynolds number, Re_t, and complex boundary layer with adverse pressure gradients, this model will be used for turbulence prediction. The reports on particle transport involving two-phases have studied the behavior of particles in the flow domain. However, there is a need to understand the influence of particles (mud) on the flow behavior across the flow domain of PDC drill bit. Hence, the VOF model which is a multiphase model will be used to study the fluid-mud behavior on the flow domain, down the hole in PDC drill bit.

2.4 The Design of Experiments (DOE) Approach

Design of Experiments (DOE) is an engineering design approach that allows an engineer to perform a series of experiments corresponding to variations in a set of predetermined design parameters (Stewart et al., 2006). Response surface methodology (RSM) is one of the statistical

techniques that saves cost and time in conducting experiments by reducing the total number of required tests (Myers, 1971). RSM helps to identify the effect of the interactions of different design parameters on the response when they are varied simultaneously.

Factorial design based experiments are used to conduct the preliminary studies in which the effect of a number of parameters are analyzed and the most significant factors are screened for further analysis. The number of design points presented by a full factorial design is the product of the number of levels for each factor. The most common full factorial design consists of *k* factors varied at two levels to evaluate the main effects and interactions. The size of a full factorial experiment increases by the power of the number of factors and will lead to an insurmountable number of experiments. Hence, in order to reduce the number of experiments and the related cost, fractional factorial designs are used. Fractional factorial design is a fraction of a full factorial design (Simpson et al., 2001). The domain of the PDC drill bit consists of large number of design parameters and the application of fractional factorial design serves in reducing the test matrix.

To estimate the quadratic effects of the significant factors that were screened using the fractional factorial experiments, a central composite design will be used. A Central Composite Design (CCD) is a two level factorial design, augmented by n_0 center points and two 'star' points positioned at $\pm\alpha$ for each factor. When α is set as 1, star points are located on the centers of the faces of the cube, giving a face-centered central composite (CCF) design (Myers, 1971).

Optimization of the hydraulic design leads to improvement in the performance of the PDC drill bit (Watson et al., 1997). A good hydraulic design is obtained when the bottomhole fluid velocity is maximum, so as to enable evacuation of the cuttings (Mortimer, 2010).

Maximizing the jet impact force would result in an increase in the bottomhole fluid velocity (Wells et al., 2008). The nozzle location, nozzle size and nozzle orientation influences the jet impact force and modification of these parameters can lead to increase the bottomhole fluid velocity; reduce recirculation (dead) zones to increase effectiveness and reduce losses; decrease the pressure differential and increase cuttings evacuation rate (Akin et al., 1997; King et al., 1990). The effect of various governing parameters on the drill bit hydraulics is typically analyzed through CFD by qualitative analysis which is based on visual observation of the flow distribution across the surface of the drill bit (King et al., 1990; Mortimer, 2010; Wells et al., 2008).

To-date, there have been no studies reported for the simultaneous effect of varying two or more parameters on PDC drill bit performance. For the case of 8¾ inch (222 mm) diameter PDC drill bit with seven nozzles and five flow paths, the hydraulic design is influenced by the nozzle design parameters such as its size, location and orientation. The factorial design based combination of design factors will be implemented on the Computer-aided design (CAD) model of the PDC drill bit and the behavior of fluid flow in terms of pressure and velocity gradients will be quantified using CFD simulations. Using the pressure and velocity gradients as the responses, RSM will be applied to calculate the extent of significance, each of the design factors has on the drilling performance. The most significant design factors will be used for CCD and the various combinations of the design factors will be applied on the CAD model followed by CFD simulations to quantify the flow behavior. RSM will be used to build a statistical model that relates the significant design factors with the drilling performance in terms of velocity and pressure gradients.

Chapter Three: Methodology

3.1 Methodology

In this chapter, the methodology for implementing CFD simulations for investigating the PDC drill bit flow field by the application of experimental design (DOE) analysis is described. It is hypothesised that utilizing the statistical DOE will aid in identifying the more influential parameters and thus reduce the number of CFD simulations for optimum performance design of the PDC drill bit.

3.2 Objectives

The main objective of this research is to improve the flow distribution across the bit face in order to avoid regrinding of cuttings and hence achieve better cleaning. This work mainly focuses on the modification of the jet nozzle size, location and orientation which will result in modified flow patterns for better bit cleaning and enhanced drilling performance.

The drill bit plays a major role in the process of drilling a hole in the ground. The proper selection of a drill bit and the operating conditions leads to the success of drilling. Drill bits are broadly classified as drag bits and rolling cutter bits based on the process of drilling. Rolling cutter bits, introduced in 1909, consist of two or more cones with cutting elements that rotate about the axis of the cones as the bit rotates at the bottom of the hole (Bourgoyne et al., 1991). Drag bits consist of a series of blades with a number cutters brazed on it that process drilling in bottomhole with a shearing force as the drill bit rotates about its axis. Since the 1980's, drag bit

had significant development on design changes which leads to one of the most used drag bit - PDC drill bit that contains the polycrystalline diamond compact cutters.

Jet impact force is a function of pressure drop at the bit, fluid density and flow rate. Maximizing the jet impact force would result in an increase in the bottomhole fluid velocity. One of the objectives is to increase the bottomhole fluid velocity which could be brought about by modifying the nozzle location and nozzle orientation. The bottomhole fluid velocity will be quantified by average fluid velocity across the cutter surface. Maximizing jet nozzle velocity results in better drilling performance. Hence the other objective is to investigate different nozzle sizes in order to improve the jet nozzle velocity. The velocity distribution profile will be used to identify the recirculation zones which are responsible for bit balling. Design parameters will be modified to reduce or eliminate the recirculation zones and hence improve the evacuation of the cuttings.

Computational Fluid Dynamics (CFD) will be used to simulate the fluid flow in the complex geometry of a drill bit. As a first step, simulations will be carried out for the case of two-phase, isothermal, incompressible turbulent flow by considering the drill bit rotation for the factorial design cases to identify the significant factors. The second step will be to perform simulations for the runs obtained from the central composite design to determine the optimum design factors based on identification of the low pressure zones in the flow distribution for drill bit design development to improve the flow pattern. The improved drill bit design simulation results will be compared with the results of actual drill bit design for minimum pressure drop and minimization of recirculation zone.

3.3 Design features of PDC drill bit:

The features of the PDC drill bit under investigation in this thesis are: outer diameter 8 ¾ inch (222mm) with seven nozzles, five blades with 65 PDC cutters (including the gage and backup cutters). All seven nozzles are of equal size of 13/32 inch (10.32 mm) each. The junk slot areas are the flow areas (channels) between the blades. These are defined as the five flow paths and numbered accordingly as shown in Figure 3-1. Each nozzle was numbered as nozzle#1 in flowpath#1, nozzle#2 and nozzle#3 in flowpath#2 and similarly in other flow paths.

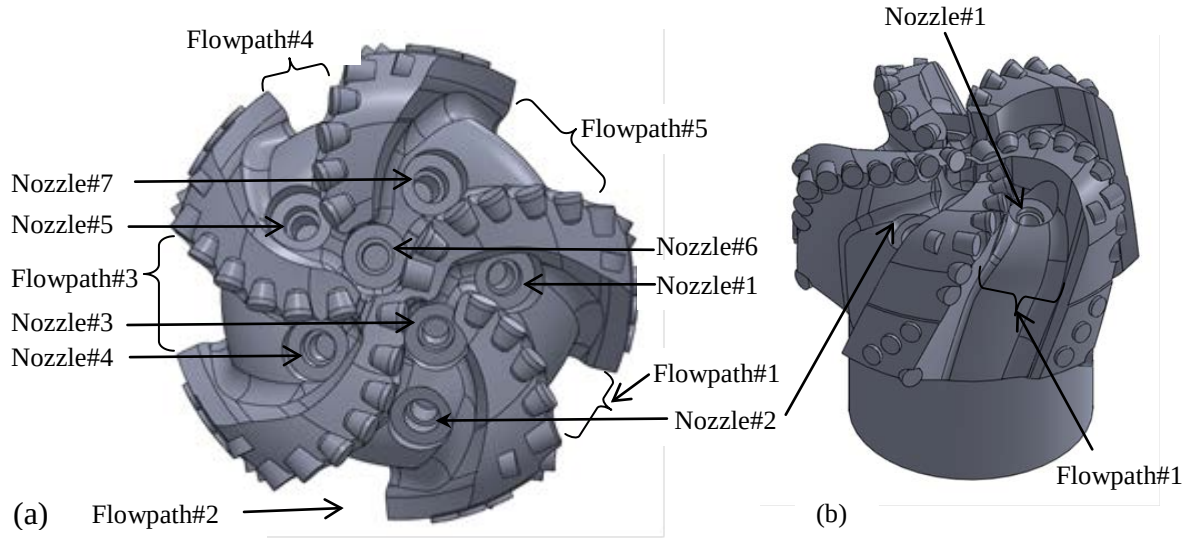

Figure 3-1. Nozzle and flow path in PDC Drill bit; (a) Bottom view of drill bit, (b) isometric view of drill bit (Hareland et al., 2009)

3.4 Governing equations for CFD

In the flow domain in the PDC drill bit, the fluid motion is governed by the conservation equations for mass and momentum and the *k-ω* turbulence model.

3.4.1 Mass Conservation Equation

The conservation of mass equation states that the change of mass inside the control volume is equal to the balance of fluid mass entering and leaving the control volume. The conservation principle is represented through the continuity equation:

$$\frac{\partial \rho}{\partial t} + \nabla . (\rho \vec{v}) \; = \; 0 \qquad \text{...(3-1)}$$

where ρ is the density, υ is the velocity, and t is the time. The first term is the unsteady term which represents the rate of change of density and the second term is the convective term which represents the net rate of mass flow through the control volume.

3.4.2 Momentum Conservation Equations

The governing equation for the conservation of linear momentum, written in conservative form, is:

$$\frac{\partial}{\partial t}(\rho \vec{v}) + \nabla . (\rho \vec{v} \vec{v}) \; = \; -\nabla p + \nabla . (\bar{\bar{\tau}}) + \rho \vec{g} + \vec{F} \qquad \text{...(3-2)}$$

where p is the static pressure, $\bar{\bar{\tau}}$ is the stress tensor, and $\rho \vec{g}$ and $\vec{F}$ are the gravitational body force and external forces.

The stress tensor $\bar{\bar{\tau}}$ is given by

$$\bar{\bar{\tau}} = \mu\left[(\nabla\vec{v} + \nabla\vec{v}^T) - \frac{2}{3}\nabla.\vec{v}I\right] \quad ...(3\text{-}3)$$

where μ is the molecular viscosity, I is the identity unit tensor, and the second term on the right hand side is the effect of volume dilation. ($\nabla.\vec{v} = 0$ for incompressible media)

The above conservation equations of mass and momentum together comprise the Navier-Stokes equations and are solved for various flow conditions in Fluent.

3.4.3 Standard k-ω Model

In addition to the Navier-Stokes equations, two more transport equations, for the turbulence kinetic energy (k) and the specific dissipation rate (turbulent frequency) (ω) are used to represent the turbulence of the fluid. The standard k-ω model comprises the transport equations for the turbulence kinetic energy (k) and the specific dissipation rate (ω) (FLUENT, 2012; Wilcox, 1998). The specific dissipation rate or turbulent frequency (ω) is defined as the ratio of ε and k, where ε is the homogeneous dissipation rate or turbulent dissipation (Wilcox, 1998). The k-ω model has the advantages of accuracy and robustness near wall region and under adverse pressure gradients and hence can be used to compute the boundary layer development in the fluid flows (Menter, 1992).

The transport equations for the standard k-ω model are as follows:

$$\frac{\partial}{\partial t}(\rho k) + \frac{\partial}{\partial x_i}(\rho k u_i) = \frac{\partial}{\partial x_j}\left(\Gamma_k \frac{\partial k}{\partial x_j}\right) + G_k - Y_k + S_k \quad ...(3\text{-}4)$$

$$\frac{\partial}{\partial t}(\rho\omega) + \frac{\partial}{\partial x_i}(\rho\omega u_i) = \frac{\partial}{\partial x_j}\left(\Gamma_\omega \frac{\partial \omega}{\partial x_j}\right) + G_\omega - Y_\omega + S_\omega \quad \text{...(3-5)}$$

where G_k represents the generation of turbulence kinetic energy due to mean velocity gradients. G_ω represents the generation of ω. Γ_k and Γ_ω represent the effective diffusivity of k and ω, respectively. Y_k and Y_ω represent the dissipation of k and ω, due to turbulence. S_k and S_ω are user-defined source terms (FLUENT, 2012; Wilcox, 1998).

3.4.3.1 Modeling the Effective Diffusivity

The effective diffusivities for the *k*-ω model are given by,

$$\Gamma_k = \mu + \frac{\mu_t}{\sigma_k} \quad \text{...(3-6)}$$

$$\Gamma_\omega = \mu + \frac{\mu_t}{\sigma_\omega} \quad \text{...(3-7)}$$

where σ_k and σ_ω are the turbulent Prandtl numbers for k and ω, respectively. The turbulent viscosity, μ_t is computed by combining k and ω as follows:

$$\mu_t = \alpha^* \frac{\rho k}{\omega} \quad \text{...(3-8)}$$

where α^* is defined below.

3.4.3.2 Low Reynolds number correction

To accommodate the transitional Reynolds number regime, the model is fitted with a low-Reynolds number correction, in which the eddy viscosity is dampened using the low-Reynolds number coefficient (α^*). It is given by,

$$\alpha^* = \alpha_\infty^* \frac{\alpha_0^* + Re_t/R_k}{1 + Re_t/R_k} \quad \text{...(3-9)}$$

where Re_t is the turbulence Reynolds number defined as,

$$Re_t = \frac{\rho k}{\mu \omega} \quad \text{...(3-10)}$$

$$\alpha_0^* = \frac{\beta_i}{3} \quad \text{...(3-11)}$$

For the case of the high-Reynolds number form of the *k-ω* model, $\alpha^* = \alpha_\infty^* = 1$. The parameters α^*, α_0^* and β_i are closure coefficients and R_k is the model coefficient (Wilcox, 1998) given in Table 3-1.

3.4.3.3 Modeling the Turbulence Generation

Generation of k:

The term G_k representing the production of turbulence kinetic energy is defined as,

$$G_k = -\rho\overline{u_i' u_j'}\frac{\partial u_j}{\partial x_i} \quad \text{...(3-12)}$$

Generation of ω:

The generation of ω is given by,

$$G_\omega = \alpha\frac{\omega}{k}G_k \quad \text{...(3-13)}$$

where the co-efficient α is given by,

$$\alpha = \frac{\alpha_\infty}{\alpha^*}\left(\frac{\alpha_0 + Re_t/R_\omega}{1 + Re_t/R_\omega}\right) \quad \text{...(3-14)}$$

where R_ω is model coefficient and α^* and Re_t are defined in eqn (3-9) and (3-10).

3.4.3.4 Modeling the Turbulence Dissipation

Dissipation of k:

The dissipation of *k* is given by,

$$Y_k = \rho\beta^* k\omega \quad \text{...(3-15)}$$

where

$$\beta^* = \beta^*_\infty \left(\frac{4/15 + \left(Re_t/R_\beta\right)^4}{1 + \left(Re_t/R_\beta\right)^4} \right) \quad \text{...(3-16)}$$

where Re_t is given by eqn (3-10), β^* is closure coefficient and R_β is model coefficient.

Dissipation of ω:

The dissipation of ω is given by

$$Y_\omega = \rho\beta\omega^2 \quad \text{...(3-17)}$$

For the incompressible flow, $\beta = \beta_i$.

Table 3-1. Model constants (Wilcox, 1998)

Turbulent Prandtl numbers	σ_k	2.0
	σ_ω	2.0
Closure coefficient	α^*_∞	1
	α_∞	0.52
	α_0	1/9
	β^*_∞	0.09
	β_i	0.072
Model coefficient	R_β	8
	R_k	6
	R_ω	2.95

3.4.4 VOF Model

The VOF model was originally proposed as surface-tracking technique applied to a fixed Eulerian mesh for tracking and resolving the interface between two or more immiscible fluids. This method implicitly allows for simulating the behaviour of mixtures of immiscible fluids.

This method is based on the assumption that each control volume contains just one phase or the interface between phases. In the VOF model, a single set of momentum equations represents the motion of the fluid mixture. The effective fluid properties of the mixture are calculated based on the individual fluid properties through the volume fraction, α. The volume fraction is forced to satisfy a consistency constraint in each control volume. The volume fraction of each of the fluids in each computational cell is tracked throughout the domain (Hirt & Nichols, 1981). The VOF formulations available in FLUENT are the explicit and the implicit scheme (FLUENT, 2012). The implicit scheme was used in this research as it focuses on obtaining a steady-state solution that depends on the initial flow conditions and there is no distinct inflow boundary for each phase. The flow pattern of gas-water, two phase flow in a horizontal pipeline was simulated in FLUENT by the application of unsteady, implicit scheme VOF method (Jie et al., 2011).

Volume Fraction Equation:

The tracking of the interface(s) between the phases is accomplished by the solution of a continuity equation for the volume fraction for each phase. For the q^{th} phase, this equation has the following form:

$$\frac{1}{\rho q}\left[\frac{\partial}{\partial t}\left(\alpha_q \rho_q\right) + \nabla.\left(\alpha_q \rho_q \vec{v}_q\right) = S_{\alpha_q} + \sum_{p=1}^{n}\left(\dot{m}_{pq} - \dot{m}_{qp}\right)\right] \quad ...(3\text{-}18)$$

where $\dot{m}_{qp}$ is the mass transfer from phase q to phase p and $\dot{m}_{pq}$ is the mass transfer from phase p to phase q. p is the drilling fluid phase and q is the mud phase. Mud is derived from a medium hard formation and since its proportion is very small compared to the drilling fluid, it was assumed that mud behaves similar to the drilling fluid in terms of rheology. The mud properties, viscosity and density are provided in Table 3-2.

The volume fraction for the primary-phase (drilling fluid) is computed based on the constraint as shown in equation (3-19). For implicit time discretization the equation solved for the volume fraction is given in equation (3-20)

$$\sum_{q=1}^{n} \alpha_q = 1 \quad ...(3\text{-}19)$$

$$\frac{\alpha_q^{n+1}\rho_q^{n+1} - \alpha_q^n \rho_q^n}{\Delta t} V + \sum_f \left(\rho_q^{n+1} U_f^{n+1} \alpha_{q,f}^{n+1}\right) = \left[S_{\alpha_q} + \sum_{p=1}^{n}\left(\dot{m}_{pq} - \dot{m}_{qp}\right)\right] V \quad ...(3\text{-}20)$$

Where *n+1* is the index for the new(current) time step, *n* is the index for the previous time step, $\alpha_{q,f}$ is the face value of the q^{th} volume fraction (mud), *V* is the volume of cell and U_f is the volume flux through the face based on normal velocity.

3.5 Solution Method

All computations are performed using the finite-volume commercial CFD code; FLUENT 14.0. The SIMPLE algorithm is applied to solve the pressure–velocity coupling. The discretization scheme used for the pressure variable is PRESTO and the first-order upwind scheme is employed to solve the momentum equation, volume fraction equation, turbulent kinetic energy and specific dissipation rate. Convergence and steady-state are examined by noting the diminishing normalized residual levels ($<10^{-3}$).

The SIMPLE solver algorithm includes setting up the boundary conditions and computing the velocity gradients. Solving the momentum equation leads to an approximation of the velocity field. The pressure gradient is calculated using the pressure distribution from the previous iteration or an initial guess. The pressure equation is formulated and solved in order to obtain the new pressure distribution. A new set of conservative fluxes is calculated from the corrected velocities.

3.6 Computational domain

A 222 mm PDC drill bit was used in the simulation. The flow channel for the simulation follows the drilling fluid from the drill bit nozzle to the drill pipe annulus. The drill pipe rotates along with the drill bit and the mud generated mixes with the drilling fluid in the flow path.

The commercial CFD software FLUENT was used to simulate the flow in the PDC drill bit. The geometric model was developed for the 222 mm PDC drill bit as shown in Figure 3-1. This five blade PDC drill bit has seven nozzles of 13/32” (10.32 mm) nozzle diameter and has 65 PDC cutters. The flow domain was developed using Solidworks along the flow path from nozzles to annulus through the junk slot area. The geometric model was cleaned from

unnecessary fillets and filled small gaps before the model was exported as an IGES file. ICEM CFD (ANSYS) was used for meshing. The IGES file was imported and the flow field was meshed as unstructured tetrahedral mesh. The mesh topology was corrected for unfilled surfaces. The mesh file was exported to the ANSYS FLUENT solver for further simulation.

3.7 Drill bit boundary conditions:

The standard operating conditions of the PDC drill bit were provided by NorthBasin Energy Services Inc (*Drill bit manufacturer in North America*) are shown in Table 3-2.

Table 3-2. Drill bit operating conditions

Drilling fluid flow rate	33.33×10^{-3} m^3/s	
Drill bit rotation	100 rpm	
Drilling fluid	Water	
	Density	1000 kg/m^3
	Viscosity	0.001 Pa-s
Lithology (Mud)	Medium hard formation (clay sediment)	
	Density	1500 kg/m^3
	Viscosity	.04 Pa-s
Rate of penetration	10 m/hr	
Drill bit thermal effect on rheology	negligible	

Inlet condition will be provided at the nozzle in the drill bit. The proportion of mud to drilling fluid is very small and hence it was assumed that mud follows Newtonian behavior. Drilling fluid flow rate was used to determine the velocity at the inlet based on the eqn (3-21) to eqn (3-24). Inlet condition of the PDC drill bit was set in terms of velocity inlet at the nozzle (57 m/s) in the direction normal to boundary as shown in Figure 3-2. Since turbulent condition exists near the inlet, it was assumed that the flow follows a uniform velocity profile. Outlet condition of the PDC drill bit was provided at the top cross section of the backflow annulus with 0 psi as the

static gauge pressure. Drill bit thermal effect on rheology was assumed to be negligible based on the cooling effect of the high fluid velocity. Though the convection heat transfer due to fluid flow is a main factor in the cooling of the cutters, its influence in fluid hydraulics is minimum. Hence, based on this assumption and from literatures based on computations simulation performed for PDC drill bit the thermal effect was neglected in calculation (Ju et al., 2013; Wells et al., 2008).

$$v = \frac{q}{3.117 A_t} \quad \text{...(3-21)}$$

$$A_t = N\frac{\pi}{4}d^2 \quad \text{...(3-22)}$$

where:

v Velocity at nozzle (ft/sec)

q Drilling fluid flowrate (gpm)

A_t Total nozzle area (in^2)

N Number of nozzle

d Nozzle diameter (in)

$$A_t = 7\left(\frac{\pi}{4}\right)\left(\frac{13}{32}\right)^2 = 0.90735\ in^2 \quad \text{...(3-23)}$$

$$v = \frac{2000 * 0.264172}{3.117 * 0.90735} = 186.81\ ft/\text{sec} = 56.94\ m/s \quad \text{...(3-24)}$$

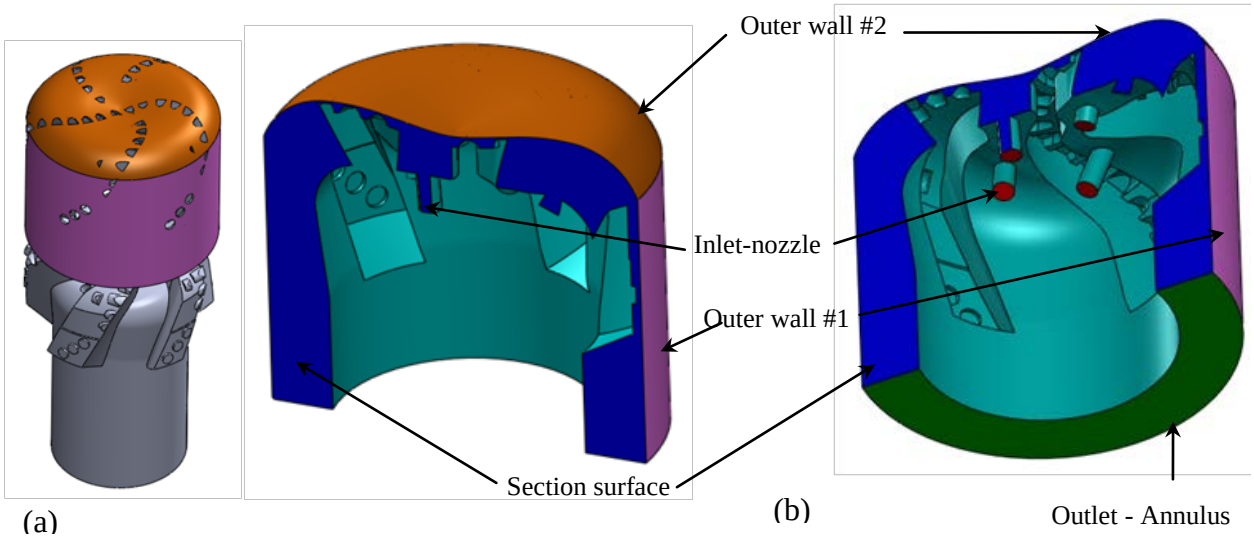

Figure 3-2. Boundary conditions a) Simulated domain versus drill bit (exploded for clarity) and b) Section view of simulated domain

Other boundary conditions were standard wall with no slip condition. The shear condition at the wall was specified as no-slip condition which indicates that the fluid sticks to the wall and moves with the same velocity as the wall, if it is moving. This means that large velocity gradients prevail at the near-wall region due to the viscous flow. The outlet domain is between the bottomhole surface and the inlet of the annular pipe. The drill bit outlet length was extended by 5 times the individual flow path length in order to achieve a fully developed flow. The static gauge pressure of the environment into which the flow exits was provided as 0 psi so as to ensure sufficient pressure gradient to facilitate the flow through the outlet.

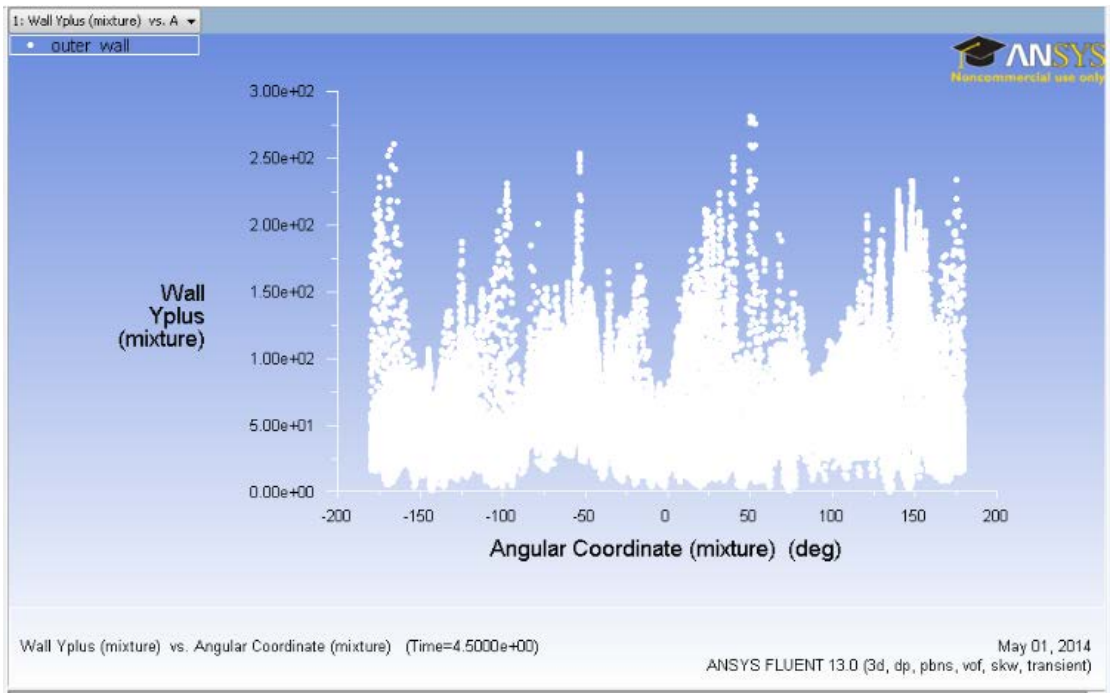

Figure 3-3. Wall y+ at the outer wall of PDC Drill bit

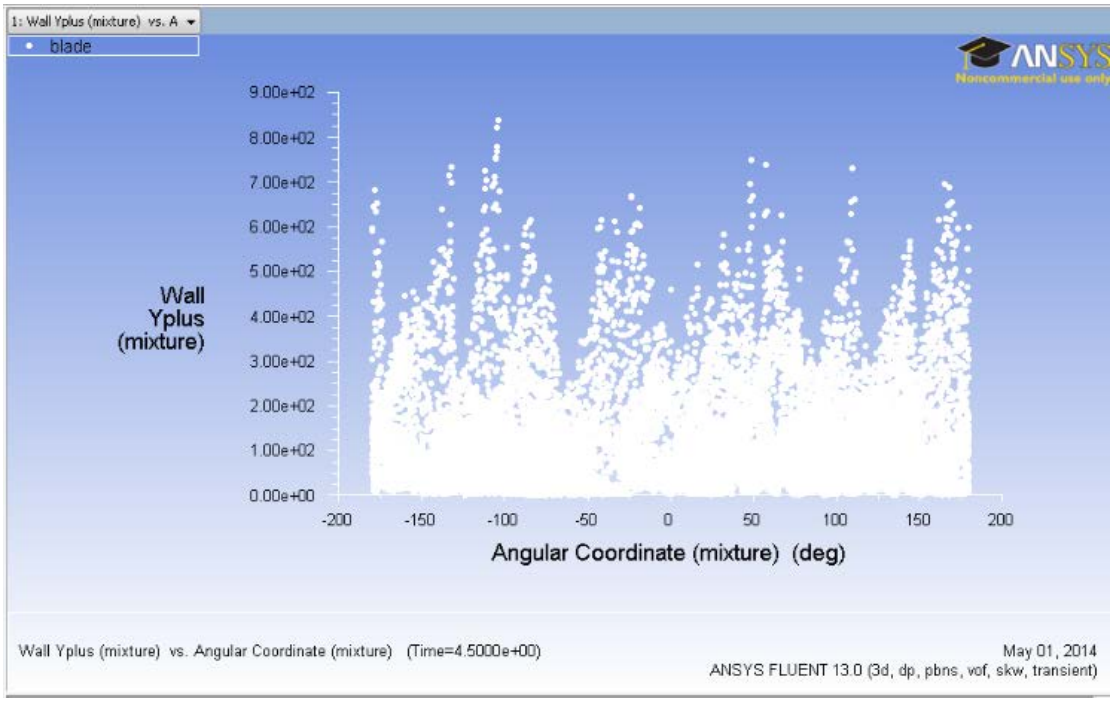

Figure 3-4. Wall y+ at the blade (inner wall) of PDC Drill bit

The wall y+ is a non-dimensional wall distance (based on local cell fluid velocity) from the wall to the first mesh node, for a wall-bounded flow which is dependent on friction velocity at the nearest wall (u^*), distance to the nearest wall (y) and local kinematic viscosity of the fluid (ν) (White, 1999). y+ in the range between 30 and 300 is desirable for turbulence model.

$$y^+ \equiv \frac{u^* y}{\nu} \qquad ...(3\text{-}25)$$

The wall conditions will be treated by FLUENT differently depending on y+. Boundary conditions for wall-function meshes will correspond to the wall function approach. The value of ω at the wall (ω_w) is specified as,

$$\omega_w = \frac{\rho(u^*)^2}{\mu}\omega^+ \qquad ...(3\text{-}26)$$

Analytical solution for the laminar sublayer is given as,

$$\omega^+ = \frac{6}{\beta_i(y^+)^2} \qquad ...(3\text{-}27)$$

and for the logarithmic region as,

$$\omega^+ = \frac{1}{\sqrt{\beta_\infty^*}}\frac{du_{turb}^+}{dy^+} \qquad ...(3\text{-}28)$$

Hence, a wall treatment defined for the ω-equation switches automatically from the viscous sublayer formulation to the wall function, depending on the grid. This blending is optimized using Couette flow (laminar flow of viscous fluid between two parallel plates) in order to achieve a grid independent solution. This improved blending is the default behavior for near wall treatment in FLUENT.

The y+ plot at the outer wall and the blade with respect the angular coordinate is shown in Figure 3-3 and Figure 3-4 respectively. For the outer wall, y+ was within the 300 limit. But for the blade, though y+ was highly concentrated within the 300 limit, some points were outside the limit. However, it is considered to be acceptable since most points were in the desirable range and the demand of y+ cannot be too strict (Qunfeng et al., 2011).

3.8 PDC drill bit simulated conditions and assumptions

The real time drill bit operation was built in the computational domain by increasing the complexity gradually. By using the simplified drill bit model (Figure 3-5), it was identified that CFD can be used as a tool to simulate the downhole condition for drilling. In the next step, CFD tool was successfully utilized for simulating the single phase system in the actual drill bit model under steady state condition. This was followed by considering two phases under unsteady state condition which closely resembles the real situation. CFD was effectively utilized to simulate the flow distribution in terms of velocity and pressure profiles.

3.8.1 Simplified drill bit model simulation

An initial CFD study was performed with a highly simplified drill bit design considering a single nozzle and a symmetric model as shown in Figure 3-5. This step is conducted to identify suitable rotating frame of reference for drill bit rotation, grid resolution and prescription of boundary conditions.

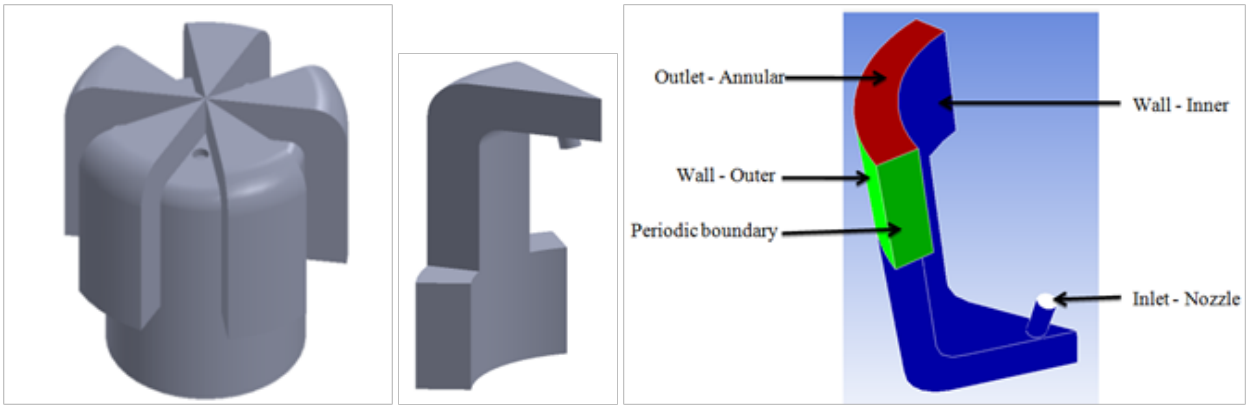

Figure 3-5. Simplified drill bit model, fluid domain and boundary conditions

The model was created with a simple profile and grid generation was done using ICEM CFD, a meshing tool. FLUENT, a commercially available CFD simulator tool was used to simulate the initially simplified model. A 3D domain with isothermal, incompressible turbulent flow, single phase and steady state Newtonian flow was considered for the initial simulation. The boundary conditions provided were the velocity inlet at the nozzle and the pressure outlet at the drill gage or junk slot area to annuli. Relative rotational motion was provided for the outer wall. Water was considered as the drilling fluid. Simulation was performed for two cases: (1) with a realizable k-ε model with standard wall function and (2) k-ω model with standard wall function. Velocity flow patterns were observed after the convergence of the simulation.

3.8.2 CFD simulation for PDC drill bit

CFD simulation was carried out for two cases, one considering steady state condition with single phase flow and the other considering two phase flow domain of mud and water with unsteady state flow condition. A brief summary of simulation details are presented in the subsequent section showing the solver parameters and the resultant flow distributions.

3.8.2.1 Model Geometry

The original CAD model for the 222mm diameter PDC drill bit was provided by NorthBasin Energy Services Inc (*Drill bit manufacturer in North America*). The CAD model was developed using SolidWorks for the computational condition as shown in Figure 3-6. Sharp fillets in the flow path were removed to avoid fine mesh near the filleted surface. Chamfer and the complex geometry at the drill bit nozzle were eliminated by assuming that chipping would fill the void areas. As discussed earlier in this section, the drill bit was assumed to be operated in a medium hard formation. At this condition, the cutter exposure will be immersed in the formation by providing the shearing force to the downhole. As the cutter exposure is not a part of the flow domain, one third of the cutter was trimmed by eliminating the immersed volume of the drill bit. This condition allows the CFD simulation to incorporate the cross flow between the flow paths as the effect of the cross flow is significant in real time operation. The developed drill bit CAD model was exported as IGES format that can be accessed by meshing software.

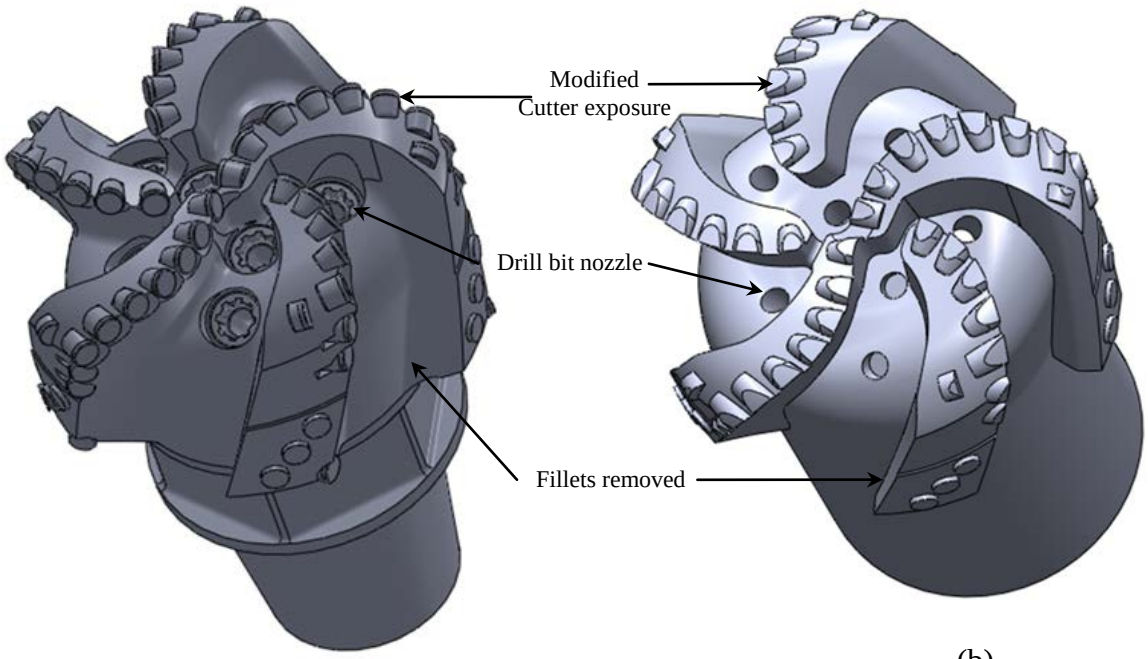

Figure 3-6. PDC drill bit geometry a) Actual PDC drill bit, b) Geometrically developed PDC drill bit

3.8.2.2 Mesh Generation

The complex geometry of PDC drill bit calls for an effective tool for mesh generation. ANSYS ICEM CFD is one of the commercial packages available for mesh generation for CFD application.

The IGES file of the drill bit flow domain was imported into ICEM package. The flow domain topology was diagnosed for any mismatched edges, additional surfaces, surface overlaps and unnecessary gaps. The outlet surface was extended by five times as the length of flow path across the blades, in order to ensure steady state condition at the outlet. All surfaces were grouped to individual parts and named as inlet, outlet, inner wall, blade, outer wall and mud inlet as shown in Figure 3-7.

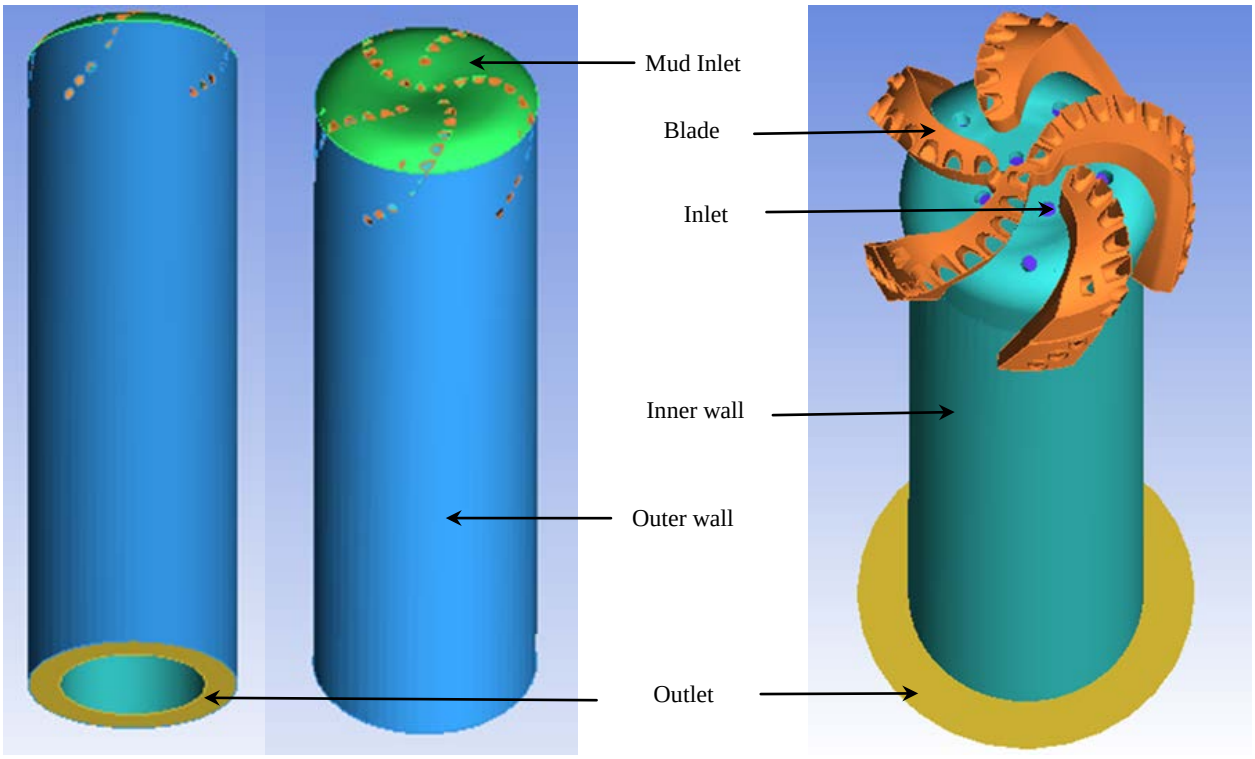

Figure 3-7. Repaired drill bit flow geometry for mesh generation. a) Outer wall b) Inner wall

Global mesh setup was made as presented in Table 3-3. Each part was provided with the mesh setup for maximum size, height and height ratio, tetra size ratio and tetra width. Volume meshing parameters were set as Tetra/mixed for mesh type and mesh type as Robust (Octree). To globally scale the model, the global parameters such as max element, min size limit, and periodicity should be multiplied by global element scale factor. The parameter Maximum element size controls the size of the largest element. Enabling the curvature based refinement automatically refines the mesh for geometry curvature and will result in larger elements on flat planar surfaces and smaller elements in areas of high curvature or within small gaps. Minimum size limit specifies the size limit for the smallest element and the mesh elements will be limited from being subdivided smaller than this value. Allowing the ignore wall thickness feature to be

ON, prevents the curvature based sizing function from refining for closely spaced parallel surfaces.

Table 3-3. Global mesh setup

Global element scale factor	.2
Maximum element size	16.0
Curvature based refinement	Enabled
Minimum size limit	0.1
Ignore wall thickness	ON

An unstructured tetrahedral mesh was generated as shown in the Figure 3-9. The mesh was checked for errors such as duplicate element edges, uncovered faces, hanging elements etc. In order to improve the mesh quality, mesh smoothing was performed to ensure that no skewed or small angled elements were present. The mesh quality was calculated based on the orthogonal quality which is the quality determined based on the vector normal to each face, the vector from the cell centroid to the centroids of each of the adjacent cells, and the vector from the cell centroid to each of its faces. The worst cells will have an orthogonal quality closer to 0, with the best cells closer to 1. The minimum orthogonal quality for all types of cells should be more than 0.01, with an average value that is significantly higher. Due to the complexity in the geometry, the minimum orthogonal quality achieved was 0.32. Since the purpose of this study is design optimization which involves simulations with several variations in the design, the mesh quality was maintained in the satisfactory level.

Inner wall and the blade mesh are shown in Figure 3-8. The mesh refinement was performed near the cutter edges in order to study the cross flow across the flow path which is the thin distance between the blade and the downhole. Figure 3-9 shows the outer wall and mud inlet

surface mesh and the interior volume meshing. The grid refinement was performed near the wall to avoid an increase in y+ value by ensuring gradual transition to the coarser mesh.

Table 3-4 shows the details of a representative mesh of a PDC drill bit. The total number of mesh nodes was maintained in the range of 650k nodes to 700k nodes which was determined based on the grid independent study (discussed in section 3.9). Unstructured tetrahedral mesh was developed at the wall with reasonably high number of elements to obtain y+ within the range of less than 500. Due to high velocity near the nozzle inlet, y+ was closer to 1000. The skewness of a grid is another important parameter that gives a measure of grid quality. For tetrahedral cells, the maximum allowable skewness limit is 0.9. Aspect ratio which is defined as the ratio of longest to the shortest side in a cell should be greater than 1.

Table 3-4. PDC drill bit mesh details

Total number of mesh nodes	692,098 nodes
y+ range for the nodes closest to the wall	<500 (~1000 close to the inlet)
Skewness of elements (max)	Max = 0.83; Mean = 0.18
Aspect ratio (max)	16
Minimum orthogonal quality	0.32

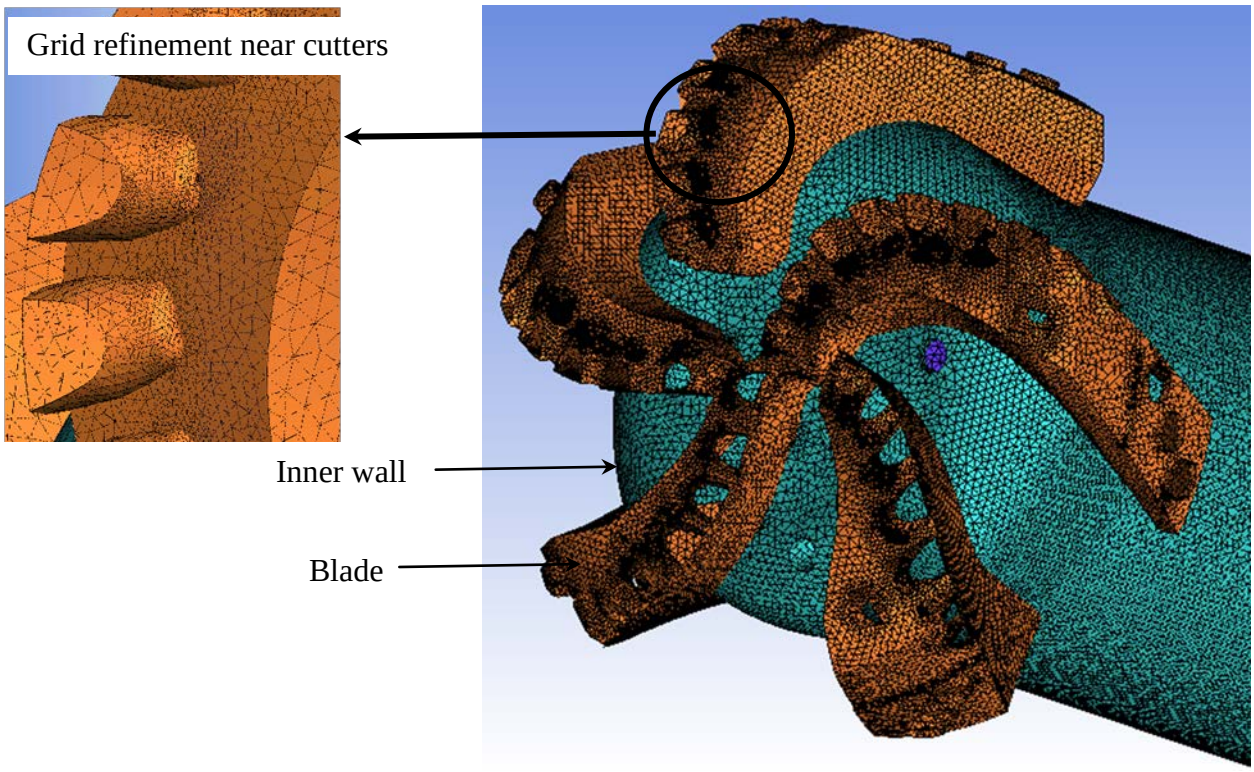

Figure 3-8. Inner wall and blade mesh

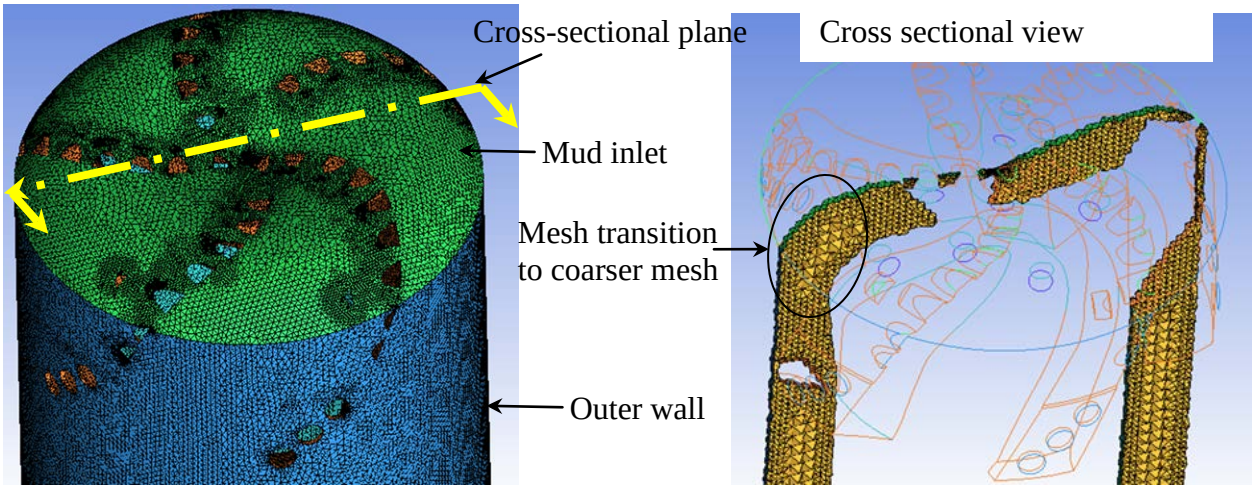

Figure 3-9. Outer wall mesh and interior volume mesh

3.8.2.3 Preliminary simulation with steady state condition

Problem solving model: The standard k-ω model was used to solve the flow field and the governing equations include equations of continuity, momentum equation and k-ω equations.

Solution methods are simple scheme for pressure-velocity coupling and discretization scheme used are PRESTO for Pressure; first order upwind for momentum, turbulent kinetic energy & specific dissipation rate.

Computational conditions: 3D space, pressure based solver with absolute velocity formulation and steady state time was used. Liquid-water material properties were obtained from the material library of FLUENT. The grid used for this simulation consisted of 28k nodes. Further study will be performed for grid independence in terms of observing the effect of change in grid fineness with respect to the convergence in result.

Boundary condition: Inlet condition of the model was given in terms of velocity inlet at the nozzle (57 m/s) in the direction normal to boundary as shown in Figure 3-2. Outlet condition of the model was given at the top cross section of the backflow annulus with 0 psi as the static gauge pressure. Other boundary conditions given are standard wall with no slip condition.

3.8.2.4 Preliminary simulation with two phase unsteady state condition

Problem solving model: The standard k-ω model was used to solve the flow field, same as in Case 1. VOF (Volume of Fluid) standard model was used to consider the two-phase system of water and mud. VOF model constants: courant number = 0.25, volume fraction cutoff = 1e-6.

Computational conditions: 3D space, pressure based solver with absolute velocity formulation and unsteady state condition were applied. Liquid water was taken to be phase-1 fluid and its material properties were obtained from the material library of the FLUENT. Mud with dynamic viscosity 0.04 kg/m-s was used as phase-2 fluid material.

Boundary condition: Phase-1 fluid inlet velocity at the nozzle (57 m/s) in the direction normal to the boundary was provided as one of the inlet boundary condition. Phase-2 fluid (mud) inlet was given as 2 m/s from the surface of bottomhole (i.e. Outlet wall #2 as shown in Figure 3-2(b). Outlet condition of the model was given at the top cross section of the backflow annulus with 0 psi as the static gauge pressure. Other boundary conditions given are standard wall condition with zero slip velocity and no penetration.

The above preliminary simulations were conducted to identify the recirculation and stagnation zones in the velocity distribution and pressure distribution profiles. Since these zones tend to decrease the drilling performance, it is necessary to reduce or eliminate them. The design parameters such as nozzle location, orientation and size will be modified and optimized to improve the drilling efficiency by eliminating or reducing the recirculation and stagnation zones.

3.9 Grid independency study

The objective of the grid independency study is to determine the most efficient grid for reliable results. Thus, different density grids are tested. The outcomes sought are to determine when the results are within an acceptable tolerance.

Meshing on the PDC drill bit computation domain was done with three different grid sizes - 178k, 314k and 887k nodes, as unstructured tetrahedral mesh with increasing grid fineness at the cutter edges (Table 3-5). CFD simulation was performed with the same operating conditions as that of the preliminary simulation as described in Table 3-6. Simulation results were compared for the flowpath#3 with nozzle#4. This flow path was chosen because it has a single nozzle and assumed to have less impact from the flow of other nozzles. The velocity profile at the cross section of the flow path was compared for the grid independency of all cases.

Table 3-5. Grid independency study - mesh size

Grid	Nodes
Mesh #1	178k
Mesh #2	314k
Mesh #3	887k

Table 3-6. Solver parameters and boundary conditions for grid independency study

Solver	Pressure based – Steady state
Viscous model	k-ω turbulence model
Fluid material	Water (Density[ρ] = 998.2 kg/m^3 & Dynamic Viscosity[μ] = .001 kg/m-s)
Boundary condition	Velocity inlet at Nozzle (57m/s) Outflow at Annulus = constant (P_{ref} = 0 Pa) Inner wall at Bit surface (standard wall condition) Outer wall at Bottomhole surface (standard wall)
Solution Methods	Pressure-Velocity coupling – Simple Discretization Scheme: Pressure – PRESTO Momentum – First order upwind Turbulent Kinetic Energy – First order upwind Specific Dissipation Rate – First order upwind

3.10 DOE method for drill bit design

DOE is a statistical tool which allows the evaluation of how a group of factors control a parameter or a group of parameters. In this study, it is required to understand the effect of varying the design parameters on the drill bit performance, in terms of recirculation zones and pressure differential across the bit. Recirculation zones were quantified by outlet velocity, mean velocity and mean vorticity in the cross section of each flow path. A two-step statistical approach comprising a fractional factorial design and central composite design based analyses was used in this study

3.10.1 Identification of significant parameters:

In the first step, fractional factorial design was applied to study the effect of 15 design parameters obtained by varying the nozzle size, nozzle location and nozzle inclination (Figure 3-10). The design parameters of the PDC drill bit was combined in various combinations based on a 2-level fractional factorial experimental design. Nozzle size will be the same for all seven nozzles and nozzle location was determined by the diameter of the orbit of nozzle placement. Nozzle inclination was measured based on the inclination of the nozzle towards the axis of the drill bit without changing the inclination of the nozzle towards the cutter or the blade. Table 3-8 shows the 15 factors and the actual level of the factors. The actual level of each factor was considered to be the base level. The base level will be increased and decreased according to the range to obtain the high level and low level respectively. All the 15 factors were analyzed according to a resolution-3, factorial design with 16 runs.

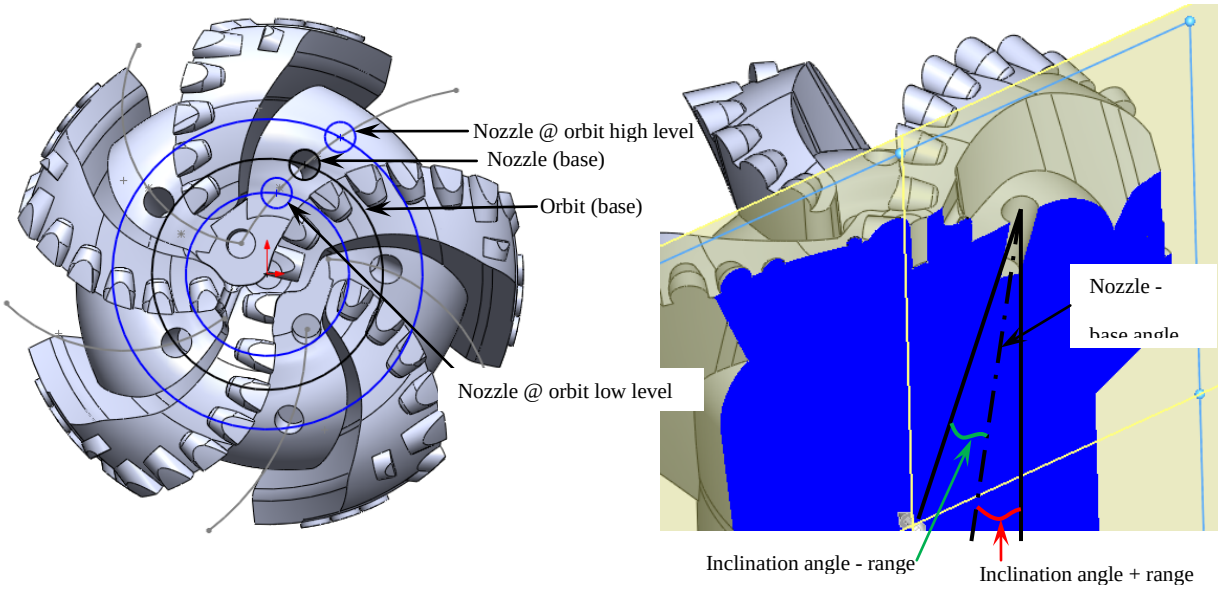

Figure 3-10. Illustration of nozzle location orbit and nozzle inclination angle as referred in DOE matrix - a representation in flowpath#5

Each of the various design combinations was implemented in the CAD model of the PDC drill bit and the behavior of fluid flow in terms of pressure and velocity gradients was quantified using CFD simulations. CFD simulations performed based on solver parameters and boundary conditions provided in Table 3-7. The factorial design based simulations were executed with two-phase, isothermal, incompressible turbulent flow condition by considering the drill bit rotation.

Table 3-7. Solver parameters and boundary conditions

Solver	Pressure based – Unsteady state
Viscous model	k-ω turbulence model
Multiphase model	VOF
Fluid material	Water (Density[ρ] = 998.2 kg/m^3 & Dynamic Viscosity[μ] = .001 kg/m-s) Mud (Density[ρ] = 1500 kg/m^3 & Dynamic Viscosity[μ] = .04 kg/m-s)
Boundary condition	Phase1-Water: Velocity inlet at Nozzle (57m/s) Phase2-Mud:Velocity inlet at bottomhole (.003m/s) Outflow at Annulus = constant (P_{ref} = 0 Pa) Frame rotation at Inner wall at Bit surface (100rpm) Outer wall at Bottomhole surface (standard wall)
Solution Methods	Pressure-Velocity coupling – Simple Discretization Scheme: Pressure – PRESTO Momentum – First order upwind Turbulent Kinetic Energy – First order upwind Specific Dissipation Rate – First order upwind

The responses obtained from CFD simulations were embedded in the design matrix and the Design Expert 8.0.6 statistical software was used to determine the model and the effects of each of the design parameters using the half normal probability plot. Analysis of variance (ANOVA) was carried out to determine the significance of the factorial model. The selected

model was validated by residual analysis using normal plot of residuals. Based on Pareto chart, the significance of the design parameters were estimated and the top five significant design parameters were chosen for the optimization studies of the PDC drill bit.

Table 3-8. Fractional Factorial Design Matrix

Sl	Nozzle#	Design Factor	Actual/ Base	High level	Low level
1	ALL	Nozzle Size # (1/32)	16	16	10
2	N1	Orbit diameter (mm)	102	132	72
3	N1	Inclination angle (deg)	18	21	15
4	N2	Orbit diameter (mm)	129	159	99
5	N2	Inclination angle (deg)	26	29	23
6	N3	Orbit diameter (mm)	59	69	49
7	N3	Inclination angle (deg)	13	16	10
8	N4	Orbit diameter (mm)	98	128	68
9	N4	Inclination angle (deg)	15	18	12
10	N5	Orbit diameter (mm)	112	142	82
11	N5	Inclination angle (deg)	20	23	17
12	N6	Orbit diameter (mm)	35	45	25
13	N6	Inclination angle (deg)	3	6	0
14	N7	Orbit diameter (mm)	100	130	70
15	N7	Inclination angle (deg)	19	22	16

3.10.2 Optimization of PDC drill bit performance:

The next step in the statistical approach was to determine the design limits of the significant design parameters for optimum performance of the PDC drill bit. The desirable characteristics are low pressure drop, improved mean velocity across the flow path and reduced mean vorticity. The focus of the objective function is to determine the point closest to the peak of each of the desired characteristics. Thus, the optimum performance is defined as the geometric layout for which the pressure drop is minimized, mean velocity across the flow path is

maximized and the mean vorticity is minimized under the constraint of predetermined operating condition as stated in Table 3-2.

The chosen design parameters were combined in a design matrix according to the face centered (α = 1), central composite design (CCD). The design parameters were varied at three levels, including the base level (Table 3-9). The CCD was constructed on a cubic domain with 10 axial points, 16 factorial points and one center point, replicated 6 times. The runs generated from the central composite design were first used to develop a CAD model of the PDC drill bit followed by CFD simulation to determine the flow behavior. The results from the simulation were used to determine the responses and the design matrix along with the response was analyzed by response surface methodology (RSM). RSM was used to establish the relationship between the response and the significant design parameters and ANOVA was applied to determine the significance of the model. The relationship between the responses and the design factors was modelled by a second order quadratic equation,

$$Y = \beta_0 + \sum_i \beta_i X_i + \sum_{ii} \beta_{ii} X_i^2 + \sum_{ij} \beta_{ij} X_i X_j \quad \text{...(3-29)}$$

where Y represents the predicted response (pressure differential, mean velocity and mean vorticity in the cross section of each flow path at two different cross sectional depths as shown in Figure 5-1), β_0 is the constant coefficient which is equal to Y when all the independent factors are zero, β_i is the linear coefficient for each factor, β_{ii} is the square coefficient for each factor and β_{ij} is the interaction or cross coefficient between factors. The developed model was validated by

residual analysis. The perturbation plot and surface plots were used to report the effect of each of the design parameters and their interaction on the responses.

Table 3-9. Significant design parameters for CCD

Sl	Nozzle#	Design Factor	Actual/ Base	High level	Median level	Low level	Range (±)
1	ALL	Nozzle Size # (1/32)	16	16	13	10	3
2	Nozzle#4	Orbit diameter (mm)	98	128	98	68	30
3	Nozzle#4	Inclination angle (deg)	15	18	15	12	3
4	Nozzle#6	Orbit diameter (mm)	35	45	35	25	10
5	Nozzle#6	Inclination angle (deg)	3	6	3	0	3

Numerical optimization was chosen to determine the design limits for optimum responses (Appendix A). The Design Expert 8.0.6 software was used to generate the possible solutions along with the desirability factor. Desirability is an objective function which ranges from zero to one, the latter being closer to the set goal. The goals were set for the responses to be either maximum or minimum.

3.10.3 Assessment of Optimization Procedure:

As there are no experimental results available for validating the optimized design, the simulation results for the optimized design of the PDC drill bit was compared with that of original design to ensure improvement in the drilling performance in terms of low pressure drop, maximum mean velocity, and minimum vorticity across the flow path. In addition, the optimized design geometry was evaluated by comparison with the recommended geometry for improved bit performance in various PDC drill bits available in the literature. The optimization procedure was carried out using water (a Newtonian fluid). Hence, to assess the results of the optimization

under drilling conditions, the VOF approach was used to simulate the influence of a water-mud mixture. The mixture behaves as a non-Newtonian fluid. The results from this simulation were compared with the simulation results for the non-Newtonian mixture by considering drilling fluid (Power law non-Newtonian fluid) later in the results and discussion chapter of the thesis.

Chapter Four: Numerical methods - Preliminary simulations

This section focuses on the preliminary simulations to develop CFD model used for design optimization. Tests were conducted to develop suitable representations of the boundary conditions (drilling fluid and mud inlet conditions, drill bit surface and downhole surface conditions, fluid condition at outlet) and fluid representation. The flow distribution in a highly simplified drill bit model was simulated first and the results assessed. This was followed by preliminary CFD simulations carried out on actual drill bit model for two cases: (a) steady state flow condition with water as a single phase, and (b) unsteady state flow condition with two phase flow domain of mud and water. A grid independency study was performed for the drill bit in order to proceed with the final simulations that are based on the methodology of design of experiments (DOE). The next chapter focuses on the selection of the design parameters and the analysis of the simulations of the optimized drill bit configuration.

4.1 Simplified drill bit model simulation

An initial CFD study was performed with a highly simplified drill bit design considering a single nozzle and a symmetric model as shown in Figure 3-4. The operating conditions and the simulation procedure are explained in section 3.8.1. Grid generation for the simplified model was performed similar to that of the actual model as discussed in section 3.8.2.2. This step was conducted to identify a suitable rotating frame of reference for drill bit rotation, grid resolution and prescription of boundary conditions, at inlet (drilling fluid and mud), outlet and solid surfaces (drill bit surface and downhole circumference). The realizable k-ε model with standard wall function was initially applied for the simulation due to its global industrial application

(Hargreaves & Wright, 2007; Moslemi & Ahmadi, 2014) and it was compared with the *k*-ω turbulence model. Figure 4-1 shows the comparison of velocity distribution for *k*-ε model and *k*-ω model at the middle of the cross sectional surface of the simplified drill bit geometry along the flow path. The velocity distribution trend is almost same for both the cases and the velocity region near the drill bit axis is low for both the models. Low velocity is due to the influence of the wall shear stress. Regions of low velocity are expected to give rise to low-Reynolds number effects, which are not well predicted using the *k*-ε model. Moreover, the influence of the wall shear stress could significantly be increased in the actual drill bit model, which has complex geometry with narrow flow path and cross flow across flow paths. The *k*-ε equation has a lack of sensitivity to adverse pressure gradients and therefore may under-predict separation and the standard *k*-ω model shows superior performance for wall-bounded boundary layer, free shear, and low Reynolds number flows and it is suitable for complex boundary layer flows under adverse pressure gradient and separation (Menter, 1993). In the PDC drill bit, the turbulent Reynolds number is very low near the wall surface, at the viscous sub layer due to high shear and is in the range between 4e-06 and 1. Reynolds number for the main stream in the flowpath was approximately 1.5e+06. Hence, the *k*-ω turbulence model was chosen for the future simulation of PDC drill bit. The inlet of the drilling fluid is the nozzle and that of mud is the downhole bottom surface. Simplified models are preferred for modeling the boundary conditions owing to less computing time. Actual drill bit operating conditions were implemented at the boundaries.

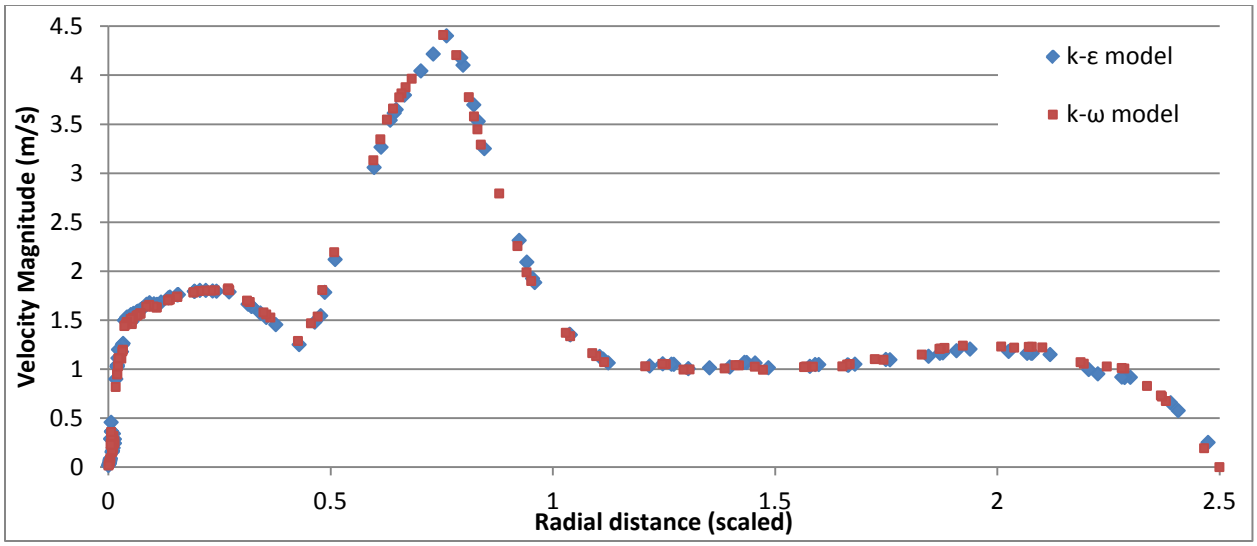

Figure 4-1. Velocity magnitude comparison for *k*-ε turbulence model and *k*-ω turbulence model at cross section (Figure 4-2(a)) of the simplified drill bit geometry along the flow path.

Illustrative sample representations of flow distribution obtained from simulation of the simplified drill bit model are shown in Figure 4-2. The velocity distribution facilitates the identification of the fluid recirculation zones and the pressure distribution contour shows the low pressure profile at the vortex zone. These observations will be used to investigate the influence of the nozzle placement and/or the nozzle inclination on the flow pattern across the bit.

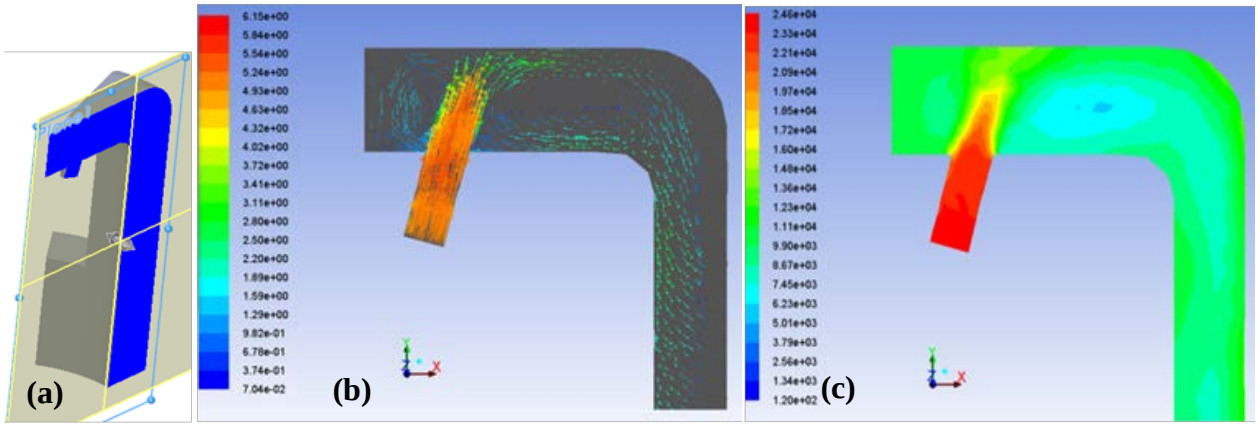

Figure 4-2. Flow distribution at the mid plane in simplified drill bit model. (a) Mid Plane cross section view, (b) Velocity Distribution (m/s) at mid plane, (c) Pressure Distribution (Pa) at mid plane

4.2 PDC drill bit preliminary simulation

The actual drill bit model geometry was developed and implanted into the computational domain as discussed in section 3.8.2.1. The grid generation was performed with unstructured tetrahedral meshes as demonstrated in section 3.8.2.2. CFD simulations were carried out by increasing the complexity from a steady state-single phase flow domain to an unsteady state-two phase flow domain. These simulations were performed in order to evaluate the applicability of boundary conditions derived from the simplified model to the actual drill bit model and to understand the flow pattern in terms of recirculation region and stagnation zones that reduce the drilling performance.

4.2.1 Numerical simulation under steady state condition - results and observation

The objective of this simulation with a single phase steady state flow is to evaluate the boundary conditions derived from the simplified geometry to the actual drill bit geometry. Each flow path was investigated for the flow pattern in terms of velocity vectors. These results will be used as a demonstration of the formation of recirculation and the velocity instabilities due to stagnation region in the flow paths.

The simulation converged after 2313 iteration with an average outlet velocity of 3.3 m/s. The convergence criterion was to obtain an absolute residual of 1e-06. Figure 4-3 shows the velocity vectors in the flow domain and Figure 4-4 shows the pressure distribution in the flow domain. These results show the flow pattern considering single phase (water) as the fluid.

The following provides an example on how the flow pattern across the bit will be evaluated to characterize bit balling. The velocity distribution profile across the bit shows the

regions of recirculation and stagnation. Recirculation zone is characterized by the velocity vector that flows in the direction from annulus to drill bit axis, whereas the desired flow stream should be in the direction from drill bit axis to annulus. It occurs always attached to the wall region. Stagnation zone in the flow field is characterized by zero velocity. One of the recirculation zones was observed between nozzle#6 & #7 in flowpath#5 as shown in Figure 4-3(c). Since these recirculating zones cause bit balling, it is essential to eliminate them. This could be achieved by shifting the nozzle position or by changing the nozzle inclination.

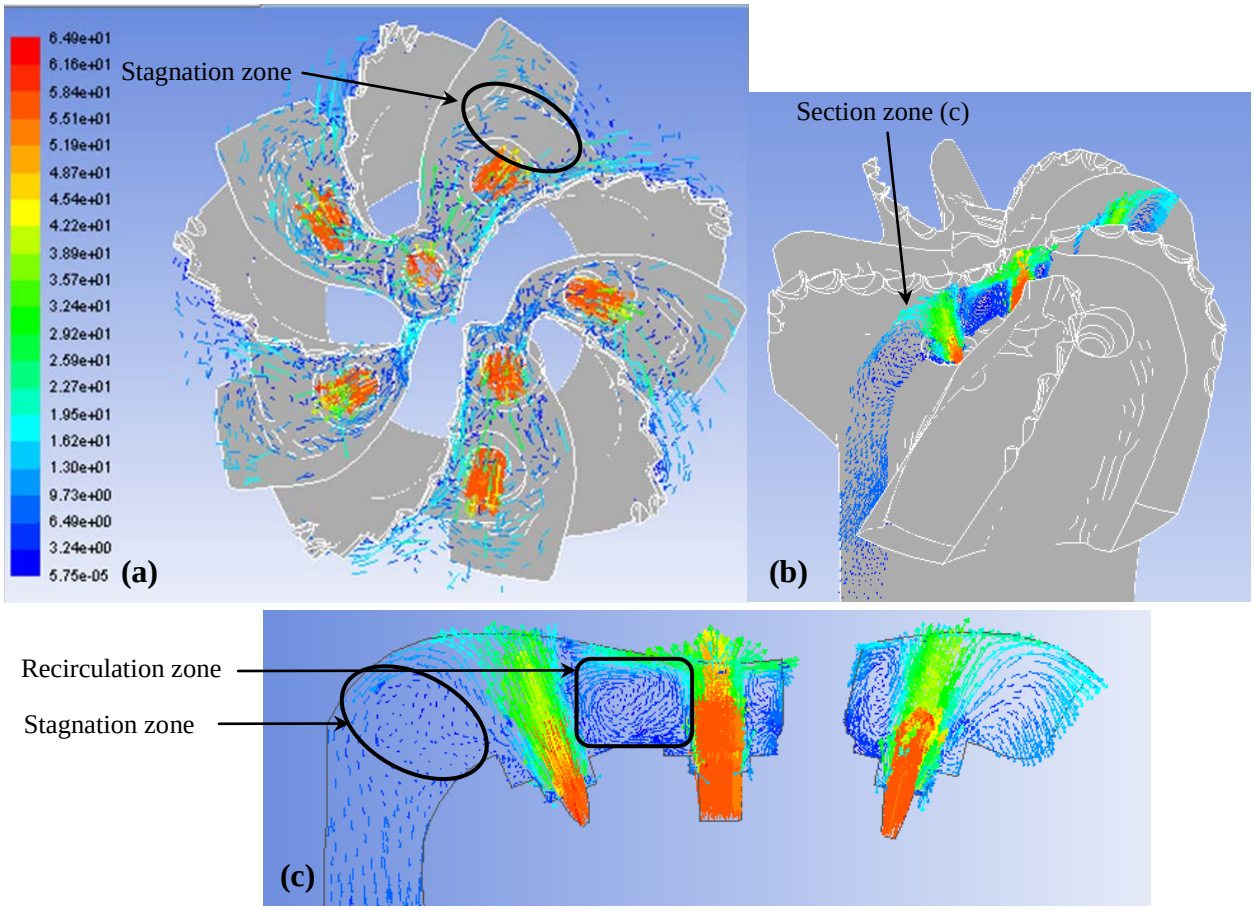

Figure 4-3. Stagnation zone (circled) and recirculation zones (squared) in the velocity distribution at steady state condition (a) Horizontal plane above the bit, (b) Location of section zone (c) passing through nozzle#6 and #7 at flowpath#5.

Stagnation zones were evident from the pressure distribution across the bit at nozzle#5 which is characterized by high pressure and zero velocity as shown in Figure 4-4(a). These zones reduce the drilling performance and hence should be removed. Possible means to avoid stagnation zones include changing the nozzle size, to modify jet nozzle velocity, or to change the geometry (nozzle location and inclination).

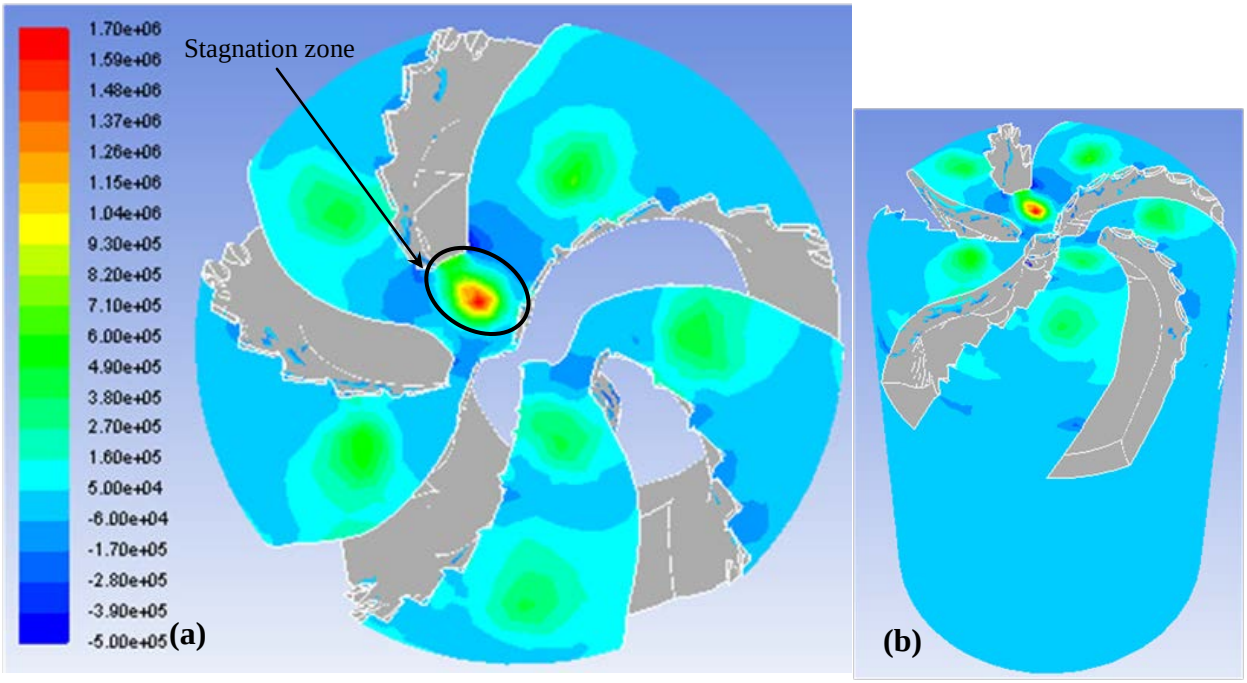

Figure 4-4. Observation of stagnation zones (circled) in the pressure distribution at steady state condition (a) Horizontal plane above the bit (b) Isometric view

4.2.2 Numerical simulation with two phases - results and observation

The objective of this section is to simulate the flow pattern for a two phase flow (mud and water mixture) with the boundary conditions arrived from the single phase steady state simulation. A steady-state solution is required for the scenario of continuous drilling where the intermediate transient flow is not relevant. As a two phase- mixing process is involved, the mixing process due to the action of the drill bit on the mud surface must be resolved. Briefly, the

steady-state solution is achieved after the initial transient period due to the mixing of the mud and water. Only after the mixture has reached equilibrium, is a steady-state solution possible. Thus it is required that the unsteady (time dependent) form of the equations be solved. In order to simulate the mixing process, the steady-state flow solution will result as the mixing reaches equilibrium. Similar to the previous case, water was considered to be the drilling fluid. In addition, mud was considered as the clay generated from the downhole bottom surface. For simplicity, mud was assumed to be a weak suspension that follows Newtonian behavior (Reeves et al., 2006). The results will be used to demonstrate the rheological behavior of the mixture of the two phases.

The simulation converged after 3600 iteration with the average outlet velocity of 6.5 m/s. Figure 4-5 shows the representation of velocity vectors distribution. These results show the flow pattern considering two phases, water and mud. As stated earlier, the phases, water (drilling fluid) and mud (generated clay) were assumed to be Newtonian. As two phases are involved, viscosity is not uniform for every shear rate. This case of fluid behavior will fall under the category of a Non-Newtonian model and hence the flow rheology is affected. Recirculation and stagnation zones were observed in the velocity distribution and pressure distribution profiles. Since these zones tend to decrease the drilling performance, it is necessary to reduce or eliminate them. The design parameters such as nozzle location, orientation and size will be modified and optimized to improve the drilling efficiency by eliminating or reducing the recirculation and stagnation zones.

The velocity distribution profile across the bit shows the regions of recirculation and stagnation. One of the recirculation zones was observed between nozzle#6 and nozzle#7 in flowpath#5 as shown in Figure 4-5(c). Since these zones are one of the causes for bit balling, it is

essential to eliminate them. This could be achieved by shifting the nozzle position or by changing the nozzle inclination.

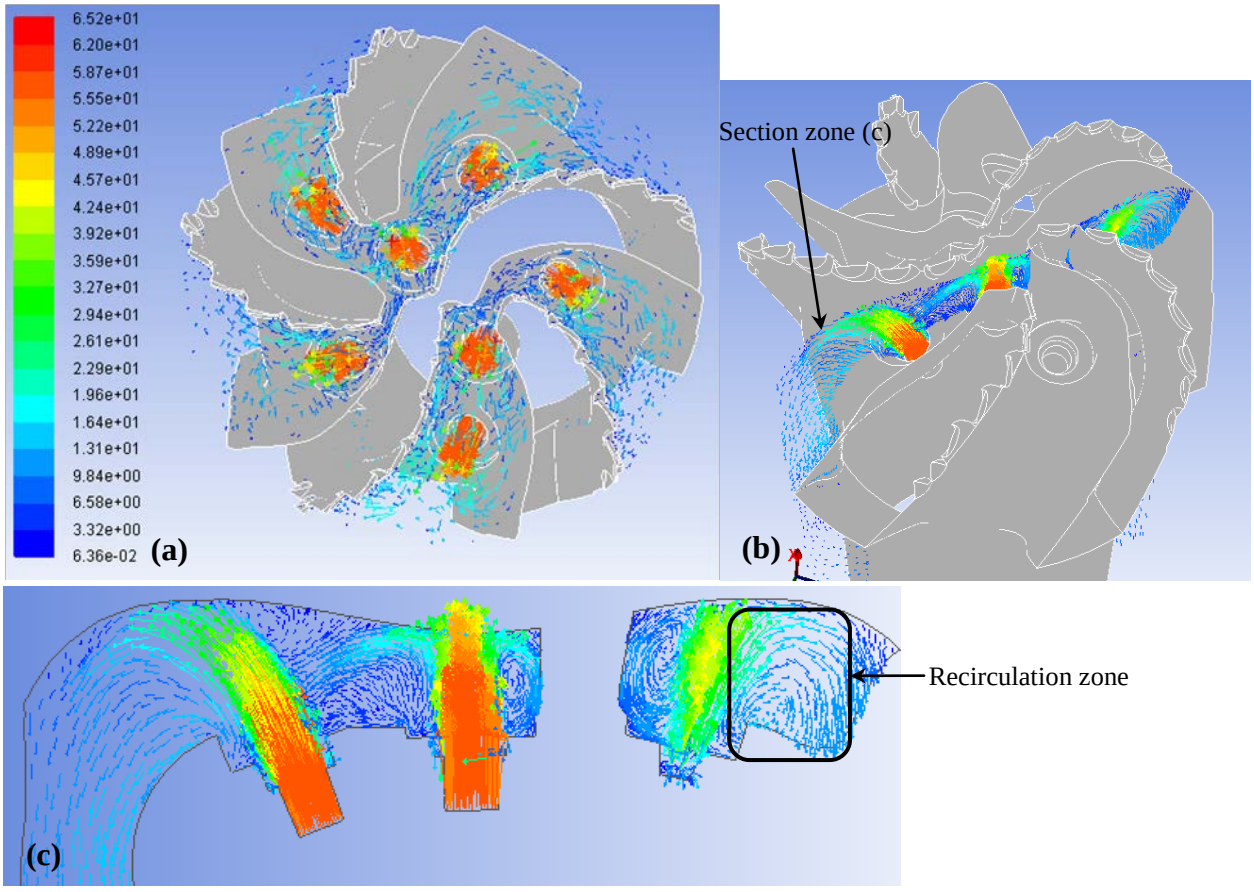

Figure 4-5. Recirculation zones (squared @ nozzle#5) in the velocity distribution at unsteady state condition for a two phase system (a) Horizontal plane above the bit, (b) Location of section zone (c) passing through nozzle#6, #7 at flowpath#5 including nozzle#4 at flowpath#3.

Figure 4-6 shows the comparison of single phase model and two phase model in terms of velocity magnitude. Flowpath#3 was chosen as a reference to demonstrate the effect of two phases in the flow domain. The total width of the junk slot area from the down-hole surface to the bit inner wall (30mm) was divided into three zones and the velocity was compared at two different heights, Ψ = 10mm and Ψ = 20mm as shown in Figure 4-12. At Ψ = 10mm, which is

closer to the downhole bottom surface, the velocity magnitude is low in the two phase model due to the mixing of high volume fraction of mud with the drilling fluid. At the same time, the presence of high volume fraction of mud causes resistance to the flow and hence results in distributing the velocity of the nozzle jet near the drill bit surface at Ψ = 20mm. Therefore, the average velocity of the two phase model at Ψ = 20mm is higher than that of the single phase model. These conditions prove the significance of using a two phase model in order to replicate the actual drill bit flow domain.

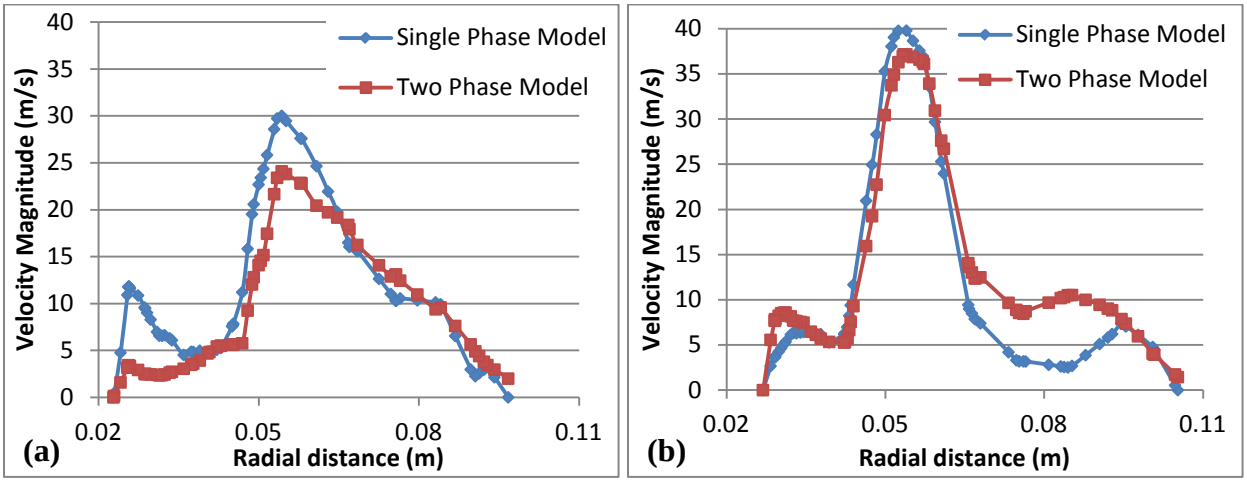

Figure 4-6. Velocity magnitude comparison for single phase model and two phase model in flowpath#3 along radial distance from drill bit axis: (a) Velocity at height Ψ = 10mm; (b) Velocity at height Ψ = 20mm.

The distribution of the effective viscosity of the mixture of drilling fluid and mud across the drill bit surface in the flowpath#3 is shown in Figure 4-7. In general, the effective viscosity was high near the downhole bottom surface at Ψ = 10mm, which is due to the high volume fraction of mud in the flow field. The viscosity of the mixture near the nozzle inlet is closer to that of water (drilling fluid), indicating that water is the predominant phase at this location. The mixture viscosity is very high near the circumference towards the exit of the flow path due to the

high proportion of mud in the mixture. These observations show the non-Newtonian behavior of the mixture of drilling fluid and mud.

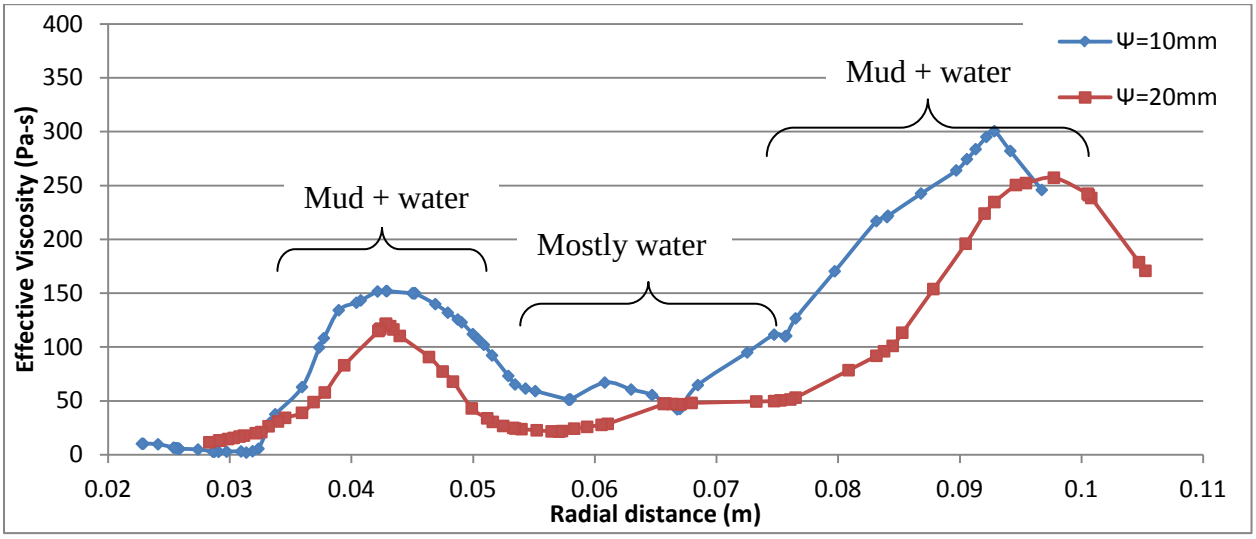

Figure 4-7. Effective viscosity distribution in flowpath#3 for Ψ = 10mm and Ψ = 20mm.

The effective viscosity for the single phase model and the two phase model were compared at Ψ = 10mm and Ψ = 20mm as shown in Figure 4-8. The comparatively high effective viscosity in the two phase model was due to the integration of mud with water that increased the viscosity of the mixture. At Ψ = 10mm, the effective viscosity was drastically increased near the nozzle jet and near the circumference of the downhole surface in the two phase model due to the high resistance to shear force created by viscous mixture. At Ψ = 20mm, the magnitude of increase in the effective viscosity was comparatively lower than that at Ψ = 10mm. This was because of water predomination in this region due to the low volume fraction of mud. Near the circumference of the downhole surface, the effective viscosity was considerably higher in the two phase model compared to that of single phase model due to the shear force exerted on the fluid mixture by the outer wall and flows towards the outlet of the drill bit.

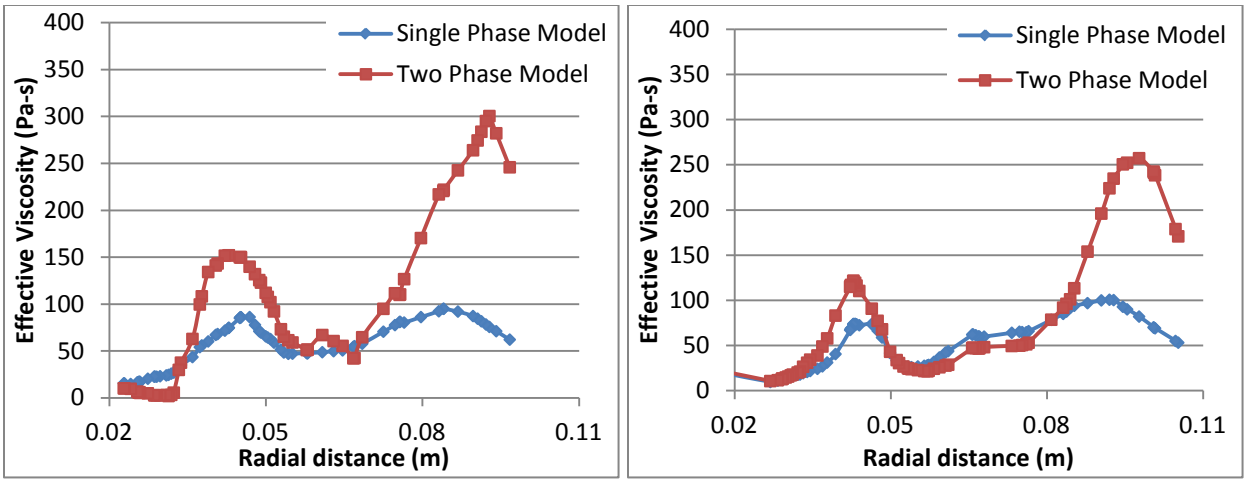

Figure 4-8. Effective viscosity comparison for single phase model and two phase model in flowpath#3 along radial distance from drill bit axis: (a) Velocity at height Ψ = 10mm; (b) Velocity at height Ψ = 20mm.

In order to simulate the real time drill bit operation, the computational domain was modified in steps of increasing complexity to evaluate (a) the selection of suitable computational models for CFD simulation of PDC drill bit (b) the implementation of boundary conditions and setting up benchmark for assessing the influence on fluid rheology (c) the two phase interaction effect on fluid rheology. By using the simplified drill bit model, it was identified that CFD can be used as a tool to simulate the downhole condition for drilling along with the identification of the boundary condition. The CFD tool was utilized for simulating the single phase system in the actual drill bit model under steady state condition. This was followed by considering two phases under unsteady state condition which closely resembles the real situation. CFD was effectively utilized to simulate the flow distribution in terms of velocity and pressure profiles, which in turn allowed the identification of recirculation and stagnation zones.

4.3 Grid independency study

CFD simulations were carried out on actual drill bit geometry as discussed in section 3.8.2.1, for three cases by varying the grid sizes to analyze grid sensitivity. A representative flow path (flowpath#3) has been chosen to compare the simulation results for the various grid sizes.

Table 4-1. Grid size and computation time

Grid	Nodes	Wall-Clock Time (HH:MM) Per 4000 iteration
Mesh #1	178k	01:30
Mesh #2	314k	02:50
Mesh #3	887k	07:30

4.3.1 Convergence results for various grid sizes

Mesh #1 with 178k nodes: Taking the rotation of the drill bit into consideration, CFD simulation was performed with single phase and steady state condition. The simulation converged at about 500 iterations. The criterion for convergence is that the residual should be equal to 1e-03. The scaled residuals and the average outlet velocity are shown in Figure 4-9.

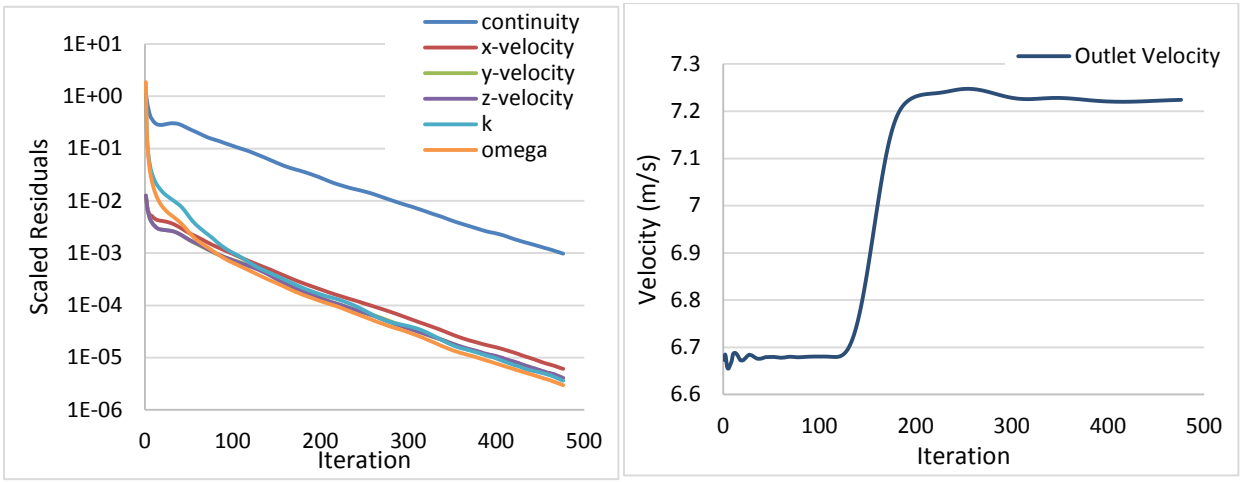

Figure 4-9. Scaled residuals versus iteration and outlet average velocity versus iteration for mesh#1

Mesh #2 with 314k nodes: CFD simulation was performed with single phase and steady state condition, considering the bit rotation. The simulation converged at about 1000 iterations. The scaled residuals and the average outlet velocity are shown in Figure 4-10.

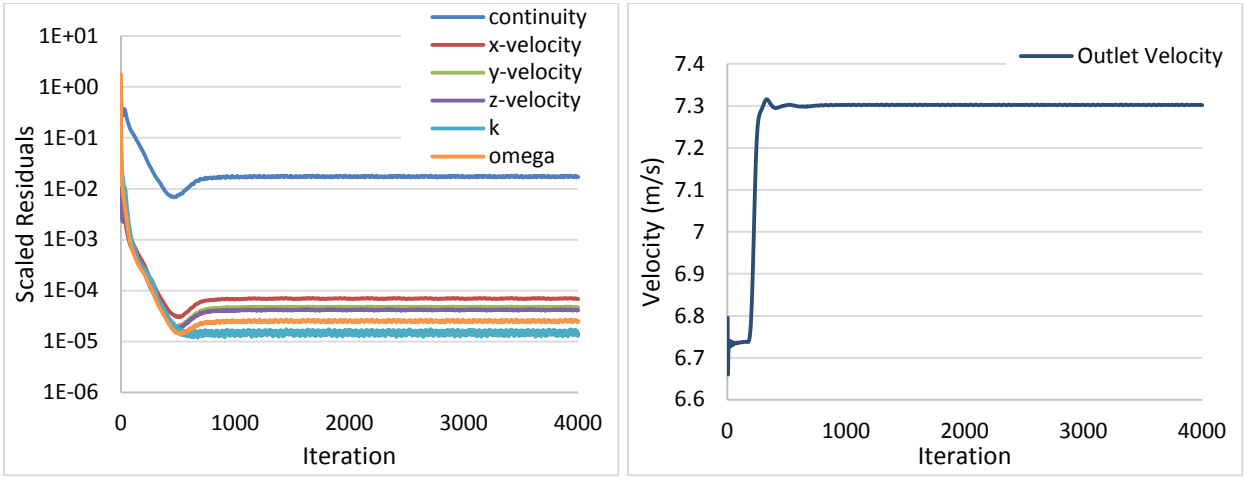

Figure 4-10. Scaled residuals versus iteration and outlet average velocity versus iteration for mesh#2

Mesh #3 with 887k nodes: CFD simulation with single phase and steady state condition was carried out considering the rotation of the drill bit. The simulation converged at about 1000 iterations. The scaled residuals and the average outlet velocity are shown in Figure 4-11.

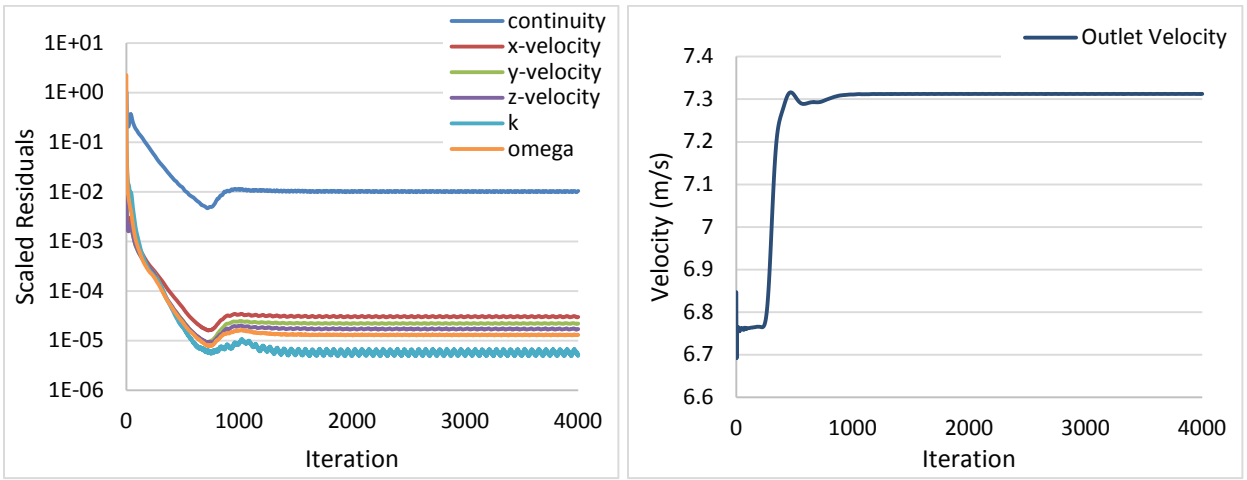

Figure 4-11. Scaled residuals versus iteration and outlet average velocity versus iteration for mesh#3

Convergence Summary: The convergence level was set to the error residual to reach 1e-03. For the mesh #1, the convergence reached within the 450 iteration. But for the mesh #2 and mesh #3 the above said convergence level is not reached but the solutions arrived to steady state condition after 1000 iteration. Surface average velocity at the outlet also reached steady value. This condition ensures the convergence in result. Table 4-1 shows the grid size and the computational time for each mesh.

4.3.2 Grid sensitivity - A comparative study

Velocity distribution profile: Results for the three mesh sizes were compared based on the velocity distribution along the flowpath#3. The cross sectional plane location and the depth line for velocity plot through the radius of the drill bit are shown in Figure 4-12(a). The velocity profile cross sections taken at the centre of the flowpath#3 are shown in the Figure 4-12 (b), (c) and (d) for mesh sizes 178k, 314k and 887k respectively. The squared areas are the low velocity zones in the jet flow path.

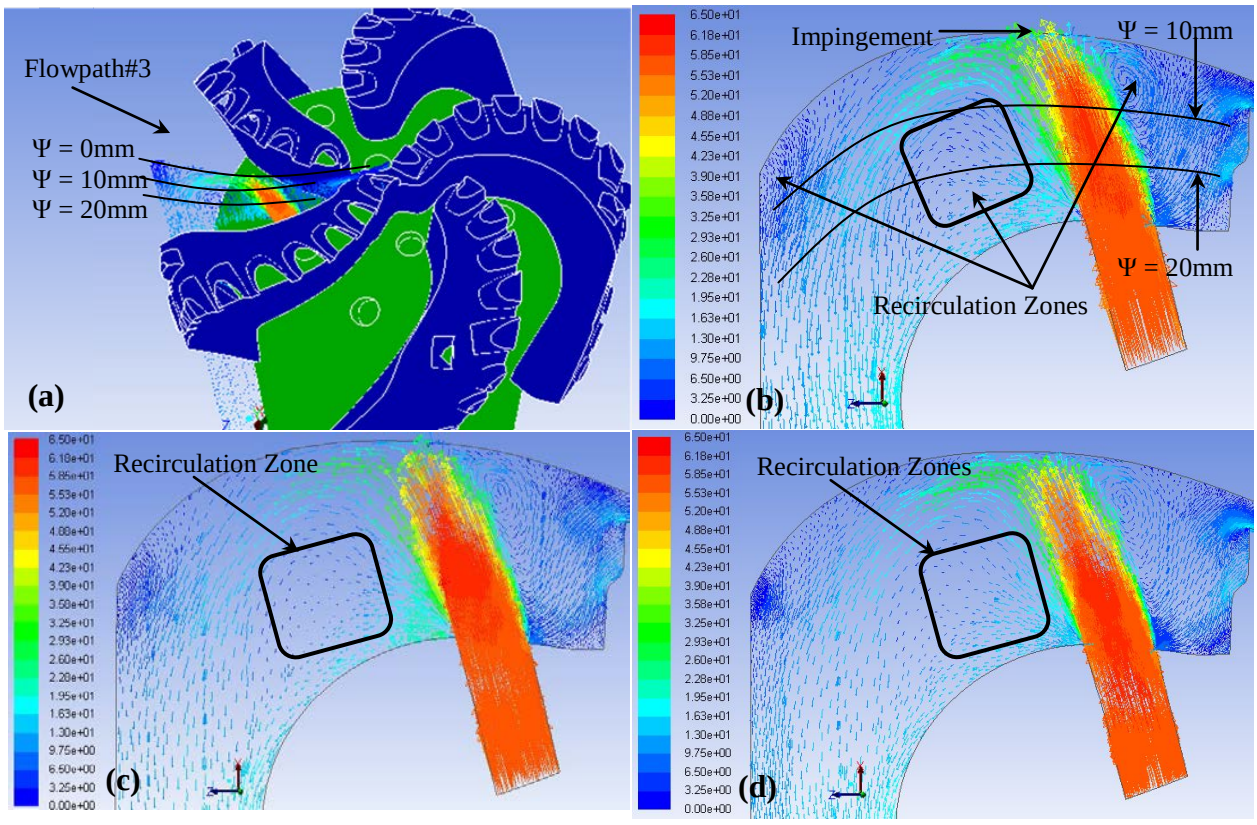

Figure 4-12. Velocity distribution profile at flowpath#3 with the squared areas shows the low velocity zone: (a) Location of cross sectional plane at flowpath#3 and the clip lines for Ψ = 10mm & Ψ = 20mm; (b) Velocity distribution for mesh#1; (c) Velocity distribution for mesh#2; (d) Velocity distribution for mesh#3.
*A representative of recirculation zones and impingement zones are marked in Figure (b)

Velocity magnitude and static pressure comparison plot: The total width of the junk slot area from the down-hole surface to the bit inner wall (30mm) was divided into three zones and the velocity was compared at two different heights, Ψ = 10mm and Ψ = 20mm. The clip lines at Ψ = 10mm and Ψ = 20mm are shown in the Figure 4-13(a) and (b). For three mesh sizes of 178k, 334k & 887k nodes, the velocity was plotted along the radial length from the drill bit axis and compared in Figure 4-13(a) at clip height of Ψ = 10mm and Figure 4-13(b) at clip height of Ψ = 20mm. Similarly static pressure plotted along the radial length from the drill bit axis was compared in Figure 4-14(a) at clip height of Ψ = 10mm and Figure 4-14(b) at Ψ = 20mm.

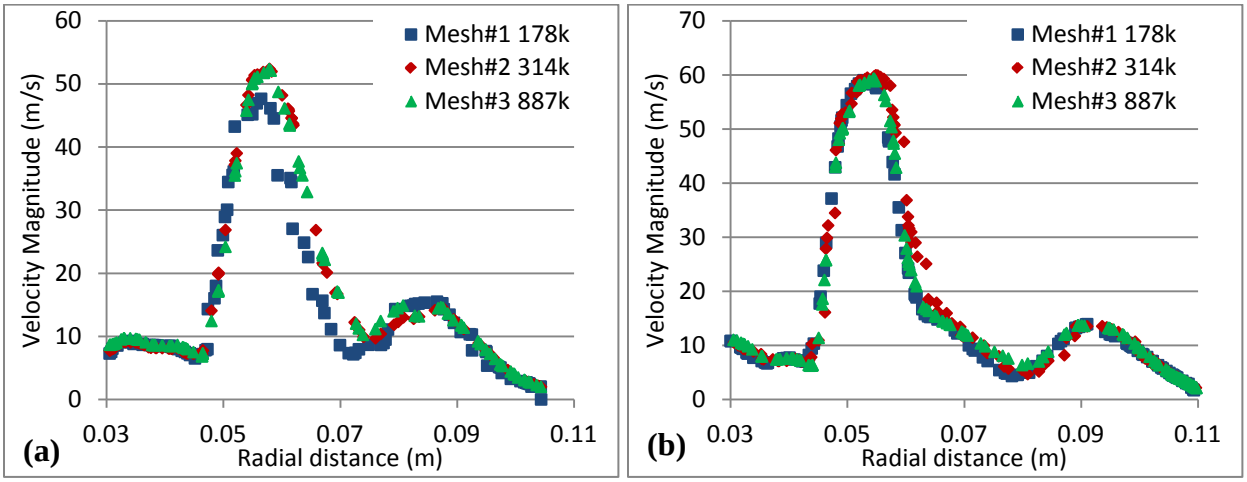

Figure 4-13. Velocity magnitude for gird sizes (178k, 334k and 887k nodes) at the center of the flowpath#3 versus radial distance from drill bit axis- (a) Velocity at height Ψ = 10mm; (b) Velocity at height Ψ = 20mm.

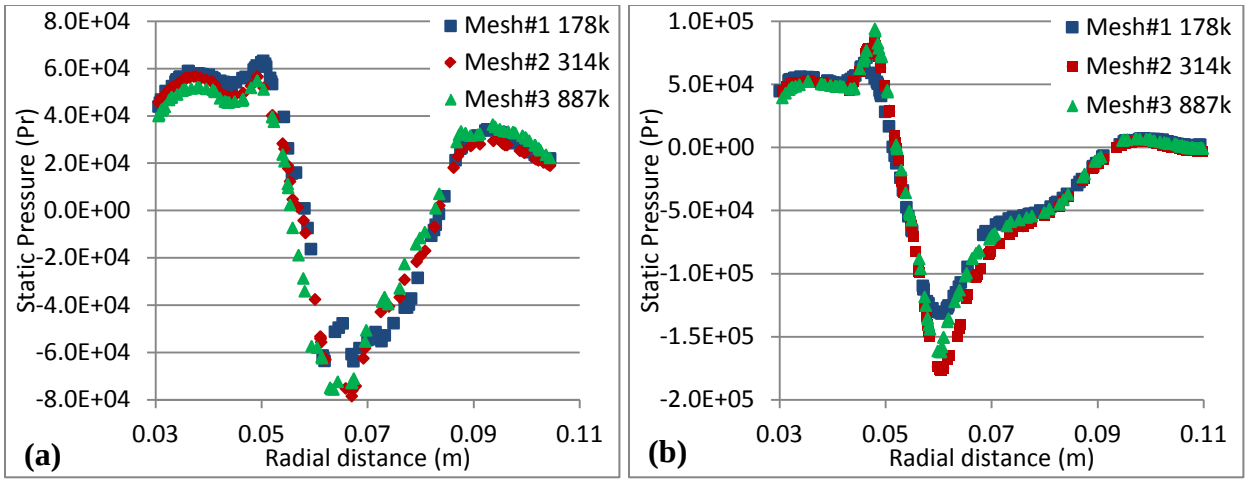

Figure 4-14. Static pressure for gird sizes (178k, 334k and 887k nodes) at the center of the flowpath#3 versus radial distance from drill bit axis - (a) Static pressure at height Ψ = 10mm; (b) Static pressure at height Ψ = 20mm.

Flow patterns remain similar for the three different mesh sizes. From Figure 4-13 and Figure 4-14, it can be observed that the results for mesh#1 (178k nodes) is differ significantly from those for the other two mesh sizes. The computational time taken for the finer mesh, 887k nodes, was three times more than the time taken for the mesh with 314k nodes. Hence, the mesh

size selection should be between 887k and 314k nodes, say mesh 650k nodes. Hence, further simulations were carried out for the mesh with 650k nodes.

The velocity distribution obtained for 650k nodes was similar to that of 887k nodes. The velocity distribution was compared between two different cross sectional depths, at Ψ = 10mm and 20mm. As shown in Figure 4-12, velocity increased at the radial distance of 60mm and decreased at 75mm (squared area in Figure 4-12) and increased along the flowpath#3 due to the jet impacts of the nozzle#4. From the velocity distribution profile in Figure 4-12, the highlighted areas are the recirculation zones, where the velocity is very low. Similarly static pressure was plotted along the radial distance for the flowpath#3 as shown in Figure 4-14(a) at 10mm clip height and Figure 4-14(b) at 20mm clip height. Pressure decreased up to the nozzle at radial distance of 65mm and increased towards the exit of the nozzle. The pressure drop was very high at the nozzle as shown in Figure 4-14. Recirculation zones and high pressure drops tend to decrease the drill bit performance. Hence, for optimization, recirculation zones and pressure differential should be reduced.

Based on the convergence summary, mesh#2 and mesh#3 shows very close results, whereas from the results of the sensitivity study, mesh#3 proves to provide better results. The computing time for mesh#3 is 3-folds higher than that of mesh#2. As the convergence of mesh#2 and mesh#3 is almost similar, optimal mesh size should be between mesh#2 and mesh#3. This serves fulfilling all the requirements of better results with feasible computing time. Hence, as conclusion, the mesh size in the range of 650k nodes to 700k nodes will be selected for further simulations.

Chapter Five: Design of Experiments and Statistical Analysis for Identification of Significant Factors

Based on the preliminary simulations described in chapter 4, the meshing process was validated using grid sensitivity analysis and it was confirmed that the CFD model can be implemented to study the flow behavior around the PDC drill bit. The next step of this research was to understand the effect of modifying the design parameters such as nozzle size, nozzle location and nozzle inclination on the bit hydraulics and hence to identify the most significant design parameters for optimization. Of the 15 design parameters taken into consideration, the five design parameters which had the highest impact on the average velocity, average vorticity and pressure drop were chosen for the optimization studies.

5.1 Identification of significant factors

There are seven nozzles in the PDC drill bit under investigation. It is known that nozzle size is an important factor that influences the pressure drop and jet impact force. Hence, nozzle size was chosen as one of the factor in the fractional factorial design of experiments. The location of the nozzle and its inclination influences the vorticity and chip carryout velocity. Therefore, the location and inclination of the seven nozzles were chosen as the other parameters. In total, 15 parameters (nozzle size, nozzle location, and nozzle inclination) were varied in the design matrix of a 2-level factorial experiment in order to identify the significant factors. The factorial levels were chosen by increasing and decreasing the actual level present in the PDC drill bit. Therefore, one level was lower than the actual level and the other was higher than the actual level. The algorithm for the fractional factorial experimental design is detailed in section 3.10.1. The 15

design parameters were embedded in the factorial design using Design Expert software. Based on a resolution-3 fractional factorial design, 16 different combinations of the design parameters varied at two levels were obtained (Table 5-1). The table shows the levels of each of the design factor for each combination. Thus, 16 different modifications to the actual PDC drill bit were obtained.

The parameters for each run were applied to develop a CAD model of the PDC drill bit and the corresponding mesh generation was carried out. CFD simulations were carried out for each run using ANSYS-FLUENT software. Based on the predicted total pressure at the outlet of the drill bit annulus, the pressure drop was calculated. The mean vorticity and mean velocity data were calculated along each of the five flow paths as shown in Figure 5-1. The cross section of each flow path (30 mm depth) was divided into three sections, 10 mm and 20 mm depth from the bottom-hole surface. Henceforth, this depth will be referred to as Ψ. The mean vorticity and mean velocity were calculated from the Ψ = 10 mm and Ψ = 20 mm depths.

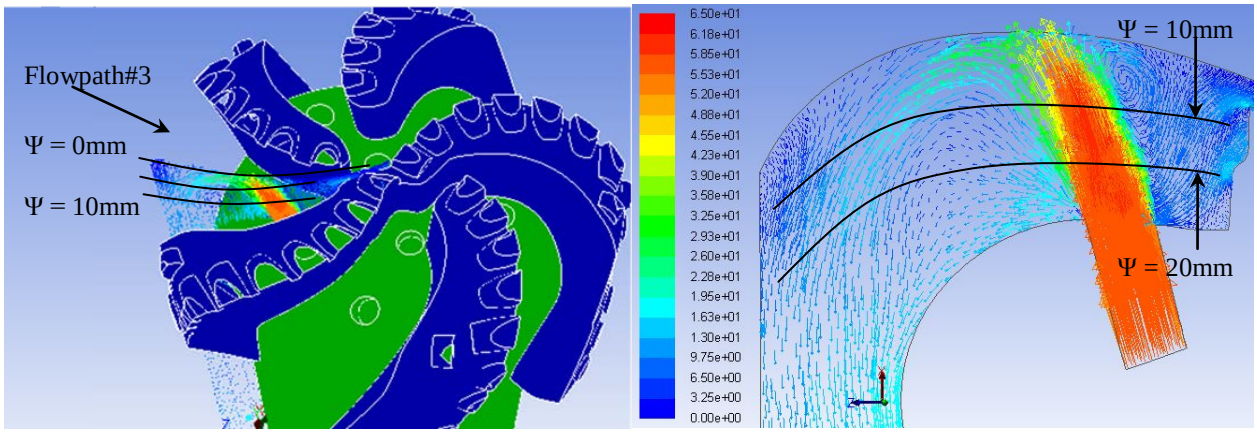

Figure 5-1. Location of cross sectional depth (Ψ) shown in flowpath#3. (a) Location of cross sectional plane at flowpath#3; (b) Clip lines for results acquisition at Ψ = 10mm & Ψ = 20mm.

Table 5-1. Fractional factorial design based 16 combinations of design parameters

Parameters	A	B	C	D	E	F	G	H	J	K	L	M	N	O	P	R1	R2	R3	R4	R5
	All Nozzle	Nozzle#1	Nozzle#1	Nozzle#2	Nozzle#2	Nozzle#3	Nozzle#3	Nozzle#4	Nozzle#4	Nozzle#5	Nozzle#5	Nozzle#6	Nozzle#6	Nozzle#7	Nozzle#7	Cross section @10mm	Cross section @20mm	Cross section @10mm	Cross section @20mm	Drill bit
Run	Size	Orbit Diameter (m)	Inclination angle (deg)	Orbit Diameter (m)	Inclination angle (deg)	Orbit Diameter (m)	Inclination angle (deg)	Orbit Diameter (m)	Inclination angle (deg)	Orbit Diameter (m)	Inclination angle (deg)	Orbit Diameter (m)	Inclination angle (deg)	Orbit Diameter (m)	Inclination angle (deg)	Velocty Magnitude (m/s)	Velocty Magnitude (m/s)	Vorticity Magnitude (1/s)	Vorticity Magnitude (1/s)	Outlet Pressure (Pa)
FR01	16	72	15	99	29	69	16	68	12	82	17	25	6	130	22	8.82	7.96	3240	1984	104557
FR02	16	72	15	159	29	49	10	128	18	82	17	45	6	70	16	7.55	6.69	2706	1703	121275
FR03	10	132	15	99	29	69	10	128	12	82	23	45	0	70	22	9.99	11.03	3789	3066	238370
FR04	10	132	21	159	23	49	10	128	12	82	17	25	6	130	22	11.72	10.74	5509	3300	163916
FR05	10	72	21	159	29	69	10	68	18	142	17	25	0	70	22	13.68	11.18	6340	3429	165483
FR06	16	72	21	99	23	69	10	128	18	82	23	25	0	130	16	9.17	7.86	3996	1859	138581
FR07	16	132	21	99	29	49	10	68	12	142	23	25	6	70	16	7.73	7.7	2937	1982	56989
FR08	10	72	15	99	23	49	10	68	18	142	23	45	6	130	22	11.02	9.37	3904	3009	117963
FR09	16	72	21	159	23	49	16	68	12	82	23	45	0	70	22	8.1	7.42	3010	1894	97420
FR10	16	132	15	159	23	69	10	68	12	142	17	45	0	130	16	6.46	6.25	2543	1635	83361
FR11	10	72	21	99	29	49	16	128	12	142	17	45	0	130	16	11.18	10.66	3932	3182	165395
FR12	10	72	15	159	23	69	16	128	12	142	23	25	6	70	16	11.88	11.19	4679	3262	162437
FR13	16	132	21	159	29	69	16	128	18	142	23	45	6	130	22	5.6	5.69	1817	1453	113543
FR14	10	132	21	99	23	69	16	68	18	82	17	45	6	70	16	10.33	10.68	4233	3210	237490
FR15	10	132	15	159	29	49	16	68	18	82	23	25	0	130	16	13.47	11.32	6337	3424	117956
FR16	16	132	15	99	23	49	16	128	18	142	17	25	0	70	22	8.34	7.83	3457	1940	104274

The responses (pressure drop, mean velocity and mean vorticity) were used as input to the statistical software for analysis of the factorial design of experiments (Table 5-1). The first part of the analysis is the suitable selection of the significant effects from the half-normal probability plot and the pareto chart (Mead, 1990). The half-normal plot is used to assess the sensitivity of the outcomes to the geometric parameters. This approach is used to determine the most significant parameters (i.e. those to be included in the model). Large effects appear in the upper-right section of the plot. The lower-left portion of the plot contains effects which are smaller, i.e. insignificant in a statistical sense. Design-Expert also performs a Shapiro-Wilk hypothesis test on the normality of the unselected parameters on the Effects plot to make sure that those parameters are insignificant. It is based on the null hypothesis that the unselected parameters come from a normal distribution. After the selection of statistically significant terms, p-value>0.10 from the Shapiro-Wilk test indicates that the unselected parameters are indeed insignificant. The Pareto chart is a graphical representation used to display the t-values of the effects. Large t-values indicate that the parameter is more significant.

5.1.1 Effect of design parameters on average velocity:

The effects of significant parameters on the velocity magnitude (Ψ = 10 mm) were observed from half-normal plot and pareto chart. All the parameters that were present at the right portion of the half-normal plot (Figure 5-2 (a)) were chosen and the pareto chart (Figure 5-3 (a)) shows the ranking of the parameters according to their significance. The highly significant parameter ranks first followed by the less significant parameters. After choosing the significant parameters, analysis of variance (ANOVA) of the factorial model with mean velocity (Ψ = 10 mm) as the response was performed. ANOVA results are shown in Table 5-2. The coefficient of

determination (R^2), 0.9957 indicates that 99.57% of total variation in data is explained by the factorial model. The p-value should be less than 0.05 for a parameter to be significant. From the ANOVA results, it can be seen that the chosen parameters are significant at 95% confidence. The signal to noise ratio is given by the adequate precision, which should be greater than 4 for adequate signal. In this case, the ratio is 45.50 which indicates that there is sufficient signal and hence the model can be used to navigate the design space. The p-value from the Shapiro-Wilk test is 0.946, which indicates that the unselected parameters are less significant.

For the case of average velocity (Ψ = 20 mm), the half-normal plot and pareto chart shown in Figure 5-2 (b) and Figure 5-3 (b) were used to choose the significant parameters. The results of ANOVA of the factorial model are shown in Table 5-2. The coefficient of determination (R^2), 0.9354 indicates that 93.54% of total variation in data is explained by the factorial model. The adequate precision 19.52 indicates that the noise in the model is very minimal. From the p-value (0.509) of the Shapiro-Wilk test, it can be observed that the unselected parameters are less significant.

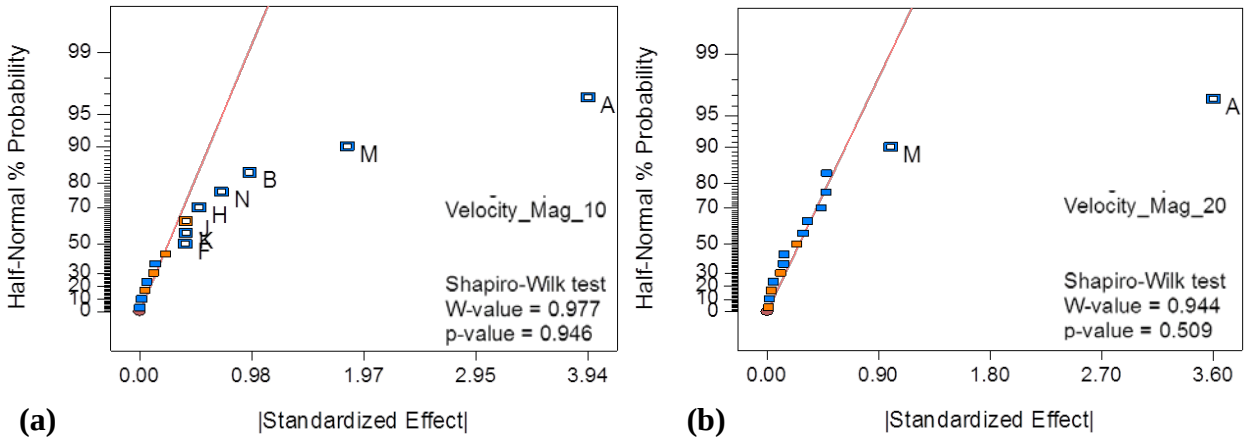

Figure 5-2. Half-normal plot for velocity magnitude residuals (a) Ψ = 10 mm, (b) Ψ = 20 mm

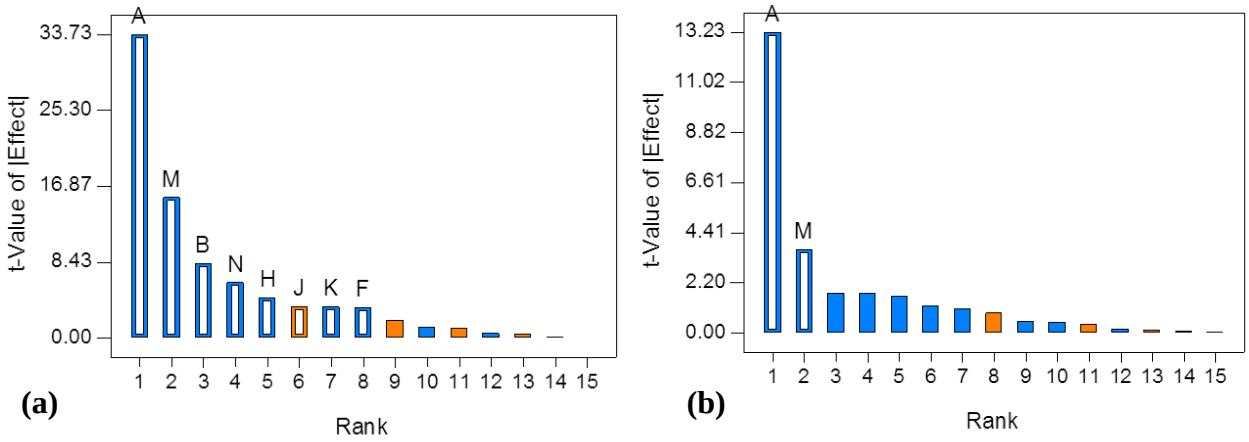

Figure 5-3. Pareto chart for velocity magnitude residuals (a) Ψ = 10 mm, (b) Ψ = 20mm

Table 5-2. Analysis of Variance for Factorial Model of Average Velocity (ANOVA)

Velocity (Ψ = 10 mm)			Velocity (Ψ = 20 mm)		
	F	p-value		F	p-value
Source	Value	Prob > F	Source	Value	Prob > F
Model	193.02	< 0.0001	Model	94.23	< 0.0001
A- Size	1137.85	< 0.0001	A-Size	174.94	< 0.0001
B-N1-Location	68.64	< 0.0001	M-N6-Location	13.51	0.0028
F-N3-Location	11.70	0.0111			
H-N4-Location	19.95	0.0029			
J-N4-Angle	12.18	0.0101			
K-N5-Location	12.17	0.0102			
M-N6-Location	243.75	< 0.0001			
N-N6-Angle	37.94	0.0005			
Std. Dev.	0.23		Std. Dev.	0.54	
Mean	9.69		Mean	8.97	
C.V. %	2.41		C.V. %	6.06	
R^2	0.9954		R^2	0.9355	
Adj R^2	0.9903		Adj R^2	0.9255	
Pred R^2	0.9764		Pred R^2	0.9022	
Adeq Precision	45.504		Adeq Precision	19.516	

Nozzle size, location of nozzles#1, #3, #4, #5, #6, inclination of nozzles#4 and #6 were the parameters that significantly influence the mean velocity (Ψ = 10 mm). As the nozzle#1 is

the major nozzle in the flowpath#1, modifying the location of nozzle#1 has significant influence on the mean velocity (Ψ = 10 mm) in the flowpath#1. Similar effect was observed in the flowpath#3 due to the change in the location and inclination of nozzle#4. The location and inclination of nozzle#6 is important because it affects the two flow paths, #4 and #5. The statistical analysis shows that the location of nozzle#5 is significant. However, the location of nozzle#6 is highly significant as it influences the flow fields of nozzle#5 and nozzle#7. The location of nozzle#3 highly influences the flow field of nozzle#2 and partially influences the flow field of nozzle#1 and therefore, it has significant effect on the mean velocity (Ψ = 10 mm).

Nozzle size and location of nozzle#6 were the only parameters that had significant impact on the mean velocity (Ψ = 20 mm). Smaller nozzle size resulted in higher velocity which would in turn improve hole-cleaning. The location of nozzle#6 is very important because its location determines the flow fields in flow paths #3, #4 and #5.

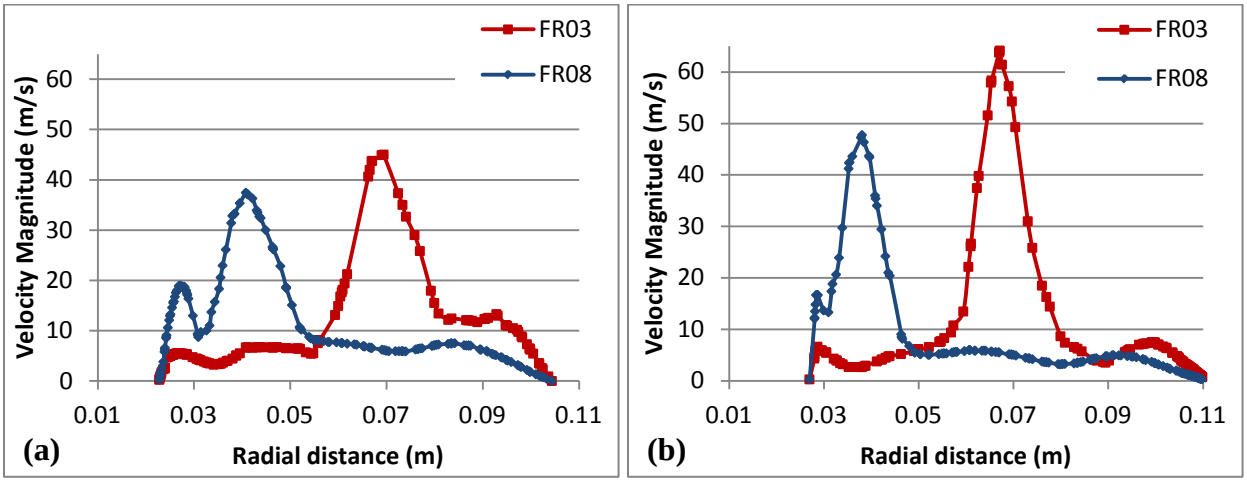

Figure 5-4. Comparison of velocity magnitude for factorial runs 3 and 8 at (a) Ψ = 10 mm, (b) Ψ = 20 mm

The flowpath#3 is used as an example to illustrate the effect of modifying the design parameters on the velocity (Ψ = 10 mm and Ψ = 20 mm). Flowpath#3 is highly influenced by nozzle#4 and partially influenced by nozzle#6. Figure 5-4 shows the comparison of mean velocity in the flowpath#3 for the factorial runs 3 and 8, in order to demonstrate its influence due to change in location of nozzle#4, from 69mm to 49mm. As shown in Figure 5-4 (a) and (b), the change in nozzle location towards drill bit axis reduces the jet velocity at both Ψ = 10 mm and Ψ = 20 mm. The limited availability of space near the drill bit axis may be the reason for the drop in the jet velocity near the nozzle. At the same time, the average velocity across the flow path is increased by 21% at Ψ = 10 mm and decreased by 18% at Ψ = 20 mm. At Ψ = 20 mm, the influence of nozzle free jet velocity is highly pronounced because the surface is near the drill bit inner wall. Ψ = 10 mm is the surface closer to the downhole surface where the nozzle jet impingement results in sudden drop in the velocity for run 8. But for the case of run 3, the jet velocity is low and hence the velocity drop is comparatively low. The increase in the average velocity shows the significance of the location of nozzle#4. Nozzle location near the axis resulted in jet impingement closer to the axis which in turn helps in chip removal. On the other hand, nozzle location closer to the annulus causes low velocity near the axis and hence results in bit balling.

On comparing the simulation results of other runs, it is observed that the mean velocity across the flow path being highly influenced by the nozzle location and size. For the case of flowpath#1, at Ψ = 10 mm the average velocity across the flow path is increased when the nozzle location closer to the drill bit axis. This is due to the limited free jet area which causes a drop in the jet velocity and increase in the average velocity towards the annulus, as discussed for the

location of nozzle#4. In the flowpath#2, the location of nozzle#2 is not significant due to the location of nozzle#3 that drives the flow path. At Ψ = 10 mm, nozzle#3 placed towards the axis of drill bit shows higher mean velocity due to the sharing of the velocity jet with the flow paths #1 and #2, through a small channel located between these two flow paths. The location and inclination of nozzle#4 play a major role on the flow distribution in the flowpath#3. Nozzle#4 placed near the drill bit axis and inclined towards the annulus shows high mean velocity because the direction of the jet is pointed towards the flow path under this condition.

In the flowpath#4, the location of nozzle#5 and nozzle#6 placed near the drill bit axis shows high mean velocity, where as the location of nozzle#7 appears to have insignificant influence on the mean velocity. This is due to the structure of the flowpath#4 and flowpath#5 where the nozzle#6 shares jet with both these flow paths and each has its own nozzle#5 and nozzle#7 respectively. The placement and inclination of the nozzle#6 drives the mean velocity characteristics in these flow paths (#4 and #5) at Ψ = 10 mm and Ψ = 20 mm. At Ψ = 20 mm, the effect of other design parameters are insignificant on velocity due to the influence of various other factors such as wall jet, and cross flow between flow paths. Change in the nozzle size exhibited high impingement velocity near the axis of the drill bit and hence resulted in increasing the velocity across the flow path. These characteristics of the drill bit design parameters proves its significance on mean velocity which in turns relates to the chip carryout velocity for an effective down-hole cleaning.

5.1.2 Effect of design parameters on average vorticity:

The half-normal plot and pareto chart shown in Figure 5-5 (a) and Figure 5-6 (a) were used to chose the parameters that had significant impact on average vorticity (Ψ = 10 mm). The results from ANOVA are shown in Table 5-3. The coefficient of determination (R^2), 0.9816 indicates that 98.16% of total variation in data is explained by the factorial model. The adequate precision 26.29 indicates that the noise accounted for in the model is very minimal.

The significant parameters were chosen from the half-normal plot and pareto chart as shown in Figure 5-5 (b) and Figure 5-6 (b). ANOVA of the factorial model was carried out with mean vorticity (Ψ = 20 mm) as the response and the results are given in Table 5-3. R^2 was determined to be 0.9813, which indicates that 98.13% of total variation in data is explained by the factorial model. The adequate precision 35.02 indicates minimal noise in the model and hence the model can be used for prediction.

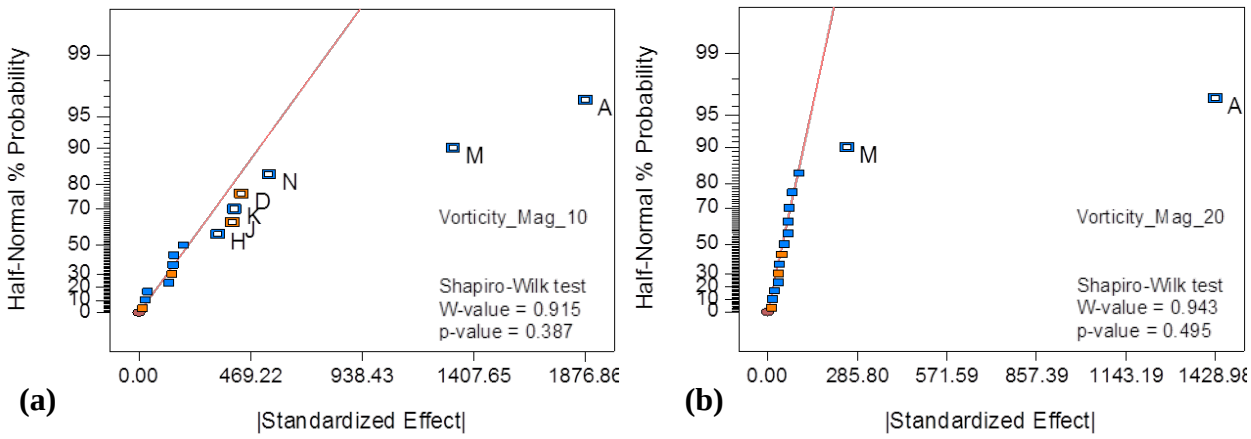

Figure 5-5. Half-normal plot for vorticity magnitude residuals (a) Ψ = 10 mm, (b) Ψ = 20 mm

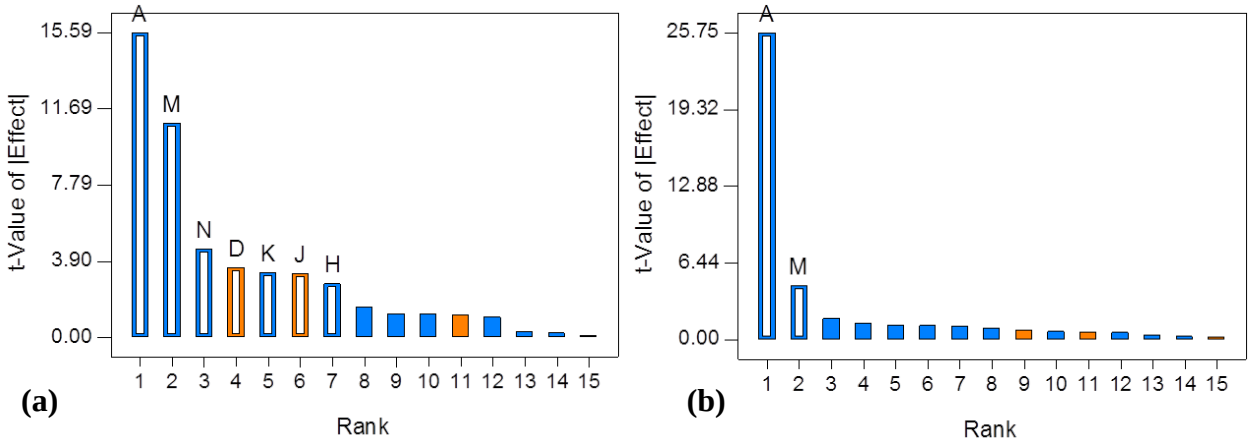

Figure 5-6. Pareto chart for vorticity magnitude residuals (a) Ψ = 10 mm, (b) Ψ = 20 mm

Table 5-3. Analysis of Variance for Factorial Model of Average Vorticity (ANOVA)

Velocity (Ψ = 10 mm)			Velocity (Ψ = 20 mm)		
	F	p-value		F	p-value
Source	Value	Prob > F	Source	Value	Prob > F
Model	60.88	< 0.0001	Model	342.07	< 0.0001
A-Size	242.99	< 0.0001	A-Size	663.24	< 0.0001
D-N2-Location	12.84	0.0071	M-N6-Location	20.90	0.0005
H-N4-Location	7.62	0.0246			
J-N4-Angle	10.69	0.0114			
K-N5-Location	11.12	0.0103			
M-N6-Location	120.23	< 0.0001			
N-N6-Angle	20.66	0.0019			
Std. Dev.	240.81		Std. Dev.	110.97	
Mean	3901.77		Mean	2520.8	
C.V. %	6.17		C.V. %	4.4	
R^2	0.9816		R^2	0.9814	
Adj R^2	0.9655		Adj R^2	0.9785	
Pred R^2	0.9263		Pred R^2	0.9718	
Adeq Precision	26.300		Adeq Precision	35.016	

The parameters that were found to have significant impact on the vorticity (Ψ = 10 mm) are nozzle size, location of nozzles #2 and #5, location and inclination of nozzles #4 and #6. Though the objective is to minimize the recirculation of fluid at the measured location, decreasing the nozzle size resulted in increasing the vorticity, which has a negative impact on the bit hydraulics. The parameters that had significant influence on the vorticity (Ψ = 20 mm) were nozzle size and location of nozzle#6. Vorticity at Ψ = 20 mm from the bottomhole surface is mainly due to the nozzle free jet zone.

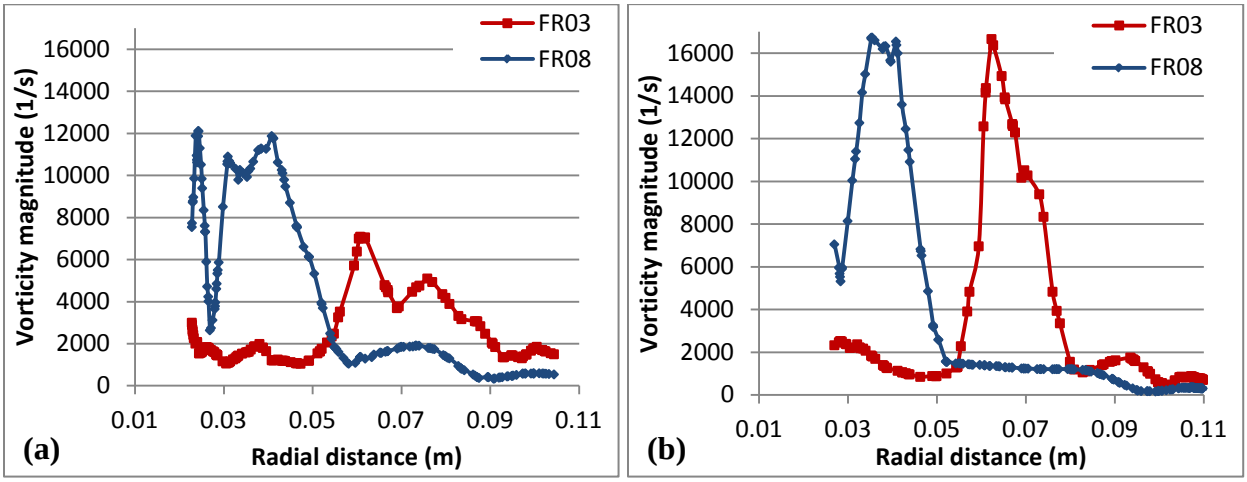

Figure 5-7. Comparison of vorticity magnitude for factorial runs 3 and 8 at (a) Ψ = 10 mm, (b) Ψ = 20 mm.

The flowpath#3 is illustrated to discuss the effect of design parameters on vorticity magnitude at different depth levels (Ψ = 10 mm and Ψ = 20 mm). Flowpath#3 is highly influenced by nozzle#4 and partially influenced by nozzle#6. Figure 5-7 shows the comparison of mean vorticity magnitude in the flowpath#3 for the factorial runs 3 and 8, where the nozzle#4 location is 69mm and 49mm respectively. Positioning the nozzle#4 away from the axis (run 3) in the flowpath#3 resulted in 51% lower average vorticity (Ψ = 10 mm) compared to run 8, which

is mainly due to the high impact force of the nozzle jet (Figure 5-7 (a)). Vorticity in this location is also influenced by the wall jet. At Ψ = 20 mm, the high vorticity zones are at the nozzle free jet zone because, the surface is closer to the nozzle. At Ψ = 20 mm (Figure 5-7 (b)), the change in the nozzle location closer to the annulus results in decreasing the mean vorticity by 10%. This is due to the high vortex zone created in the flow path near the center of the drill bit for the case of run 8 due to limited space for the flow development. But for the case of run 3, where the nozzle is away from the centre of drill bit, there is enough free space for the flow development that generates low vorticity. By comparing the overall mean vorticity in this flow path, vorticity is decreased by 30% for the nozzle placed closer to the annulus of the drill bit compared to that of nozzle placed near the drill bit axis. High shear prevailing near the wall surface causes the vorticity, which in turn affects the flow pattern across the bit surface.

In general, vorticity in the other flow paths are reduced for the bigger nozzle size. This is due to the low jet velocity generated by the bigger nozzle. Thus, the size of the nozzle is a very critical factor that influences the formation and intensity of the recirculation zone and hence bit balling. In the flowpath#1, the nozzle#1 location and inclination appears to be less significant on the mean vorticity. In the flowpath#2, nozzle#2 location placed closer to the drill bit axis results in decreasing the vorticity due to the structure of the nozzle arrangement in this flow path, where the two nozzles, nozzle#2 and nozzle#3 influence the flow development. Modifying the location or inclination of nozzle#3 does not show any significance on the vorticity. In flowpath#3, placing the nozzle#4 location away from the drill bit axis and inclining it towards the drill bit axis resulted in low mean vorticity. This is because of the widening of flowpath#3 when the nozzle is shifted away from drill bit axis. When the nozzle#4 is inclined towards the drill bit axis, there is

a drop in the jet velocity due to the channel that is located between the flowpath#3 and #5, and hence, results in reducing the vorticity. The flowpath#4 and #5 are connected, with the nozzle#6 placed at the center of the flow paths, and nozzle#5 placed in the flowpath#4 and nozzle#7 in the flowpath#5. Hence the vorticity field developed in these flow paths are mainly related to the characteristics of the nozzle#6. The results of the factorial runs show the significance of nozzle#6 which results in low vorticity when placed away from drill bit axis and inclined away from drill bit axis. This condition is when the nozzle jet is directly pointed at the centre of both the flow path, where the flow is divided equally and therefore yields low mean vorticity. Based on the above inferences, the low vorticity level is preferred which is an indication of low recirculation velocity is desirable for improved bit hydraulics.

5.1.3 Effect of design parameters on the pressure drop across the drill bit:

The parameters that had significant impact on the pressure drop were chosen from the half-normal plot and pareto chart as shown in Figure 5-8. Based on the ANOVA of the factorial model with pressure drop as the response, the R^2 was 0.8329, which means that 83.29% of total variation in data is explained by the factorial model (Table 5-4). The adequate precision 12.35 is sufficiently high for the model to be used for navigating the design space with less noise.

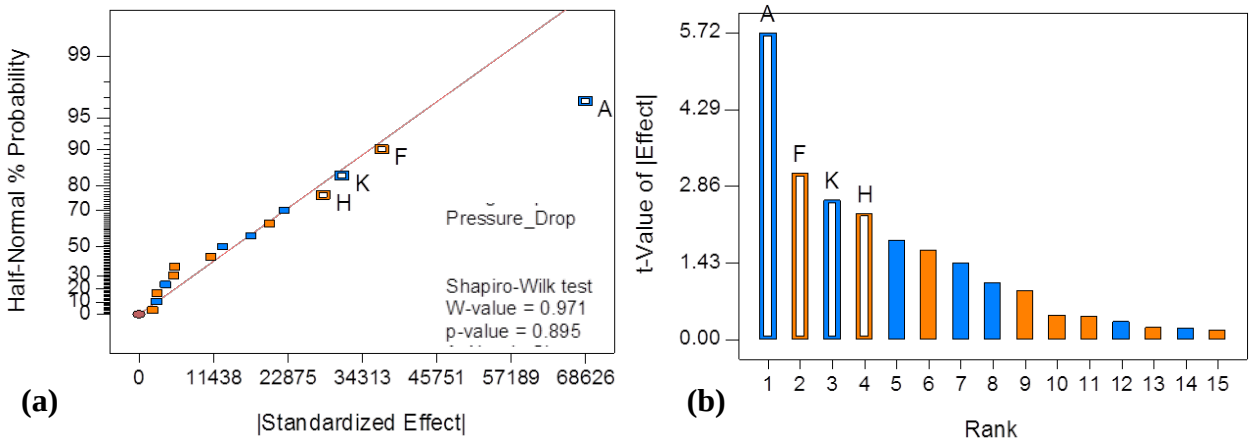

Figure 5-8. Effects plot for pressure drop a) Half-normal plot, (b) Pareto chart

Table 5-4. Analysis of Variance for Factorial Model of Pressure drop (ANOVA)

Source	F Value	p-value Prob > F
Model	13.71	0.0003
A-Size	32.76	0.0001
F-N3-Location	9.69	0.0099
H-N4-Location	5.58	0.0377
K-N5-Location	6.80	0.0244
Std. Dev.	23981.36	
Mean	136813.13	
C.V. %	17.53	
R^2	0.8329	
Adj R^2	0.7721	
Pred R^2	0.6464	
Adeq Precision	12.348	

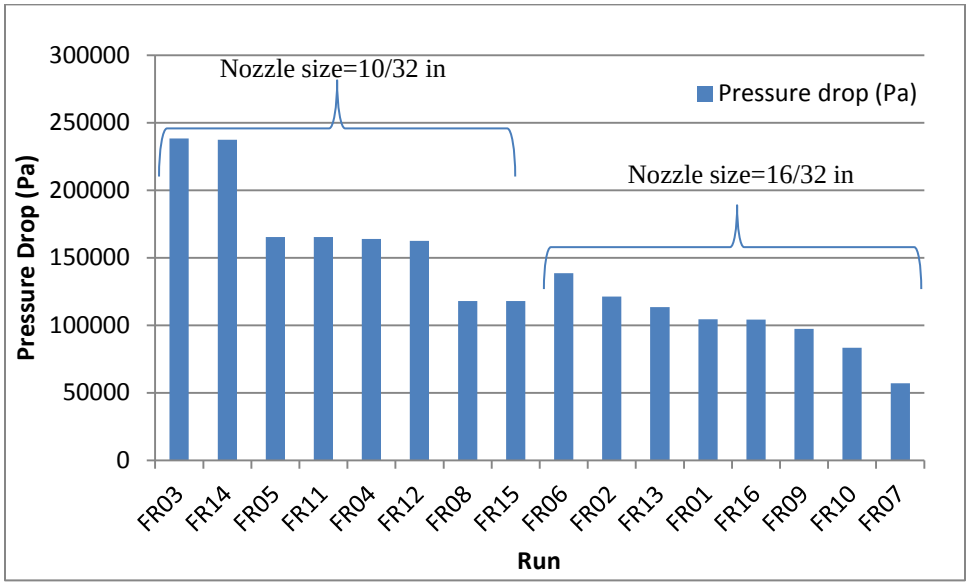

Figure 5-9. Comparison of outlet pressure for all factorial runs.

From the Figure 5-9, the change in nozzle size shows the highest impact on the pressure drop. Smaller nozzle size shows high pressure drop across the drill bit for factorial runs 3, 4, 5, 11, 12 and 14, whereas low pressure drop was observed for larger nozzle size in the factorial runs 1, 7, 9, 10, 13 and 16. The nozzle location for nozzles #3, #4 and #5 which was positioned closer to the annulus of the drill bit led to low pressure drop across the flow path. In order to decrease the pressure drop in the drill bit, the nozzle placements need to be placed near the annulus of the drill bit.

Based on the statistical analyses of the factorial models, it can be concluded that a high average velocity could be achieved by placing a smaller sized nozzle near the axis of the drill bit. However, the above arrangement also considerably increases the average vorticity in the respective flow path. Nozzle placement should be carefully selected in order to achieve high velocity that helps to increase chip carry velocity without generating any recirculation zone by

changing the nozzle inclination. Low pressure drop is obtained by small nozzle size. Nozzle placement near the annulus generates less pressure drop than when placed closer to the axis. But, a low pressure drop could be achieved only at the expense of low average velocity which would in turn lower the chip carryout velocity and hence cause bit balling.

5.1.4 Ranking and selection of top five significant design parameters

The influence of various design parameters on the responses were investigated by the effects plot and the pareto chart. For each response, the level of significant contribution of the design parameters was obtained from the pareto chart.

Table 5-5. Ranking of design parameters based on their level of significance on the responses

	Nozzle#	**Design Factor**	10mm		20mm		**Total Pressure drop**	**Overall Significant Parameter**
			Vorticity Magnitude	**Velocity Magnitude**	**Vorticity Magnitude**	**Velocity Magnitude**		
A	ALL	Nozzle Size #	1	1	1	1	1	✓
B	N1	Orbit diameter	9	3	10	10	11	
C	N1	Inclination angle	11	15	11	13	9	
D	N2	Orbit diameter	4	9	14	6	7	
E	N2	Inclination angle	14	11	15	11	14	
F	N3	Orbit diameter	10	8	6	15	2	
G	N3	Inclination angle	12	13	9	8	15	
H	N4	Orbit diameter	7	5	3	14	4	✓
J	N4	Inclination angle	6	6	12	7	10	✓
K	N5	Orbit diameter	5	7	5	4	3	
L	N5	Inclination angle	8	10	8	12	8	
M	N6	Orbit diameter	2	2	2	2	6	✓
N	N6	Inclination angle	3	4	7	5	12	✓
O	N7	Orbit diameter	15	14	4	3	5	
P	N7	Inclination angle	13	12	13	9	13	

Table 5-5 shows the responses and design parameters with their ranking. Ranking was done in ascending order starting from design parameters with high to low significance. The highlighted cells indicate the design parameters which were found to be significant using the factorial model analysis. Comparing the ranks, the most significant five design parameters were chosen and it is shown in the last column of Table 5-5. The chosen five parameters will be used in the next step of this research for the determination of the optimum design limits for each of the chosen design parameters by the application of response surface methodology.

5.2 Response Surface Methodology for optimization of design parameters of the PDC drill bit

The identification of the most influential parameters on the flow domain of the PDC drill bit is followed by determination of the optimum parameters in terms of bit hydraulics. Optimum performance is characterized by low pressure drop, minimum recirculation velocity, and enhanced mean velocity across the flow path. The identified significant factors were varied at three levels, using a central composite design. The runs generated from the central composite design were simulated and the results were used to identify the optimum levels for the significant factors. The optimized design results were compared with that of original design for maximum velocity, minimum pressure drop and small recirculation zones.

5.2.1 Central Composite Design (CCD) and CFD simulation

As stated in the methodology chapter (section 3.10.2), the five most significant design parameters (nozzle size, location and inclination of nozzle#4, location and inclination of nozzle#6) were varied at three levels (Table 3-9). The corresponding coded values for each of the

design factors are shown in Table 5-6. The face-centered CCD consisted of 32 test runs comprised of 10 axial points, 16 factorial points and one center point that was replicated 6 times. Table 5-7 shows the various combinations of the significant design parameters. Each test run is a variation in the design of the PDC drill bit. Therefore, for each run, a CAD model was developed using Solidworks, imported to ICEM CFD for meshing and then followed by CFD simulation in FLUENT. The pressure drop was calculated as the difference between the total pressure at the inlet and at the outlet of the drill bit annulus. The mean vorticity and mean velocity data were calculated from each of the five flow paths as shown in Figure 5-1.

The average velocity, average vorticity, and pressure drop for each simulation were input to the Design Expert software as the responses. ANOVA was applied to determine the significance of the model. The relationship between the responses and the design factors was modeled by a second order quadratic equation given in eqn 3-27. The values of the corresponding regression coefficients were calculated and the equations were fitted for predicting the responses.

The ANOVA results, residual analysis, and the developed statistical models are discussed separately for each response in the subsequent sections.

Table 5-6. Central composite design – Actual and coded values of design parameters

Factor	Design Factor	Actual Values			Coded Values		
		Low	Median	High	Low	Median	High
A	Nozzle Size # (1/32 inch)	10	13	16	-1	0	1
B	Nozzle#4-Orbit diameter (mm)	68	98	128	-1	0	1
C	Nozzle#4-Inclination angle (deg)	12	15	18	-1	0	1
D	Nozzle#6-Orbit diameter (mm)	25	35	45	-1	0	1
E	Nozzle#6-Inclination angle (deg)	0	3	6	-1	0	1

Table 5-7. Central composite design based 32 combinations of design parameters

Parameter	A	B	C	D	E	R1	R2	R3	R4	R5
	Nozzle Size (Nos)	Nozzle#4 Orbit Diameter (mm)	Nozzle#4 Inclination angle (deg)	Nozzle#6 Orbit Diameter (mm)	Nozzle#6 Inclination angle (deg)	Velocty Magnitude @ Ψ = 10mm (m/s)	Velocty Magnitude @ Ψ = 20mm (m/s)	Vorticity Magnitude @ Ψ = 10mm (1/s)	Vorticity Magnitude @ Ψ = 20mm (1/s)	Pressure Drop (MPa)
CCD01	13	49	15	18	3	9.29	7.49	2891	2055	1.87
CCD02	10	64	12	23	6	10.96	10.73	3579	3079	5.59
CCD03	13	49	15	18	3	9.29	7.49	2891	2055	1.87
CCD04	16	34	12	13	0	8.99	7.79	3433	1942	0.72
CCD05	16	64	18	23	6	6.8	6.82	1969	1587	0.76
CCD06	13	34	15	18	3	10.17	9.4	3394	2688	1.84
CCD07	10	34	18	13	0	15.5	13.45	6429	4044	5.41
CCD08	16	34	18	23	0	8.04	7.9	2314	1891	0.75
CCD09	13	49	15	18	3	9.29	7.49	2891	2055	1.87
CCD10	13	49	12	18	3	9.23	8.6	2856	2154	1.83
CCD11	13	49	15	23	3	8.79	9.02	2744	2186	1.84
CCD12	10	64	18	13	6	13.42	12.15	5393	3537	5.44
CCD13	13	49	15	18	3	9.29	7.49	2891	2055	1.87
CCD14	13	49	15	13	3	10.79	9.47	3944	2428	1.82
CCD15	16	64	12	23	0	7.41	7.07	2119	1685	0.77
CCD16	10	34	18	23	6	11.7	10.23	4071	3048	5.47
CCD17	13	49	15	18	6	9.32	9.39	3079	2346	1.84
CCD18	13	49	15	18	0	10.2	9.5	3753	2403	1.84
CCD19	16	34	18	13	6	8.84	8.07	3031	2081	0.74
CCD20	10	64	18	23	0	11.13	11.44	3425	3101	5.45
CCD21	16	49	15	18	3	7.95	7.3	2736	1759	0.77
CCD22	10	34	12	23	0	12.09	10.41	4465	3210	5.47
CCD23	10	34	12	13	6	13.6	12.62	5409	3951	5.44
CCD24	13	64	15	18	3	9.5	9.43	3374	2376	1.86
CCD25	10	64	12	13	0	14.9	12.98	5913	3816	5.51
CCD26	16	64	18	13	0	9.68	8.31	3305	1989	0.76
CCD27	16	64	12	13	6	8.72	7.83	3191	1828	0.77
CCD28	16	34	12	23	6	7.73	7.16	2554	1736	0.72
CCD29	13	49	15	18	3	9.29	7.49	2891	2055	1.87
CCD30	13	49	15	18	3	9.29	7.49	2891	2055	1.87
CCD31	13	49	18	18	3	9.75	9.39	3332	2379	1.84
CCD32	10	49	15	18	3	12.95	11.8	4703	3434	5.50

5.2.2 Relationship between average velocity and significant design parameters and their interactions

Table 5-8 shows the ANOVA results for average velocity measured at 10 mm and 20 mm depths. The second order polynomial equation developed for the velocity (Ψ = 10 mm) and velocity (Ψ = 20 mm) are provided in eqn (5-1) and (5-2) respectively.

$$\text{Velocity } (\Psi = 10 \text{ mm}) = 9.50 - 2.34\,A - 0.23\,B + 0.066\,C - 1.10\,D - 0.38\,E + 0.33\,AD + 0.12\,AE - 0.16\,BC - 0.19\,BD - 0.11\,CD + 0.19\,DE + 0.86\,A^2 + 0.25\,B^2 \quad \ldots(5\text{-}1)$$

$$\text{Velocity } (\Psi = 20 \text{ mm}) = 8.51 - 2.09\,A - 0.015\,B + 0.14\,C - 0.66\,D - 0.21\,E + 0.33\,AD + 1.16\,A^2 \quad \ldots(5\text{-}2)$$

where A is the nozzle size, B is the location of nozzle#4, C is the inclination of nozzle#4, D is the location of nozzle#6 , and E is the inclination of nozzle#6.

ANOVA explains whether the model adequately fits the variations in the response with respect to the factor levels. If the F-test for the model is significant at the 5% level ($p<0.05$), then the model is good and can adequately explain the variation observed. The model F-value for both velocities were high and the p-value was <0.0001, indicating that both the models are highly significant and that there is only 0.01% probability that F-value this large could occur due to noise. The R^2 value for the velocity (Ψ = 10 mm) was 0.9924 which implies that 99.24% of the variability in the data could be explained by the model. Similarly, for the velocity (Ψ = 20 mm), 88.15% of the variability in the data is explained by the corresponding model. For both responses, the predicted R^2 was close to the adjusted R^2, indicating that the models can be used

for navigating the design space. The variability in the data measured by the coefficient of variation (C.V.%) was less than 10%. The signal to noise ratio given by the adequate precision indicates that there was adequate signal, so that the models can be used to predict the design space.

Table 5-8. Analysis of Variance for Response Surface Reduced Quadratic Model for Velocity (ANOVA)

Velocity (Ψ = 10 mm)			Velocity (Ψ = 20 mm)		
Source	F Value	p-value Prob > F	Source	F Value	p-value Prob > F
Model	180.32	< 0.0001	Model	25.52	< 0.0001
A-Size	1692.05	< 0.0001	A-Size	140.31	< 0.0001
B-N4- Location	16.34	0.0008	B-N4- Location	7.11E-03	0.9335
C-N4-Angle	1.36	0.2586	C-N4-Angle	0.65	0.4297
D-N6- Location	374.03	< 0.0001	D-N6- Location	14.04	0.001
E-N6-Angle	44.9	< 0.0001	E-N6-Angle	1.48	0.2353
AD	30.21	< 0.0001	AD	3.19	0.0869
AE	3.94	0.0625	A^2	18.95	0.0002
BC	7.37	0.0142			
BD	9.98	0.0054			
CD	3.28	0.0867			
DE	9.64	0.0061			
A^2	44.26	< 0.0001			
Std. Dev.	0.24		Std. Dev.	0.75	
Mean	10.12		Mean	9.16	
C.V. %	2.38		C.V. %	8.16	
R^2	0.9924		R^2	0.8815	
Adj R^2	0.9869		Adj R^2	0.8470	
Pred R^2	0.9682		Pred R^2	0.833	
Adeq Precision	54.178		Adeq Precision	16.605	

The model adequacy was validated by residual analysis. From the normal probability plot shown in Figure 5-10, it can be seen that the residuals follow the straight line and hence are

normally distributed. Therefore, the models for velocity are adequate for predicting the responses within the design space. The equation is provided in terms of coded factors and can be used to make predictions about the response for given levels of each factor. By default, the high levels of the factors are coded as +1 and the low levels of the factors are coded as -1. The coded equation is generally used to identify the relative impact of the factors by comparing the factor coefficients. The magnitude of the coefficient for each independent factor gives the magnitude of the effect that variable has on the response. The sign of the coefficient (positive or negative) gives the direction of the effect on the response. When the independent factor increases by one, the response increases by the magnitude of the corresponding positive coefficient and vice versa. The correlation between the actual simulated response and the response predicted by the developed statistical models is very high (Figure 5-11). The models predict the velocity responses very close to that of actual values.

From the perturbation plot shown in Figure 5-12(a) and (b), the individual effect of each of the design factor on the velocity at Ψ = 10 mm and Ψ = 20 mm can be observed. Small nozzle size, location of nozzles#4 and #6 closer to the drill bit axis, and inclination of nozzle#6 towards the drill bit axis favor higher velocity (Ψ = 10 mm). But, the inclination of nozzle#4 closer to the drill bit axis lowered the velocity. For the case of velocity (Ψ = 20 mm), the factors that had significant impact are nozzle size and location of nozzle#6. Small nozzle size and location of nozzle#6 closer to the drill bit axis resulted in high velocity. Other design parameters had less influence on this velocity.

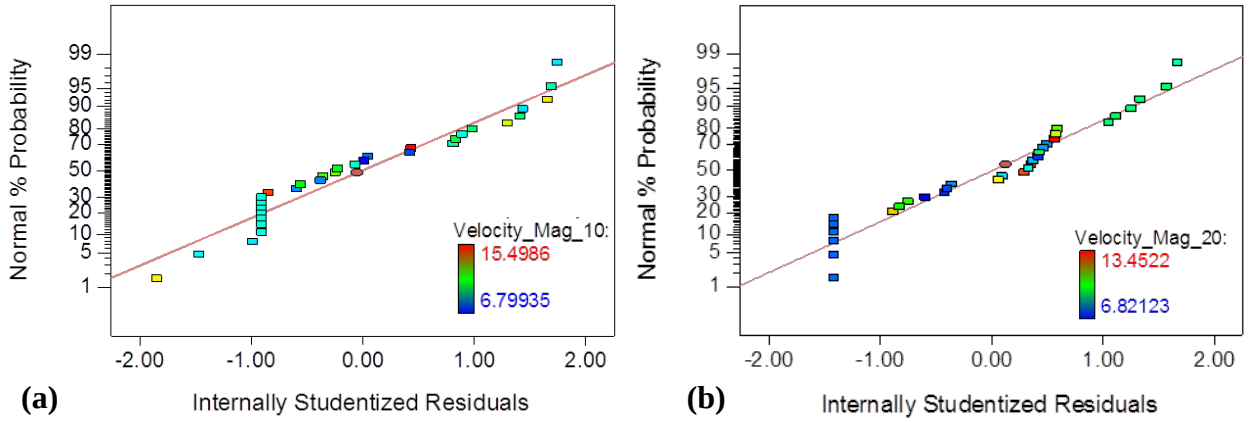

Figure 5-10. Normal probability plot for velocity magnitude residuals (a) Ψ = 10 mm, (b) Ψ = 20 mm

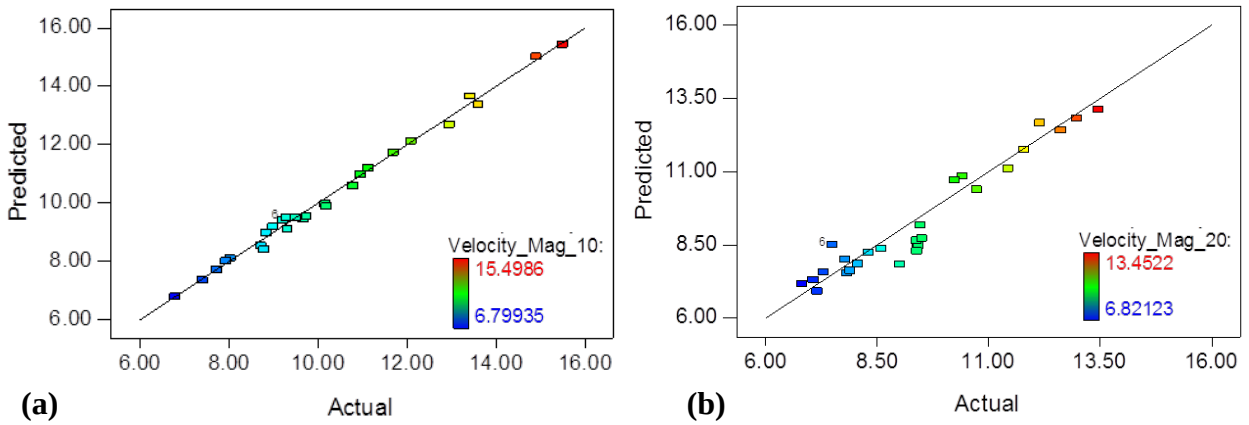

Figure 5-11. Predicted versus actual velocity magnitude (a) Ψ = 10 mm, (b) Ψ = 20 mm

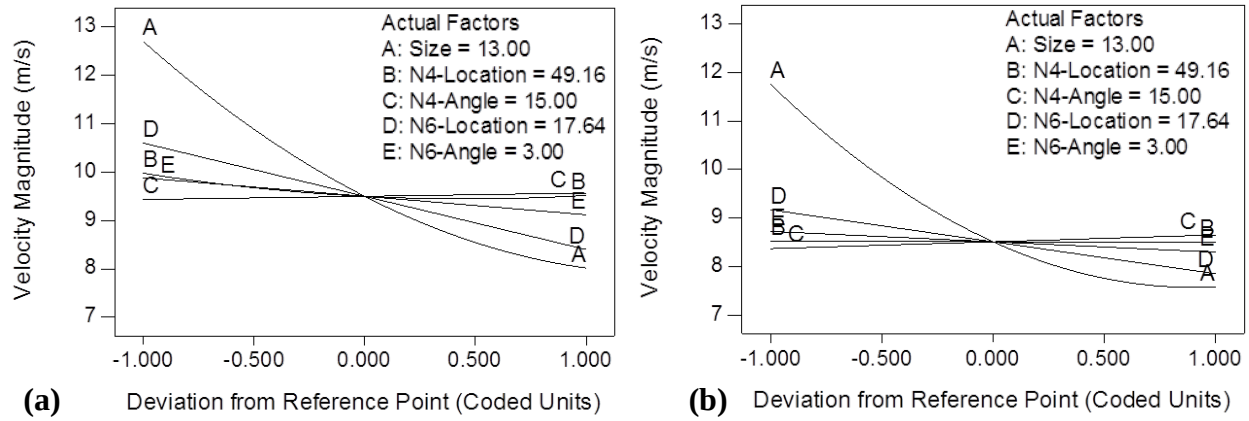

Figure 5-12. Perturbation plot (a) velocity (Ψ = 10 mm), (b) velocity (Ψ = 20 mm)

The effects of significant interactions on velocity (Ψ = 10 mm) are shown in the contour plot (Figure 5-13(a)). Smaller nozzle size combined with location of nozzle#6 closer to the drill bit axis resulted in 19.1% higher velocity when compared to the location of nozzle#6 closer to the annulus. The magnitude of velocity increase due to the interaction of the location of nozzle#6 with the nozzle size was higher than that caused by the individual effect of the location of the nozzle#6 closer to the drill bit axis. The velocity was observed to be 36.6% higher for small nozzle size and the inclination of nozzle#6 towards the drill bit axis than that observed for large nozzle size. Higher velocity was observed when the location of nozzle#4 was closer to the drill bit axis and its inclination was towards the annulus. When the location of nozzle#6 and nozzle#4 were closer to the drill bit axis, the velocity was increased by 23.62% compared to the location of nozzles#4 and #6 placed closer to the annulus. For the case of nozzle#4 inclination towards the drill bit axis, positioning the nozzle#6 closer to the axis resulted in 18.54% higher velocity than its position closer to the annulus. High velocity was observed when the angle and location of nozzle#6 were towards the drill bit axis. When the inclination and location of nozzle#6 was closer to the axis, the velocity magnitude was 22.36% higher than when the location of the nozzle#6 was closer to the annulus. The only significant interaction effect that was observed for velocity (Ψ = 20 mm) was that between nozzle size and location of nozzle#6 (Figure 5-12(b)). Small nozzle size and location of nozzle#6 closer to the drill bit axis resulted in high velocity. For the case of nozzle#6 location closer to the drill bit axis, small nozzle size increased the velocity by 37.35% compared of that large nozzle size. When the nozzle size was small, moving the nozzle#6 closer to the annulus resulted in 15.62% decrease in velocity compared to the position of nozzle#6 closer to the axis.

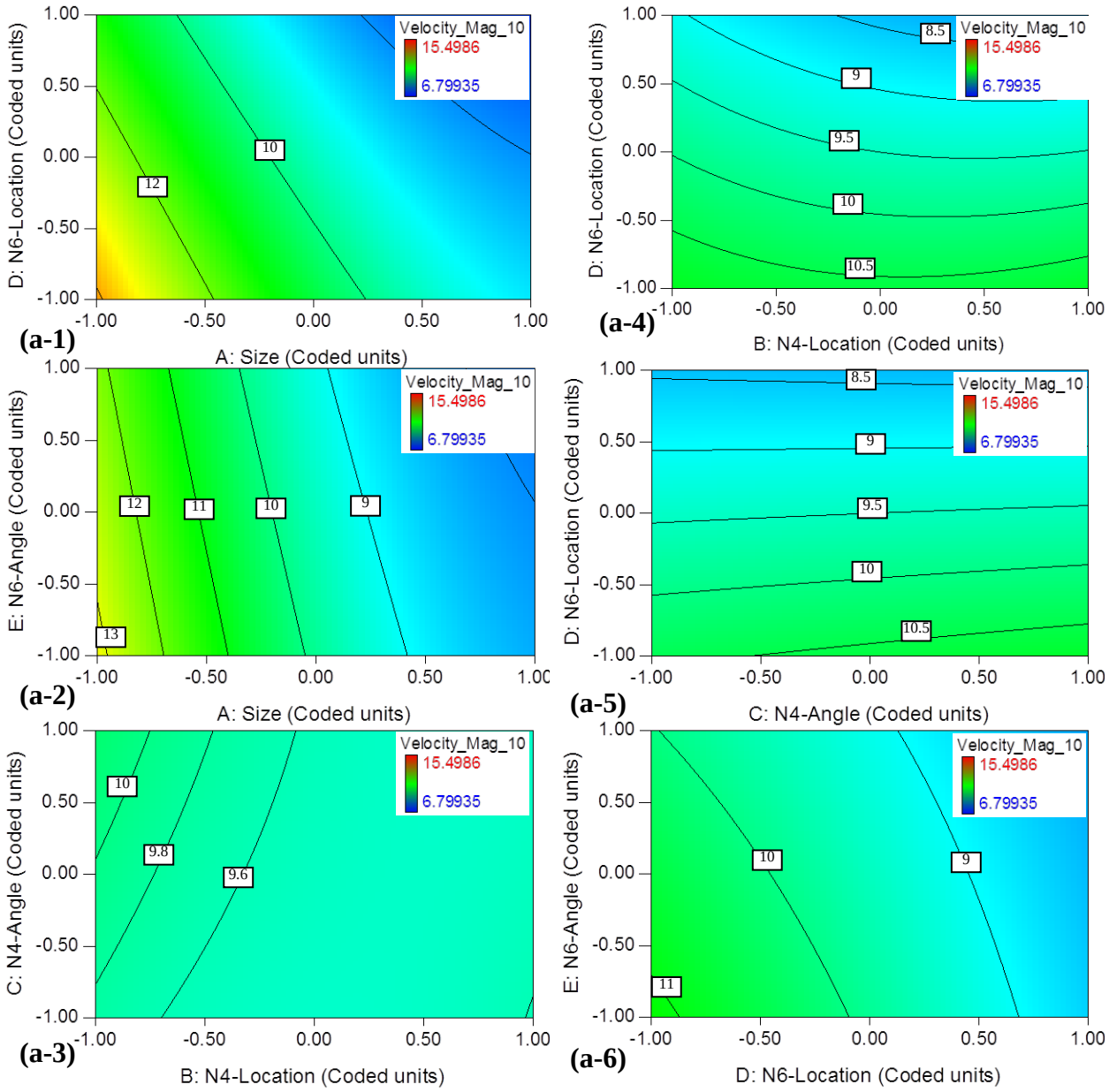

Figure 5-13. Contour plots for interaction effects on (a) velocity magnitude (m/s) (Ψ = 10 mm): (a-1) A x D; (a-2) A x E; (a-3) B x C; (a-4) B x D; (a-5) C x D; (a-6) D x E; (b) velocity magnitude (m/s) (Ψ = 20 mm): (Continued))

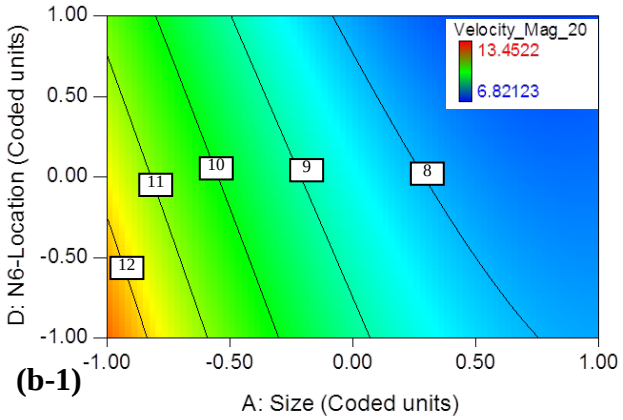

Figure 5-13. Contour plots for interaction effects on (b) velocity magnitude (m/s) (Ψ = 20 mm): (b-1) A x D

Each run in the CCD is composed of a unique combination of design parameters. To comprehend the effect of the various combinations, two runs were chosen as a representative to explain the influence on velocity magnitude. Runs, 22 and 28 were compared to understand the effect of nozzle size and the inclination of nozzle#6 on the velocity magnitude in the flowpath#3, while all other design parameters were held constant. Decreasing the nozzle size resulted in 36% and 31% increase in the velocity magnitude at Ψ = 10 mm and Ψ = 20 mm, respectively. The Figure 5-14 shows the velocity magnitude in flowpath#3 at Ψ = 10 mm and Ψ = 20 mm compared for runs 22 and 28. The velocity magnitude is high near the nozzle jet and decreases along the flowpath. Decreasing the nozzle size by 38% resulted in increasing the nozzle jet velocity by 75%. The wall jet impact on velocity magnitude was negligible for both runs at Ψ = 10 mm. Due to the high wall jet created by the small nozzle, a small recirculation zone was observed in run 22 at Ψ = 10 mm between 22 mm and 30 mm radial distance in the flowpath. Compared to run 28, velocity magnitude was increased by 50% in run 22 along the flow path towards the annulus due to the decrease in the nozzle size.

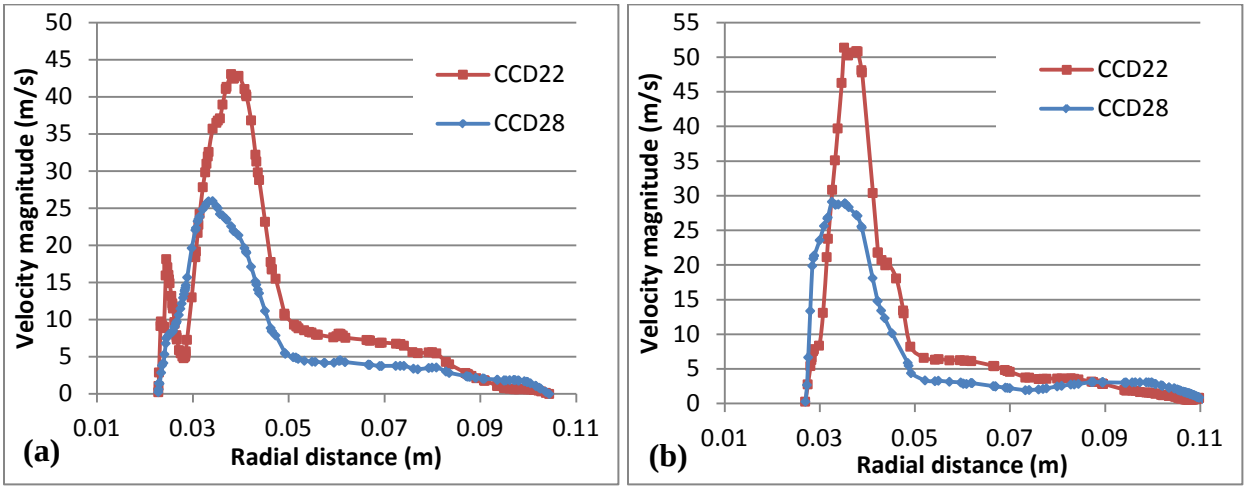

Figure 5-14. Comparison of velocity magnitude for CCD22 and CCD28 at (a) Ψ = 10 mm, (b) Ψ = 20 mm

The influence of the nozzle size, location and inclination of nozzle#6 and location of nozzle#4 was significant on velocity (Ψ = 10 mm), whereas, only nozzle size and location of nozzle#6 had significant effect on velocity (Ψ = 20 mm). As the nozzle#6 is the origin of the flow for the two flow paths, flowpath#4 and flowpath#5, it proves its significance at different cross-sectional depths in flow path. Whereas the nozzle#4 supplies only for flowpath#3 and hence its significance is limited to the depth of Ψ = 10 mm. The effect of interactions between the design parameters was significant for the velocity (Ψ = 10 mm). This could be due to the effect of the cross flow between the flow paths that shows the significance of interaction effects at Ψ = 10 mm which is closer to the downhole surface. However, for the velocity (Ψ = 20 mm), the only significant interaction was between size and location of nozzle#6. The possibility of cross-flow is less at the depth Ψ = 20 mm which is closer to the inner wall of the drill bit.

5.2.3 Relationship between average vorticity and significant design parameters and their interactions

The ANOVA results for average vorticity measured at 10 mm and 20 mm as the responses are shown in Table 5-9. The regression coefficients of the individual effects and those of significant two-way interaction and higher order effects were used to fit a second order polynomial equation. The developed quadratic model for vorticity @ Ψ = 10 mm and vorticity @ Ψ = 20 mm as the responses are given in eqn (5-3) and (5-4) respectively.

$$\text{Vorticity } (\Psi = 10 \text{ mm}) = 3130.07 - 1040.84\,A - 157.43\,B - 13.84\,C - 711.52\,D - 159.94\,E + 224.97\,AD - 113.11\,BD + 119.04\,DE + 649.81\,A^2 \quad \ldots(5\text{-}3)$$

$$\text{Vorticity } (\Psi = 20 \text{ mm}) = 2206.36 - 817.81\,A - 88.44\,B + 14.33\,C - 227.32\,D - 49.38\,E + 123.14\,AD + 265.33\,A^2 + 201.59\,B^2 \quad \ldots(5\text{-}4)$$

where A is nozzle size, B is the location of nozzle#4, C is the inclination of nozzle#4, D is the location of nozzle#6 , and E is the inclination of nozzle#6.

The model F-value of 57.31 and 96.97 implies that the models are significant and there is only a 0.01% chance that an F-value this large could occur due to noise. R^2 *which* is a statistical measure of how close the data are to the fitted regression line was 0.9591 for vorticity (Ψ = 10 mm) and 0.9712 for vorticity (Ψ = 20 mm). This ensures that 95.91% and 97.12 % of the variation in the respective responses could be explained by the developed models. The co-efficient of variation (C.V.%) which is the measure of relative variability in the data was low (7.35% and 5.61%) for both the vorticity responses.

Table 5-9. Analysis of Variance for Response Surface Reduced Quadratic Model for Vorticity (ANOVA)

Vorticity (Ψ = 10 mm)			Vorticity (Ψ = 20 mm)		
Source	F Value	p-value Prob > F	Source	F Value	p-value Prob > F
Model	57.31	< 0.0001	Model	96.97	< 0.0001
A-Size	295.06	< 0.0001	A-Size	626.68	< 0.0001
B-N4-Location	6.75	0.0164	B-N4- Location	7.33	0.0126
C-N4-Angle	0.052	0.8214	C-N4-Angle	0.19	0.6649
D-N6- Location	137.88	< 0.0001	D-N6- Location	48.42	< 0.0001
E-N6-Angle	6.97	0.015	E-N6-Angle	2.29	0.1442
AD	12.25	0.002	AD	12.63	0.0017
BD	3.1	0.0923	A^2	12.8	0.0016
DE	3.43	0.0775	B^2	7.39	0.0123
A^2	50.31	< 0.0001			
Std. Dev.	257.08		Std. Dev.	138.6	
Mean	3495.58		Mean	2469	
C.V. %	7.35		C.V. %	5.61	
R^2	0.9591		R^2	0.9712	
Adj R^2	0.9424		Adj R^2	0.9612	
Pred R^2	0.9091		Pred R^2	0.9486	
Adeq Precision	28.804		Adeq Precision	32.187	

The close agreement between the predicted R^2 and the adjusted R^2 and high signal to noise ratio measured as adequate precision indicate that the models can be used to predict the vorticity within the design space. A model is adequate if the residuals of regression are normally distributed. Therefore, model adequacy was further evaluated by residual analysis. Figure 5-15 (a) and (b) shows the normal probability plot of residuals for vorticity (Ψ = 10 mm) and vorticity (Ψ = 20 mm). There was no definite pattern observed in the normal probability plot and the residual points were closer to the straight line. This indicates that both the statistical models are adequate for predicting the responses. The response vorticity predicted using the eqn (5-3) and

(5-4) were plotted against the simulation results (actual) in Figure 5-16 and it can be observed that the predicted values are in close agreement with the simulation values.

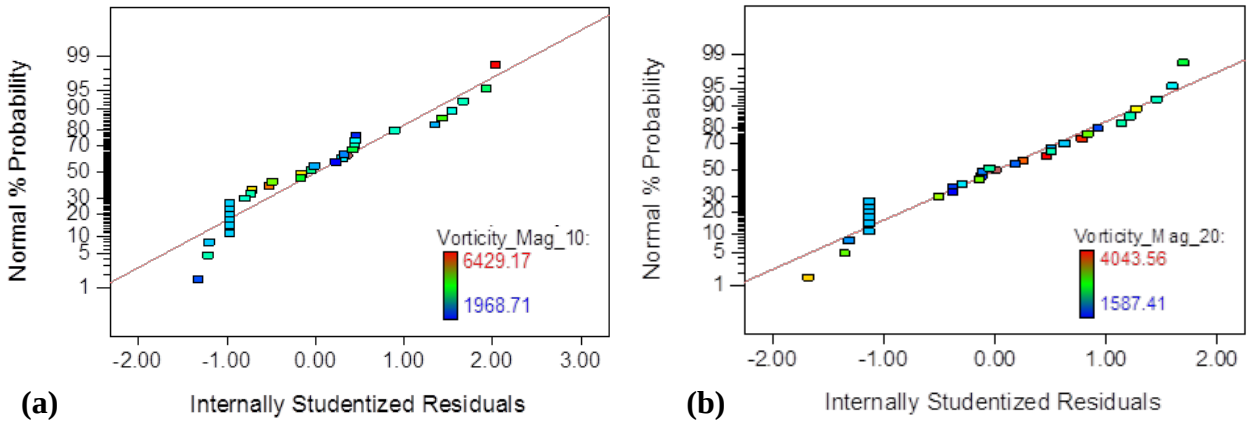

Figure 5-15. Normal probability plot for vorticity magnitude residuals (a) Ψ = 10 mm, (b) Ψ = 20 mm

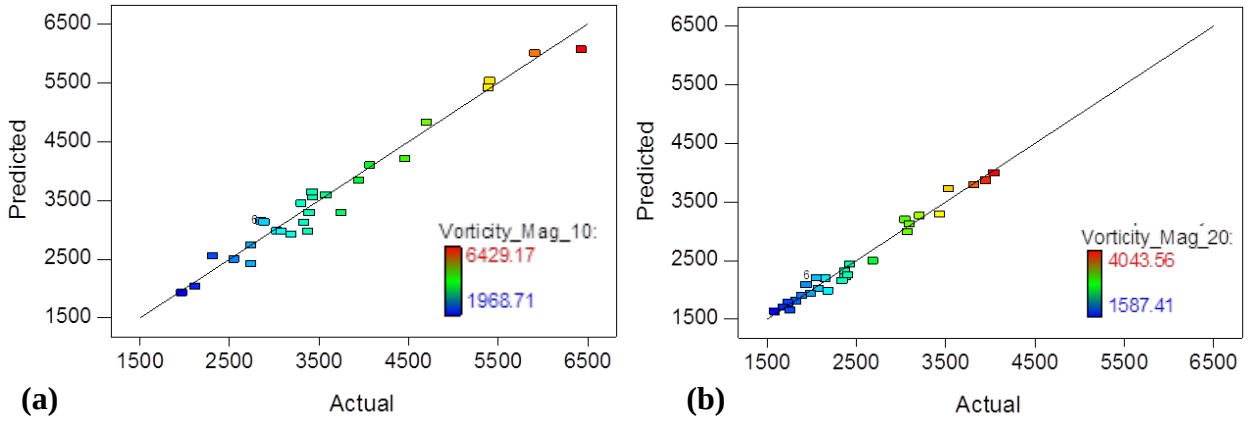

Figure 5-16. Predicted versus actual vorticity magnitude (a) Ψ = 10 mm, (b) Ψ = 20 mm

The perturbation plot compares the effect of all the factors at a particular point in the design space. The response is plotted by changing only one factor over its range while holding all the other factors constant. The perturbation for vorticity is shown in Figure 5-17. Small nozzle size resulted in high vorticity compared to that of big nozzle size at both 10 mm and 20

mm depths. The location of nozzle#6 was an important factor in determining the vorticity (Ψ = 10 mm), whereas it had less impact on the vorticity (Ψ = 20 mm). The location and inclination of nozzle#4 and inclination of nozzle#6 had significant effect on both vorticities, but the extent of the effect was comparatively low.

The contour plots show the effect of significant interactions on vorticity (Figure 5-18). In the presence of large nozzle size, positioning the nozzle#6 closer to the annulus resulted in 32.28% decrease in vorticity (Ψ = 10 mm) compared to its position closer to the drill bit axis. The interaction plot between the parameters *B* and *D* suggest that longer the radial distances of nozzles#4 and #6, smaller will be the vorticity (Ψ = 10 mm). For the condition of nozzle#4 location closer to the drill bit axis, the vorticity (Ψ = 10 mm) was decreased by 30% when the location of nozzle#6 was away from the drill bit axis compared to its position closer to the drill bit axis. For the case of nozzle#6 inclined towards the drill bit axis, positioning the nozzle#6 closer to the annulus decreased thee vorticity (Ψ = 10 mm) by 38.48% compared to its position closer to the drill bit axis.

The radial distance of nozzle#4 from the drill bit axis was observed to have significant influence on the vorticity (Ψ = 20 mm). Moving the nozzle#4 towards the drill bit axis or moving it towards the annulus resulted in increasing the vorticity. On the other hand, moving the nozzle#6 closer to the annulus decreased the vorticity (Ψ = 20 mm). The inclination of nozzles#4 and #6 were found to have less effect on vorticity (Ψ = 20 mm). The effect of the interaction between the nozzle size and radial distance of nozzle#6 on the vorticity (Ψ = 20 mm) was similar to that observed for vorticity (Ψ = 10 mm). Small nozzle size and locating the nozzle#6 closer to the annulus resulted in lowering the vorticity (Ψ = 20 mm) by 51% compared to large nozzle

size. On the other hand, locating the nozzle#6 away from the drill bit axis resulted in 18% lower vorticity (Ψ = 20 mm). Therefore, large nozzle size combined with nozzle#6 location closer to the annulus is recommended for minimum vorticity.

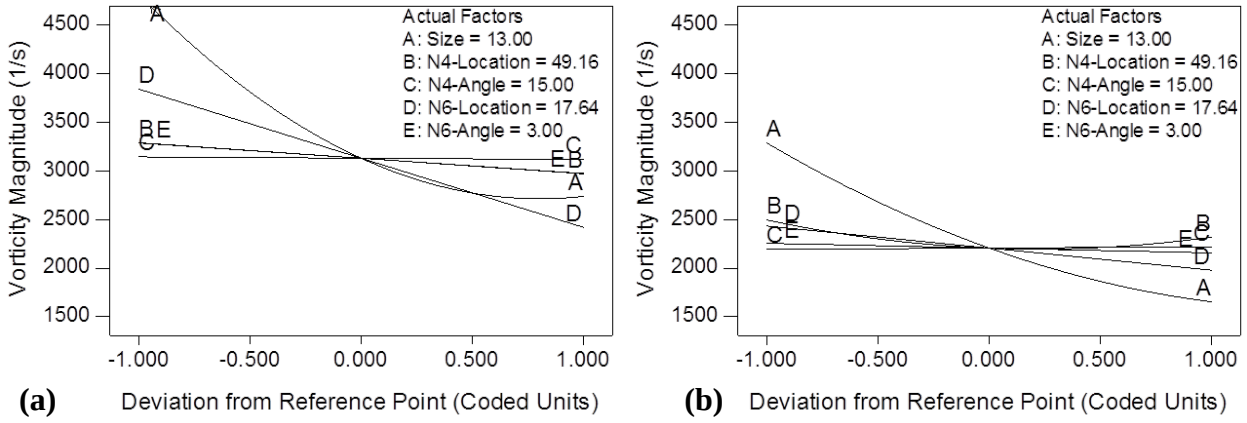

Figure 5-17. Perturbation plot (a) vorticity magnitude (Ψ = 10 mm), (b) vorticity magnitude (Ψ = 20 mm)

The influence of the nozzle size, location and inclination of nozzle#6 and location of nozzle#4 was significant on vorticity magnitude (Ψ = 10 mm and Ψ = 20 mm). Almost all the selected factors have shown strong influence due to the formation of high vorticity magnitude in the free jet zone. The effect of interactions between the design parameters was significant for the vorticity magnitude at Ψ = 10 mm. This could be due to the effect of the cross flow between the flow paths that shows the significance of interaction effects at Ψ = 10 mm which is closer to the downhole surface. However, for the vorticity magnitude at Ψ = 20 mm, only significant interaction was between size and location of nozzle#6. The possibility of cross-flow is negligible at the depth Ψ = 20 mm which is closer to the inner wall of the drill bit.

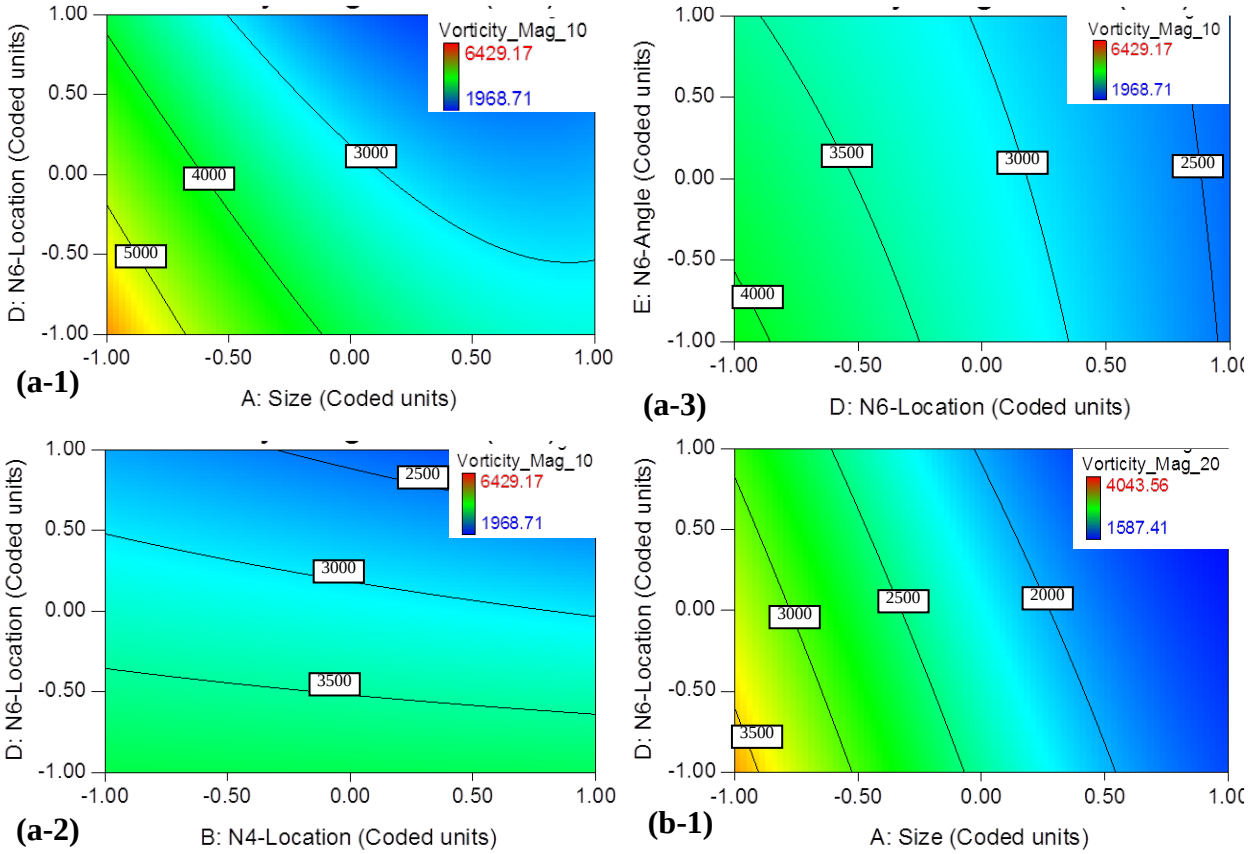

Figure 5-18. Contour plots for interaction effects on (a) vorticity magnitude (Ψ = 10 mm): (a-1) A x D; (a-2) B x D; (a-3) D x E; (b) vorticity magnitude (Ψ = 20 mm): (b-1) A x D

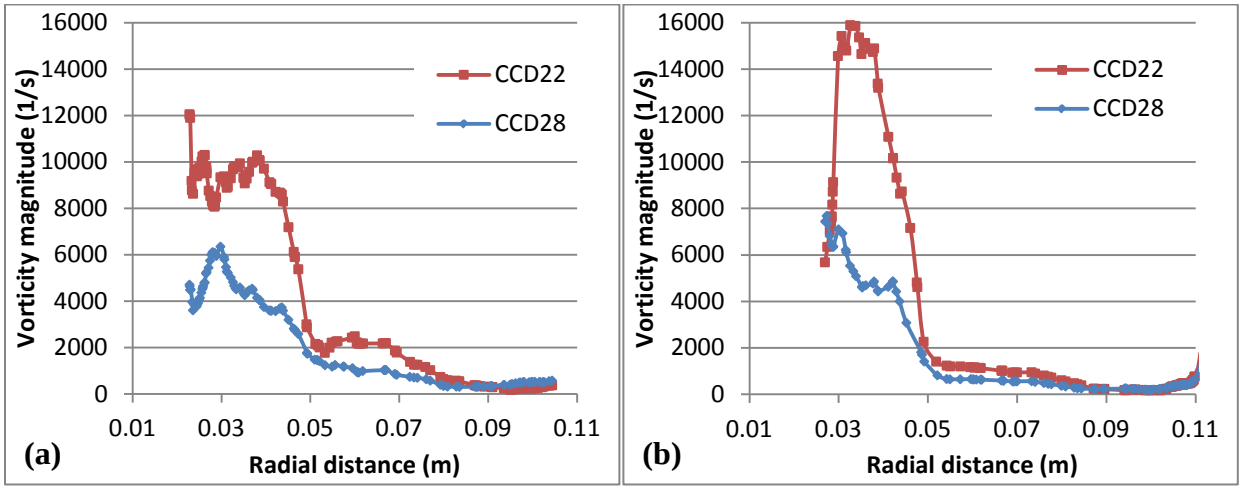

Figure 5-19. Comparison of vorticity magnitude for CCD22 and CCD28 at (a) Ψ = 10 mm, (b) Ψ = 20 mm

5.2.4 Relationship between pressure drop and significant design parameters and their interactions

The pressure drop across the drill bit which is the difference between the pressure inlet at the nozzle and pressure outlet at the annulus was measured as one of the responses which is affected by the design parameters of the drill bit. The simulation based pressure drop was fitted into a second order polynomial equation. The ANOVA results are shown in Table 5-10.

$$\text{Pressure drop} = 1.853e{+}006 - 2.361e{+}006\ A + 18198.24\ B - 11827.73\ C + 12157.10\ D + 4503.98\ E + 17167.98\ AC - 10954.45\ AD - 6946.77\ AE - 15385.34\ BC + 7810.00\ DE + 1.282e{+}006\ A^2 - 23891.58\ D^2 \quad \ldots(5\text{-}5)$$

where *A* is nozzle size, *B* is the location of nozzle#4, *C* is the inclination of nozzle#4, *D* is the location of nozzle#6 , and *E* is the inclination of nozzle#6.

The model was highly significant which is evident from the high F-value. There is only 0.01% chance that F-value this high could have occurred due to noise. The R^2 value was 1, indicating that 100% of the variability in the data could be explained by the model. The coefficient of variation (C.V.%) was very small indicating that the error in the data is minimum. The predicted R^2 was same as the adjusted R^2 and the signal from the data was significantly higher than the noise. This indicates that the developed model for pressure drop was sufficiently good for navigating the design space. The residual analysis was performed to check the model adequacy. From the Figure 5-20 (a), it can be observed that almost all the residual points follow the straight line. This implies that the residuals are normally distributed and hence the model is

adequate for predicting the pressure drop within the design space. The relationship between the predicted and actual pressure drop is shown in Figure 5-20 (b). The close agreement between the predicted and actual values indicates that the model predicts the pressure drop to an agreeable extent.

Table 5-10. Analysis of Variance for Response Surface Reduced Quadratic Model for Pressure drop (ANOVA)

Pressure drop		
Source	F Value	p-value Prob > F
Model	49065.87	< 0.0001
A-Size	5.23E+05	< 0.0001
B-N4- Location	31.07	< 0.0001
C-N4-Angle	13.13	0.0018
D-N6- Location	13.87	0.0014
E-N6-Angle	1.9	0.1837
AC	24.58	< 0.0001
AD	10.01	0.0051
AE	4.02	0.0593
BC	19.74	0.0003
DE	5.09	0.0361
A^2	29898.92	< 0.0001
D^2	10.39	0.0045
Std. Dev.	13850.41	
Mean	2.56E+06	
C.V. %	0.54	
R^2	1	
Adj R^2	0.9999	
Pred R^2	0.9999	
Adeq Precision	550.471	

The influence of each of the design parameter on the pressure drop is shown in the perturbation plot (Figure 5-21). Nozzle size was observed to be the most significant factor affecting the pressure drop. Pressure drop is high for small nozzle size and vice versa. The location of the nozzles#4 and #6 closer to the drill bit axis lowered the pressure drop and re-locating the nozzles closer to the annulus increased the pressure drop. The pressure drop was increased when the inclination of the nozzle#4 was towards the drill bit axis, but decreased when the inclination was shifted towards the annulus. The effect of nozzle#6 inclination was converse to that of nozzle#4. The pressure drop was low when the inclination of nozzle#6 was towards the drill bit axis and high when the nozzle#6 inclination is towards the annulus. The contour plots in Figure 5-22 show the effect of significant interactions on the pressure drop. From the interaction of nozzle size with inclination of nozzles#4 and #6, and location of nozzle#6 in Figure 5-22 (a), (b) and (c), it can be observed that the effect of nozzle size is dominating and the effect of other parameters is comparatively low. In the presence of nozzle#4 inclination towards the axis, reducing the nozzle size from 16/32 inch to 10/32 inch resulted in decreasing the pressure drop by 85.68%. For the case of nozzle#6 location and inclination closer to the drill bit axis, large nozzle size decreased the pressure drop by approximately 86.13% compared to that of small nozzle size. When the inclination of nozzle#4 was closer to the drill bit axis, placing the nozzle#4 closer to the drill bit axis decreased the pressure drop by 3.68% compared to its position closer to the annulus. Positioning the inclination and location of nozzle#6 closer to the drill bit axis decreased the pressure drop by 1.16% compared to the positioning of inclination and location of nozzle#6 closer to the annulus. When the inclination of nozzle#6 was towards the annulus, the location of nozzle#6 closer to the drill bit lowered the pressure drop by 2% compared to its location away from the drill bit axis.

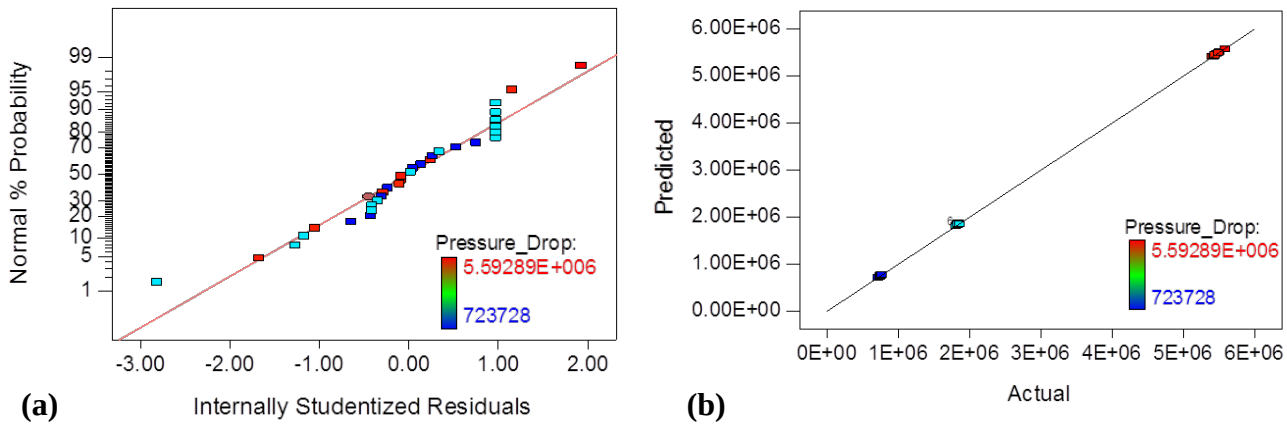

Figure 5-20. (a) Normal probability plot for residuals of pressure drop, (b) Predicted pressure drop versus actual pressure drop

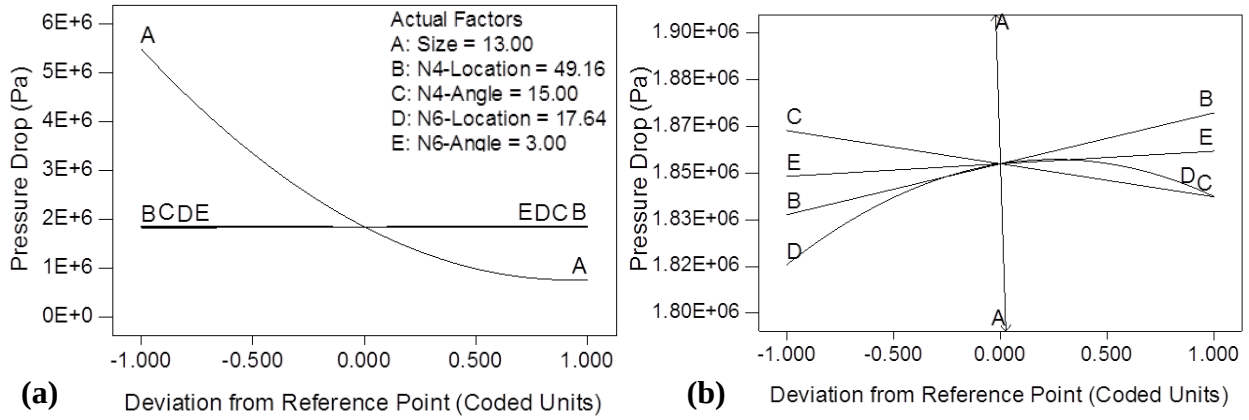

Figure 5-21. Perturbation plot for pressure drop (a) Pressure drop - full range scale, (b) pressure drop - scaled to range 1.8E06 to 1.9E06

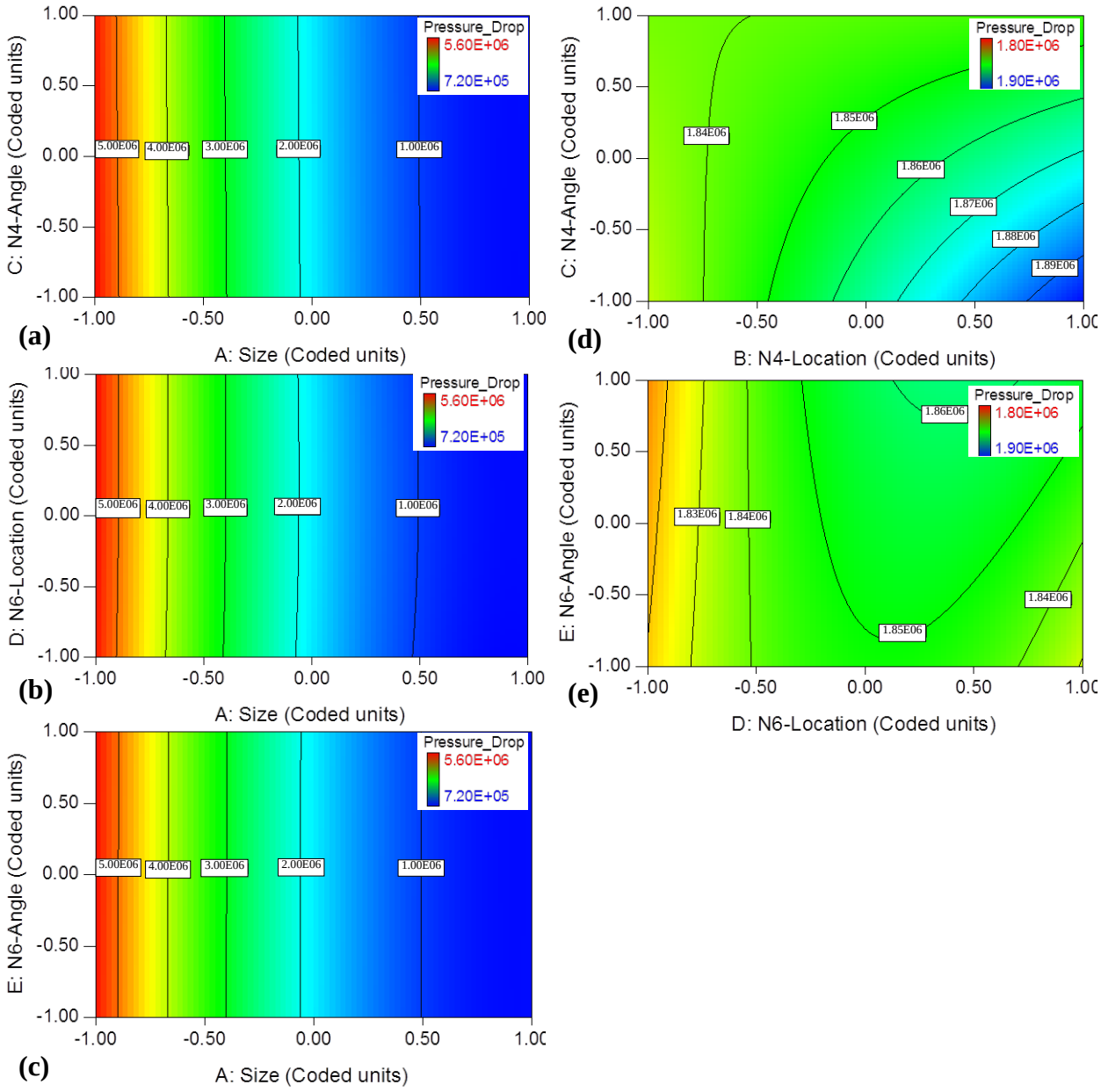

Figure 5-22. Contour plots for interaction effects on the pressure drop: (a) A x C; (b) A x D; (c) A x E; (d) B x C; (e) D x E

The Figure 5-23 shows the pressure drop compared for all the runs sorted according to the nozzle size (10/32 inch, 10/32 inch and 16/32 inch). Nozzle size 16/32 inch shows very low pressure drop in the range of 0.75 MPa when compared to that of nozzle size 10/32 inch for

which the pressure drop is in the range of 5.50 MPa. As the nozzle size was increased by 19%, the pressure drop increased by 2.5-folds and as the nozzle size was increased by 38%, the pressure drop increased by 7-folds. At a constant nozzle size of 10/32 inch, the variability in the pressure drop was 1%, which is due to the effect of the other design parameters. Similarly, for nozzle sizes 13/32 inch and 16/32 inch, the variability was 1% and 2.5% respectively.

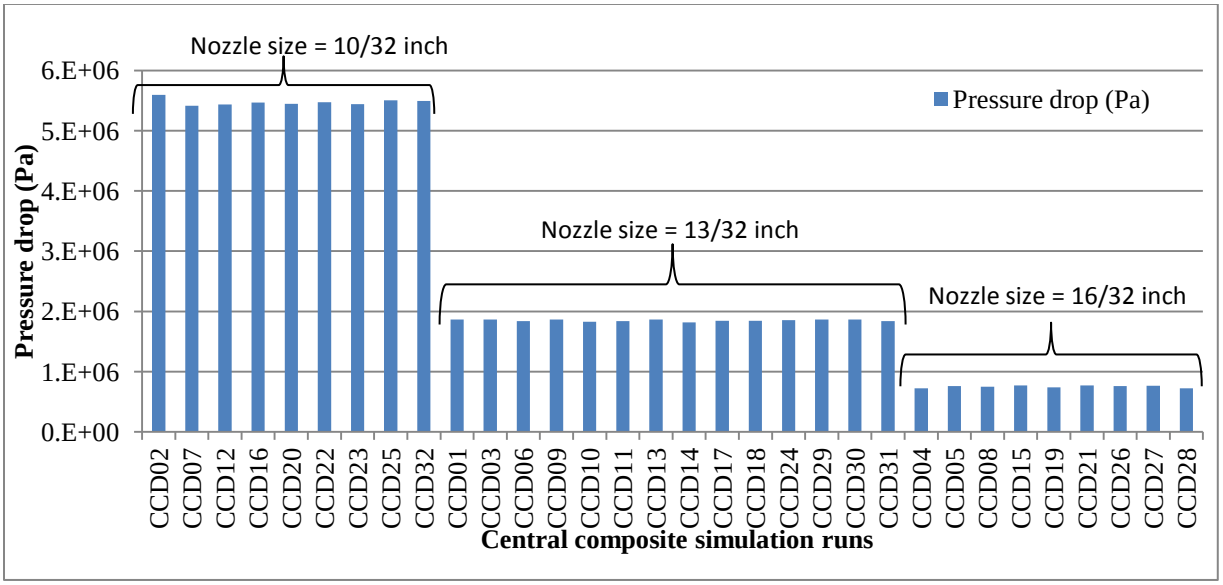

Figure 5-23. Pressure drop plot for central composite simulations sorted by nozzle sizes

This shows that in the presence of small nozzle size, nozzle size controls the pressure drop and the effect of other design parameters is small. On the other hand, the effect of other parameters on the pressure drop is significant when the nozzle size is large.

5.2.5 Discussion on the results of CCD and RSM

At Ψ = 10 mm, the velocity and the vorticity magnitude were highly influenced by the nozzle size, location & inclination of nozzle#6 and location of nozzle#4. This is because Ψ = 10

mm is closer to the downhole surface and the flow here is mainly affected by the jet impact force and the wall jet across the downhole surface. The wall jet is the shear flow directed along a wall where, by virtue of the initially supplied momentum, at any station, the streamwise velocity over some region within the shear flow exceeds that of the free stream (Launder & Rodi, 1979). The reason for increased vorticity is due to the jet impingement on the downhole surface (Schwarz & Cosart, 1961). The interactions between design parameters have strong impact on velocity and vorticity at Ψ = 10 mm. The effect due to interaction between nozzle size and location of nozzle#6 is due to the position of nozzle#6, which mainly supplies flow to the flowpaths #4 and #5, and at the same time, there is a channel open to flowpath#3 closer to Ψ = 10 mm. Though this interaction favors increase in velocity, it is also accompanied by an increase in the vorticity which is due to the nozzle jet. The interactions between location and inclination for nozzle#4 and nozzle#6 are quiet obvious as both the parameters influence their own nozzle jet in their respective flow paths. The effect due to the channel flow between flowpaths #3 and #5 is the reason for the interaction of the location of nozzle#4 & nozzle#6 on the velocity.

The formation of free jet at Ψ = 20 mm is significantly influenced by the nozzle size, location of nozzle#4 and nozzle#6. A free jet with high velocity is formed when a fluid flows through a nozzle due to the sudden pressure drop. At the nozzle exit, the jet expands radially and the jet boundary forms an expanded shape (Hatanaka & Saito, 2012). The expansion waves generated at the nozzle exit reflects at the jet boundary and results in angular motion of the fluid. For nozzle#4, the angular motion of the fluid and hence the vorticity magnitude, is high when the nozzle is displaced from its current location. On the other hand, the vorticity magnitude decreases when the nozzle#6 is moved towards the annulus because the extent of angular motion

is less at this location. The velocity at Ψ = 20 mm is high when the location of nozzle#6 is closer to the drill bit axis and nozzle size is small. The effect due to nozzle size is because of the formation of free jet which results in high velocity. When the nozzle#6 is closer to the drill bit axis, the free jet is unobstructed by the channel towards the flowpath#4, and this reflects in increasing the overall velocity at Ψ = 20 mm.

The nozzle exit velocity increases as the nozzle outlet diameter is reduced. While the velocity increase is desired (for mud removal), it is also accompanied by an increased potential for pressure loss. This is due to (1) as the exit velocity increases, the static pressure decreases (Bernoulli effect) potential giving rise to adverse pressure gradient in the channel and, (2) minor losses tend to scale with the velocity squared. Hence, the influence of the nozzle size is very high on the pressure drop (Garcia-Gavito & Azar, 1994; Lim & Chukwu, 1996). The location and inclination of nozzle#4 has impact on pressure drop due to the reduction in the frictional pressure drop that occurs when the nozzle#4 location is closer to the drill bit axis and its inclination is away from the drill bit axis. The location of nozzle#6 placed closer to the drill bit axis results in less pressure drop because the nozzle jet velocity is shared by the flow paths#3, #4 and #5.

Thus, by the application of CCD and RSM, the effect of the selected design parameters and their interactions on the average velocity, average vorticity and pressure drop was investigated to understand the PDC drill bit hydraulics and hence to improve the drill bit design for improvement of the performance.

5.2.6 Optimization of design parameters for improved performance of PDC drill bit

The design factors, nozzle size, location and inclination of nozzle#4, and location and inclination of nozzle#6 were optimized for improved PDC drill bit performance. The criteria for improved PDC drill bit performance are maximum average velocity, minimum average vorticity and minimum pressure drop. Numerical optimization was chosen for the purpose of determining the optimum limits of the design factors. The goals for the factors and the responses can be set as maximize, minimize, target, within range, or can be set to an exact value (factors only.) The importance of the goal of each response can be changed in relation to the other responses. The goals for each of the five design factors were chosen to be within range which implies that the optimum values for the design factors will be between the assigned high and low levels. The goals are combined into an overall desirability which is an objective function that ranges from zero outside of the limits to one at the goal. The numerical optimization aims to determine a point that maximizes the desirability function. The goal seeking begins at a random starting point and proceeds up the steepest slope to a maximum.

Table 5-11. Optimum levels of design parameters for the corresponding responses

Response	Goal	Significant design parameters					Optimum response
		Nozzle size (1/32 inch)	Nozzle#4 location (mm)	Nozzle#4 inclination (Deg)	Nozzle#6 location (mm)	Nozzle#6 inclination (Deg)	
Velocity (m/s) (Ψ = 10 mm)	Maximize	10	34.16	18.00	12.64	0.00	15.44
Velocity (m/s) (Ψ = 20 mm)	Maximize	10	34.16	18.00	12.64	0.00	13.12
Vorticity (1/s) (Ψ = 10 mm)	Minimize	15	63.60	17.91	22.38	5.94	1879
Vorticity (1/s) (Ψ = 20 mm)	Minimize	16	50.69	15.43	18.40	5.85	1586
Pressure drop (Pa)	Minimize	16	34.16	12.00	22.64	6.00	717558

In order to achieve a maximum velocity at the cross sectional depth Ψ = 10 mm, the goal for set to be maximum and the design parameters were set to be in the range as taken for the study. The optimum levels of nozzle size, location and inclination of nozzle#4, location and inclination of nozzle#6 were determined as shown in Table 5-11. In the similar fashion, optimum levels of the design parameters were determined for the other responses: maximum velocity (Ψ = 20 mm), minimum vorticity (Ψ = 10 mm) and (Ψ = 20 mm), and minimum pressure drop. All the optimum levels of the design parameters and the corresponding responses are shown in Table 5-11.

The main purpose of the response surface methodology was to establish the optimum conditions for simultaneous increase in velocity, decrease in vorticity and decrease in pressure drop. The goals were set for all the responses simultaneously as follows: maximize for average velocity; minimize for average vorticity and minimize for pressure drop. The optimum levels were determined as, nozzle size →14/32 inch; location of nozzle#4 → 34.96 mm; inclination of nozzle#4 → 18.00 deg; location of nozzle#6 → 12.64 mm; inclination of nozzle#6 → 6.00 deg for a maximum velocity (Ψ = 10 mm) of 9.85 m/s; maximum velocity (Ψ = 20 mm) of 9.07 m/s; minimum vorticity (Ψ = 10 mm) of 3241.09 /s; minimum vorticity (Ψ = 20 mm) of 2378.50 /s; and minimum pressure drop of 1156720 Pa. An assessment of the optimization procedure will be performed with the optimum design parameters identified from simultaneous optimization of the responses.

5.3 Assessment of Optimization Procedure

The optimization procedure assessment was carried out by comparing the flow domain of base/original drill bit design with that of statistically optimized drill bit design for two cases: (1) Newtonian fluid flow model and (2) non-Newtonian fluid flow model in order to simulate the real time down-hole condition. The design parameters that were different from the base design and optimized design are the nozzle size, location and inclination of nozzle#4, location and inclination of nozzle#6. The nozzle#4 highly influences the flowpath#3 and the nozzle#6 influences the flowpath#4 and flowpath#5. Chip carryout was measured in terms of velocity at the cross-sectional surface at two depth levels, Ψ = 10mm and Ψ = 20mm. Vorticity was also measured at these two locations as a measure of recirculation. Pressure drop across the bit was measured as the difference between the inlet and outlet pressure.

5.3.1 Newtonian flow comparison between base/original drill bit design and statistically optimized drill bit design

Newtonian flow simulations were carried out based on two phases, unsteady state condition, similar to all the simulations carried out for selection and optimization of design parameters. The primary phase, water was considered to be the drilling fluid and the secondary phase, mud was considered to be the clay generated from the downhole. The results were compared in terms of the cross sectional velocity, recirculation magnitude and vorticity level and finally the pressure drop across the bit.

For a better understanding, the velocity vectors are compared for the flowpath#3 as shown in Figure 5-24. The velocity at the nozzle was significantly increased in the modified drill bit design due to the change in nozzle size, but, the velocity across the flow path was almost similar for both the cases. The change in nozzle location reduced the stagnation area at the right of the nozzle towards the drill bit axis as marked in Figure 5-24. Similarly the other flow paths were analyzed for a smooth flow stream.

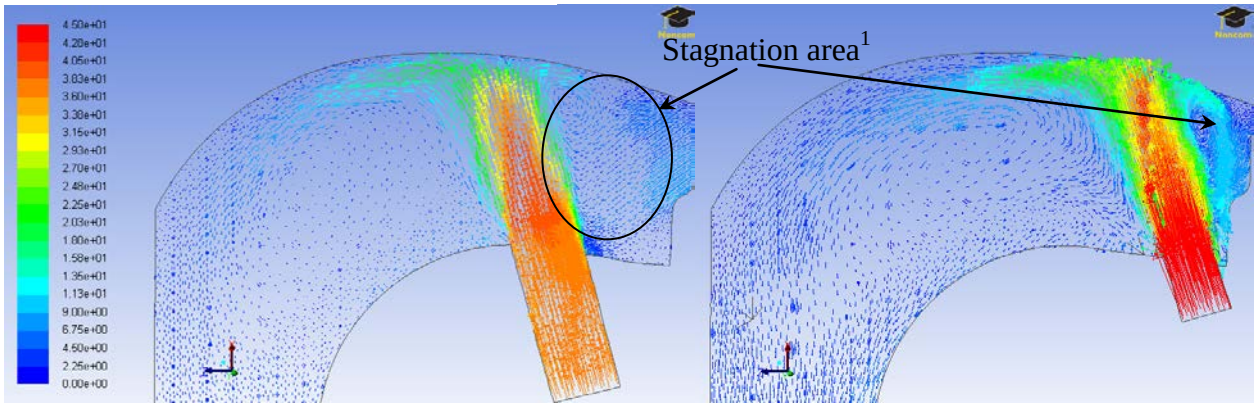

Figure 5-24. Velocity vectors in flowpath#3 (a) Original drill bit design (b) modified drill bit design

[1] Stagnation area located to the right of nozzle#4 in flowpath#3 is reduced in the modified drill bit design; Average velocity across the flow path is increased in the modified drill bit design.

The velocity across the flow path was measured at the cross sectional surface at two different levels of Ψ = 10mm and Ψ = 20mm from the downhole surface. The chip carry velocity was compared at each level in the flow paths, #3, #4 and #5 as shown in Figure 5-25. In general, modifying the design of the drill bit, resulted in very low impact on the maximum jet velocity in the flowpath#3 at both depth levels. This can be understood from the Figure 5-25 (a) and (b) where the difference in the velocity pattern across the flowpath#3 is due to the change in location of nozzle#4. Compared to the base/original design, the average velcoity in modified design was increased by 2% at Ψ = 10mm and decreased by 15% at Ψ = 20mm in the flowpath#3 . For the flowpath#4, the velocity trend was similar for both the designs with approximately 15% increase in maximum jet velocity at Ψ = 10mm and Ψ = 20mm. The average velcoity in this flow path was increased by 14% at Ψ = 10mm and decreased by 6% at Ψ = 20mm compared to that of base/original design. The flowpath#5 has the similar velocity trend as of flowpath#4 with increase in average velocity by 45% and 53% at Ψ = 10mm and Ψ = 20mm respectively. Compared to the original design, the overall average velocity for all the flow paths was increased by 14% in the modified design.

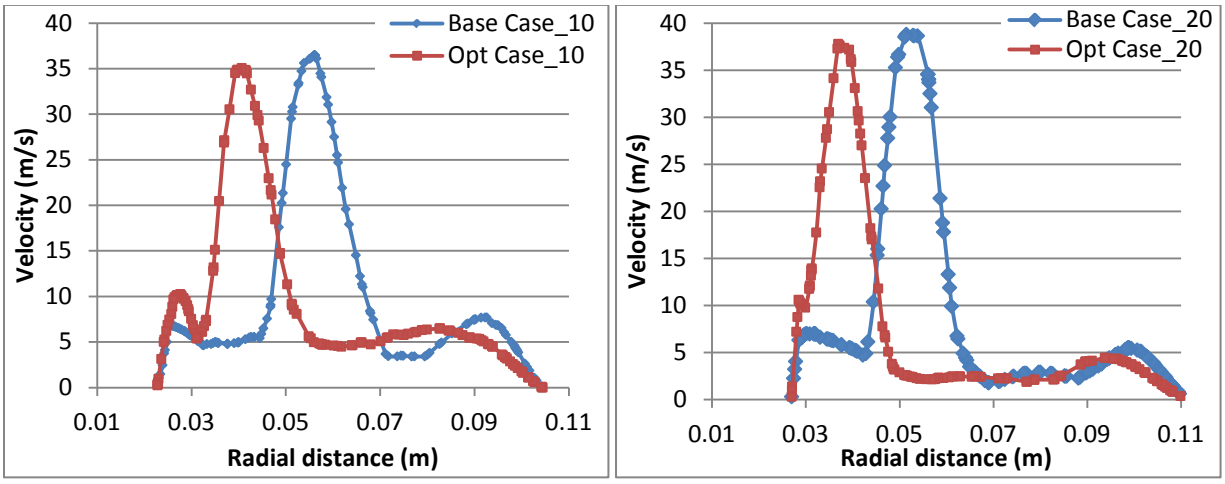

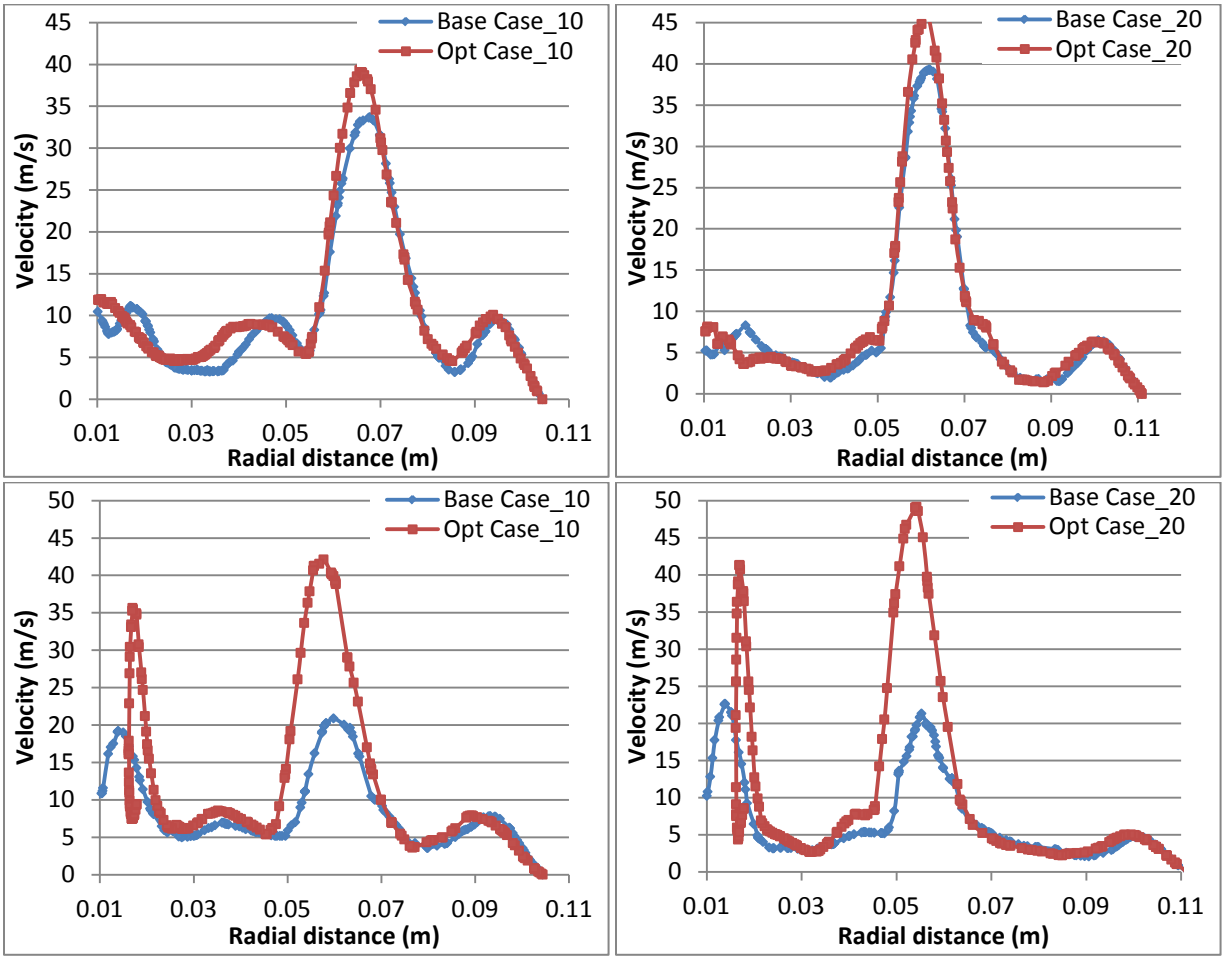

Figure 5-25. Velocity across the flowpath comparison for original drill bit design to the modified drill bit design (a) Flowpath#3 at Ψ = 10mm (b) Flowpath#3 at Ψ = 20mm (c) Flowpath#4 at Ψ = 10mm (d) Flowpath#4 at Ψ = 20mm (e) Flowpath#5 at Ψ = 10mm (f) Flowpath#5 at Ψ = 20mm

The recirculation velocity was studied in terms of radial velocity that flows opposite to the flowpath#3 and towards the axis of the drill bit. Figure 5-26 shows the recirculation velocity in the flowpath#3 for both the original and optimized drill bit designs. The change in nozzle#4 location plays a significant role in the recirculation zone. The area of high intense recirculation zone, observed in flowpath#3 as marked in Figure 5-26 was decreased in modified design. Increase in the size of high intense recirculation zone will lead to bit balling. A similar study was performed for the all the flow paths to observe the recirculation zone. The overall recirculation

velocity was decreased by 20% in the modified drill bit design when compared to that of the original design.

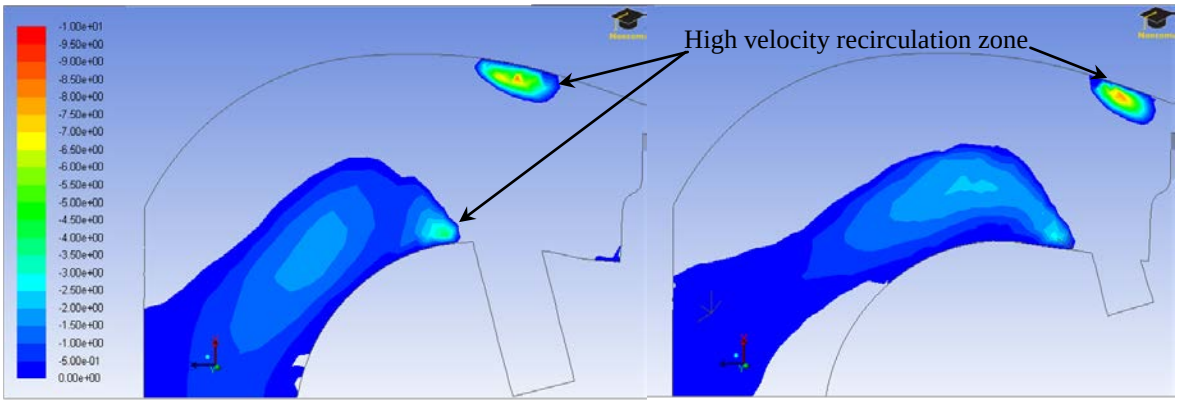

Figure 5-26. Recirculation velocity vectors in flowpath#3 (a) Original drill bit design (b) modified drill bit design

The vorticity magnitude was compared between the original and the modified drill bit design at the cross sectional surface for each flow paths. Flowpath#3 was chosen as a representation of the other flow paths to exhibit the vorticity in the flow domain as shown in Figure 5-27. A high magnitude vorticity was observed near the nozzle circumference in both the designs. However, the vorticity magnitude in the modified design at the nozzle free jet zone was higher than the original design due to the change in the nozzle size.

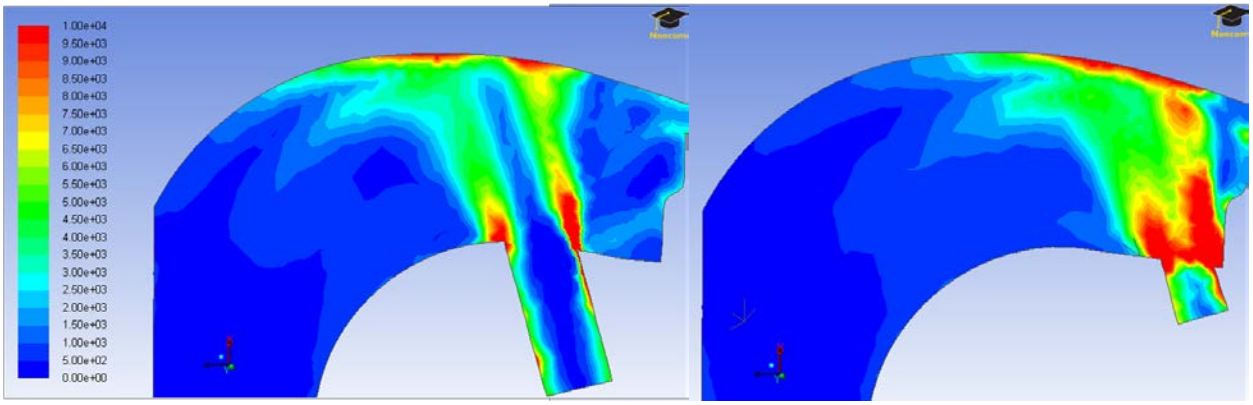

Figure 5-27. Vorticity magnitude in flowpath#3 (a) Original drill bit design (b) Modified drill bit design

The vorticity magnitude was compared across the flow path at Ψ = 10mm and Ψ = 20mm for each flow path as shown in Figure 5-28. On overall comparison, the vorticity at the nozzle jet was significantly increased in the modified design. Vorticity across the flow path was almost similar for both the cases. For flowpath#3, the average vorticity was increased by 46% and 63% at Ψ = 10mm and Ψ = 20mm respectively. For the case of flowpath#4, the average vorticity was increased by 34% and 37% at Ψ = 10mm and Ψ = 20mm respectively. In the flowpath#5, the increase in vorticity was significantly low when compared to the other flow paths. Vorticity was increased by 6% at Ψ = 10mm and decreased by 16% at Ψ = 20mm. The overall average vorticity was increased by 24% in the modified drill bit design when compared to the original drill bit design.

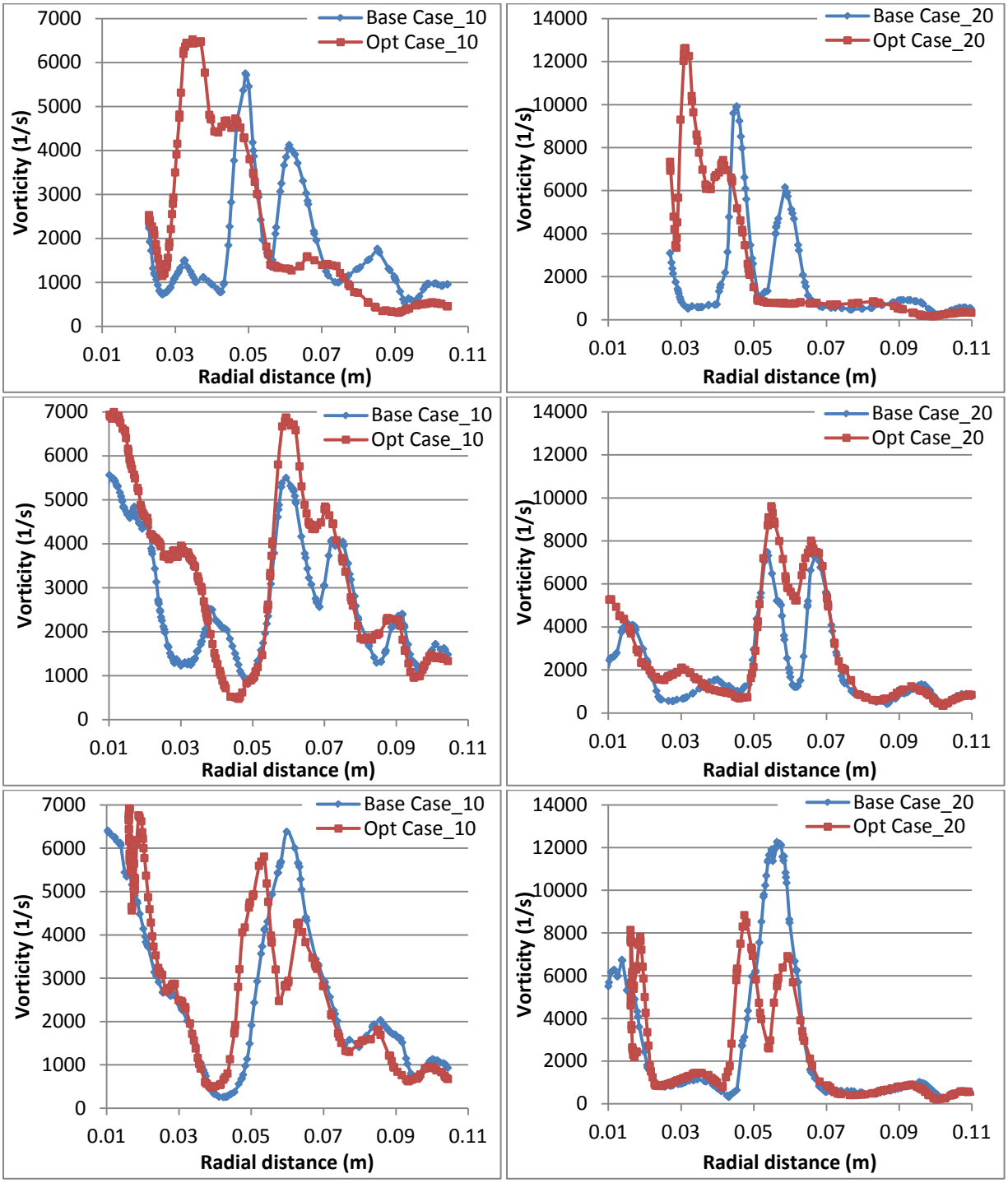

Figure 5-28. Vorticity magnitude across the flowpath comparison for original drill bit design to the modified drill bit design (a) Flowpath#3 at Ψ = 10mm (b) Flowpath#3 at Ψ = 20mm (c) Flowpath#4 at Ψ = 10mm (d) Flowpath#4 at Ψ = 20mm (e) Flowpath#5 at Ψ = 10mm (f) Flowpath#5 at Ψ = 20mm

Table 5-12. Newtonian flow results comparison for original and modified drill bit design

Response	Original drill bit design	Modified drill bit design	% difference
Pressure drop (Pa)	46408	29283	-37%
Average Velocity (m/s)	8.97	10.23	14%
Average Vorticity (1/s)	2391	2965	24%
Recirculation velocity (%)	5%	4%	-20%

The overall comparison of results for the Newtonian flow for both the original and modified drill bit designs are shown in Table 5-12. Compared to the original design, the total pressure drop was decreased by 37% in the modified design. The average velocity across the drill bit was increased by 14%. This increase in velocity across the flow path aids in faster chip removal by the prevention of chip regrinding. At the same time, the recirculation velocity was decreased, which helps to avoid the bit balling due to the stagnation of cuttings in the recirculation zone.

5.3.2 Non-Newtonian flow comparison for base/original drill bit design and statistically optimized drill bit design

Non-Newtonian flow simulations were carried out based on two phases, unsteady state condition, by incorporating the power law viscosity model for the drilling fluid with the boundary conditions similar to all the simulations carried out for selection and optimization of design parameters. The primary phase, drilling fluid, was considered as power law fluid with Consistency factor (K) = 0.06557 $kg\, s^{n-2}/m$ and Flow behavior index (n) = 0.82. The secondary phase, mud, was chosen to represent the clay generated from the downhole. One of the limitation of FLUENT is that, there is no option to choose turbulence model with non-Newtonian power law model and hence, laminar flow was selected for these simulations (FLUENT, 2012). The results were compared in terms of the cross sectional velocity, recirculation magnitude and

vorticity magnitude and finally the pressure drop across the bit similar to that of the Newtonian flow model.

Flowpath#3 was used as a model to illustrate the flow domain across the drill bit for the Non-Newtonian flow. Figure 5-29 shows the velocity vectors compared for the both the cases of original drill bit design and modified drill bit design. In general, due to the dynamic viscosity of a fluid that resists the shear near the inner wall, the fluid flow was directed along the down-hole surface. The velocity at the nozzle jet is high for the modified design due to the reduction in the nozzle size. The stagnation zone between the nozzle and the centre of the drill bit (i.e., to the right of the nozzle) was significantly reduced due to the offset of nozzle location towards the drill bit axis. The width of the flow development area is widened near the outer surface due to the improved nozzle velocity as marked in Figure 5-29. Similarly the other flow paths were analyzed for significant improvement in the flow stream.

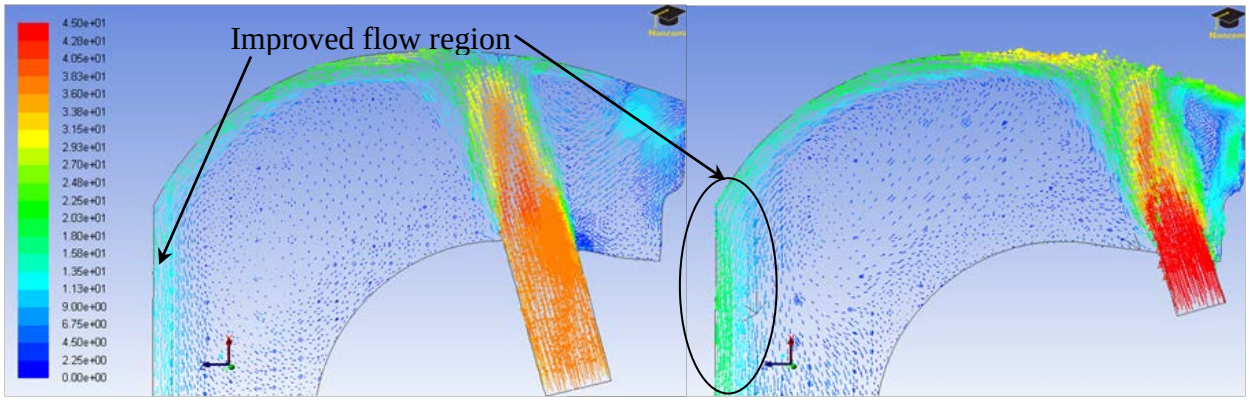

Figure 5-29. Velocity vectors in flowpath#3 (a) Original drill bit design (b) modified drill bit design

The modified drill bit design has the major design change in the nozzle size, which influences all the flow paths; location and inclination of nozzle#4, which influcences the flowpath#3; location and inclination of nozzle#6, which influences the flowpath#4 and #5. For a detailed understanding, the flow paths, #3, #4 and #5 were selected to understand the velocity impact at two different depth levels, Ψ = 10mm and Ψ = 20mm from the downhole surface as shown in Figure 5-30. On the whole, reduction of the nozzle diameter shows significant increase in the nozzle jet velocity in almost all the flow paths. However, in the flowpath#3, the influence of nozzle size was not a major one because the influence of nozzle location and inclination were more significant. Figure 5-30 (a) and (b) shows the velocity trend in the flowpath#3 at different depth levels, Ψ = 10mm and Ψ = 20mm respectively. At Ψ = 10mm, the jet velocity is low and hence results in decreasing the average velocity by 6% compared to that of original design. The jet velocity is high at Ψ = 20mm, which increases the average velocity by 7%. Hence, there is not much improvement on the overall velocity in this flow path. For the flowpath#4, the velocity trend was similar in both the optimal and original designs. Compared to the original design, the maximum jet velocity at Ψ = 10mm and Ψ = 20mm were increased by approximately 20% and 30% respectively in the optimal design. The average velocity in this flow path was increased by 9% at Ψ = 10mm and decreased by 7% at Ψ = 20mm compared to that of base/original design. The flowpath#5 has very high peak for the jet velocity at nozzle#7 which, is due to the reduction in the nozzle size and its placement in center of the flow path with more space for the free jet development. The average velocity in this flow path is increased by 65% at both the depths, Ψ = 10mm and Ψ = 20mm. Compared to the original design, the overall average velocity for all the flow paths was increased by 21% in the modified design.

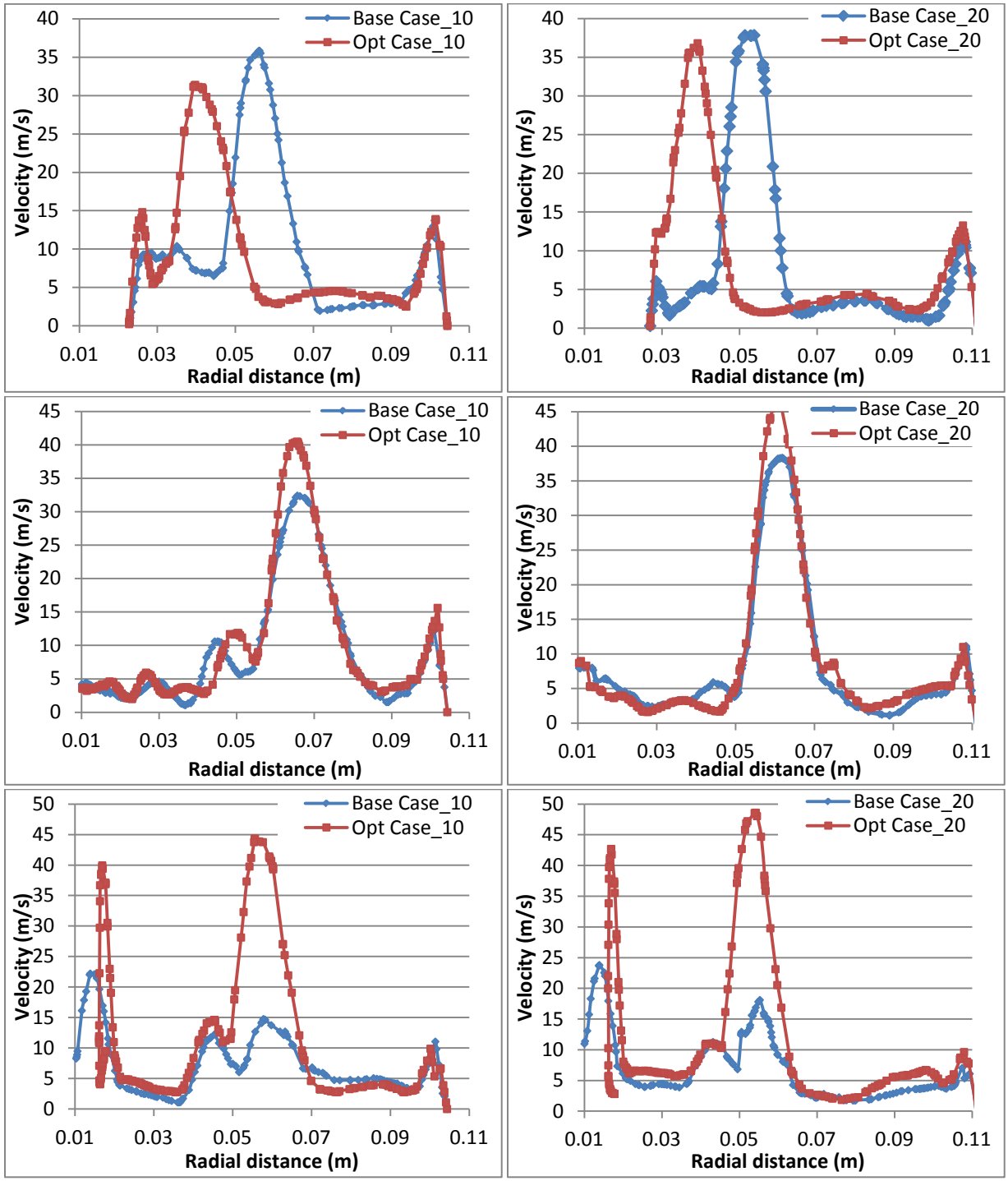

Figure 5-30. Velocity across the flowpath comparison for original drill bit design to the modified drill bit design (a) Flowpath#3 at Ψ = 10mm (b) Flowpath#3 at Ψ = 20mm (c) Flowpath#4 at Ψ = 10mm (d) Flowpath#4 at Ψ = 20mm (e) Flowpath#5 at Ψ = 10mm (f) Flowpath#5 at Ψ = 20mm

The velocity vectors that flow in the direction towards the axis of the drill bit, which is against the intended direction, i.e. towards the annulus, is chosen as the recirculation velocity. Figure 5-31 shows the recirculation velocity in the flowpath#3 for both the original and optimized drill bit designs. The intensity of the recirculation zone is significantly reduced based on the change in the location of the nozzle#4 as marked in Figure 5-31. At the same time, the recirculation area for the modified design is increased near the inner wall shear layer. From the figure, it can be observed that the recirculation velocity appears to be low for the modified drill bit design, but the average recirculation velocity at the two pre-defined cross sectional levels (Ψ = 10mm and Ψ = 20mm) is increased by seven-folds. The overall recirculation velocity for all flow paths was increased by 25% in the modified drill bit design when compared to that of the original design. This increase in recirculation velocity was not desirable for the Non-Newtonian fluid; a further investigation needs to be performed in future to avoid the increase in recirculation velocity.

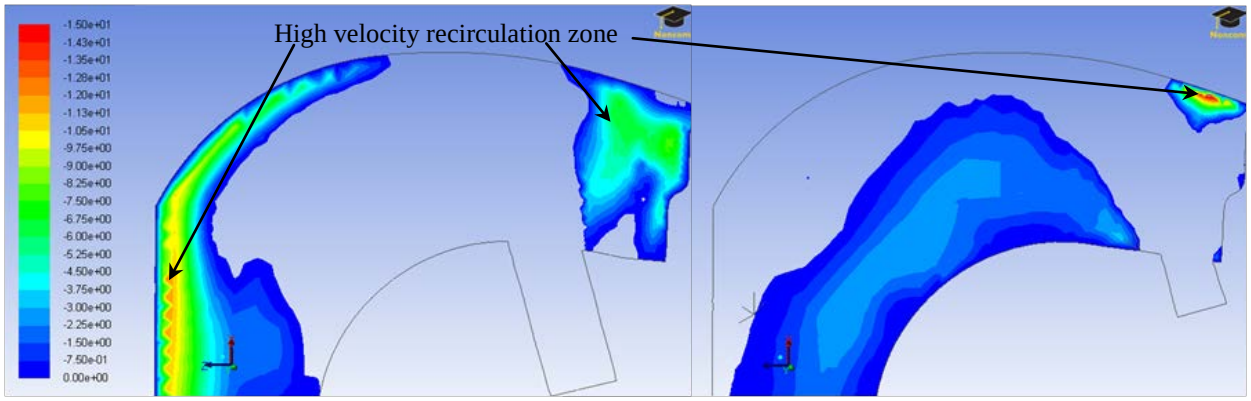

Figure 5-31. Recirculation velocity vectors in flowpath#3 (a) Original drill bit design (b) modified drill bit design

The vorticity magnitude was compared at the flowpath#3 for both the original and modified drill bit design. Offsetting the nozzle location towards the drill bit axis increased the vorticity at the cross sectional surface as shown in Figure 5-32. The zones of high vorticity magnitude are at the circumference of the nozzle free jet zone and near the downhole surface. This is due to the high velocity distribution in these regions. In the modified drill bit design, the vorticity magnitude was relatively high near the nozzle because of the reduction in the nozzle size and the limited area for the nozzle free jet. The average vorticity magnitude in this flow path is increased by 58% at the cross sectional depths, Ψ = 10mm and Ψ = 20mm.

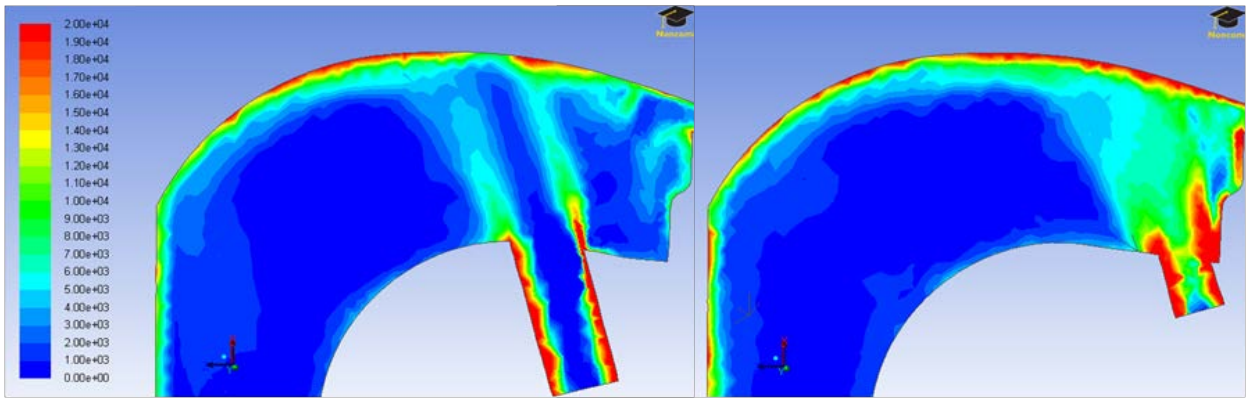

Figure 5-32. Vorticity magnitude in flowpath#3 (a) Original drill bit design (b) Modified drill bit design

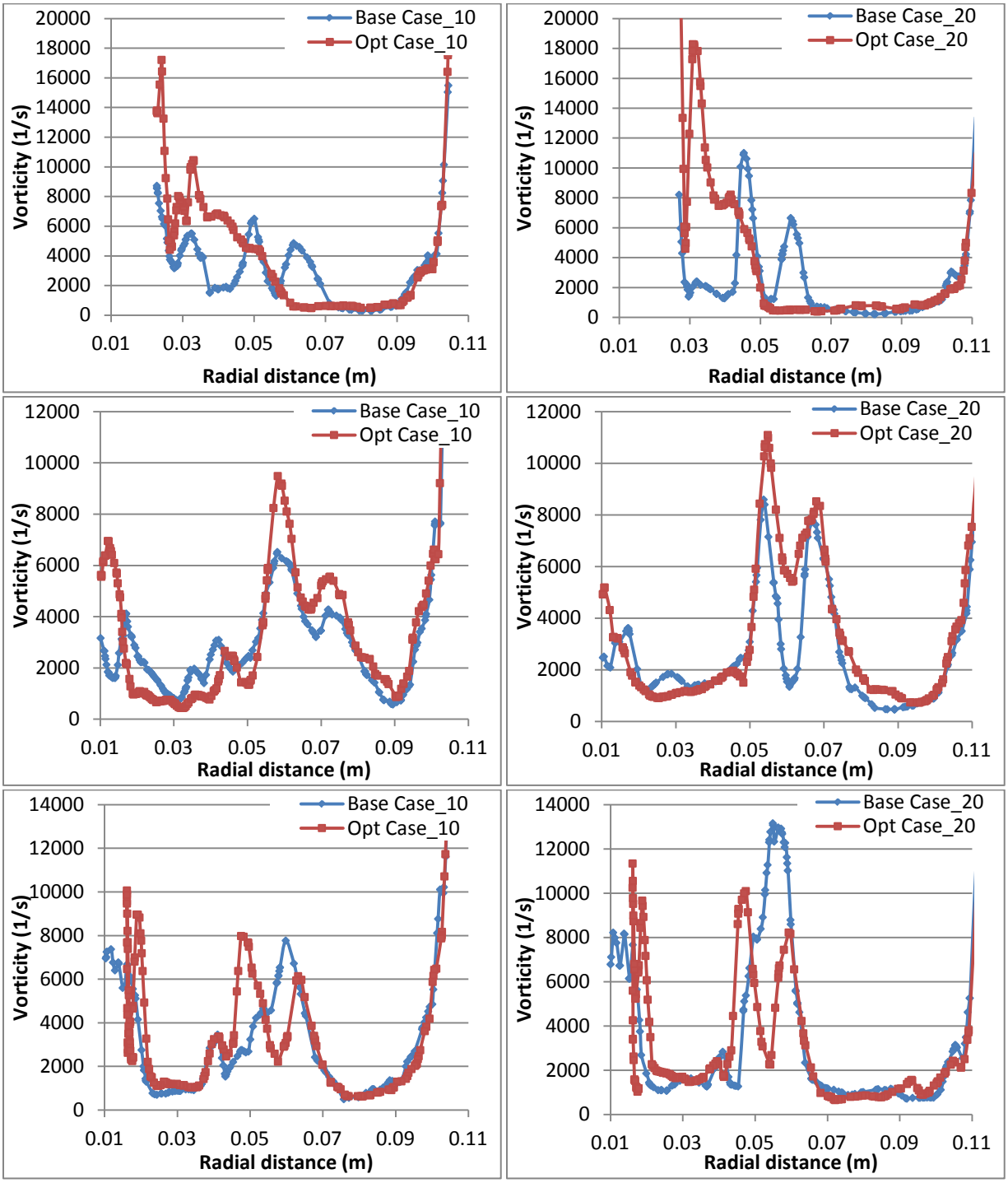

Figure 5-33. Vorticity magnitude across the flowpath comparison for original drill bit design to the modified drill bit design (a) Flowpath#3 at Ψ = 10mm (b) Flowpath#3 at Ψ = 20mm (c) Flowpath#4 at Ψ = 10mm (d) Flowpath#4 at Ψ = 20mm (e) Flowpath#5 at Ψ = 10mm (f) Flowpath#5 at Ψ = 20mm

Figure 5-33 shows the comparison of vorticity magnitude at Ψ = 10mm and Ψ = 20mm for the flow paths #3, #4 and #5. When comparing the vorticity magnitude for all the flow paths, the high vorticity regions are almost similar; these regions were observed to be 1) near the nozzle jet circumference and 2) at the downhole outer surface. Figure 5-33 (a) and (b) shows the effect of vorticity in the flowpath#3, which is mainly influenced by nozzle location (as discussed in previous section). For the flowpath#4, the vorticity pattern was almost similar for both the designs at Ψ = 10mm and Ψ = 20mm with a small increase in the vorticity magnitude. The average vorticity was increased by 7% and 23% at Ψ = 10mm and Ψ = 20mm respectively.

For the flowpath#5, the maximum vorticity region occurs at the center of the nozzle jet in the original drill bit design, but, for the optimized design with smaller nozzle size, the maximum vorticity occurs at the circumference of the nozzle free jet.The average vorticity was increased by 2% at Ψ = 10mm and decreased by 5% at Ψ = 20mm. The reduction in the nozzle size increases the nozzle free jet circumference, which inturn, reduces the vorticity at Ψ = 20mm in the flowpath#5. Overall average vorticity across the drill bit for all the flow path is increased by 19% in the modified drill bit design.

Table 5-13. Non-Newtonian flow results comparison for original and modified drill bit design

Response	Original drill bit design	Modified drill bit design	% difference
Pressure drop (Pa)	27869	36525	31%
Average Velocity (m/s)	8.55	10.32	21%
Average Vorticity (1/s)	4108	4874	19%
Recirculation velocity (%)	4%	5%	25%

The overall comparison of results for the Non-Newtonian flow for both the original and modified drill bit designs are shown in Table 5-13. Compared to the original design, the total pressure drop was increased by 31% in the modified design. The average velocity across the drill bit was increased by 21%. This increase in velocity across the flow path aids in faster chip removal by the prevention of chip regrinding. On the other hand, the recirculation velocity was increased by 25%, which could potentially lead to the generation of stagnation zone. But the increase in the mean velocity would help to overcome the issues generated by the recirculation zone. A detailed analysis needs to be performed on the drill bit design to improve its performance for a Non-Newtonian fluid in order to replicate the real time drilling condition.

Chapter Six: Conclusions and Recommendations for Future Work

6.1 Conclusions

The motivation for this research was to develop a CFD base for improving the design of a PDC drill bit. The objective of this work was to develop an optimization procedure to improve the drilling performance. To this end, the parameters related to bit geometry - jet nozzle size, nozzle location and nozzle orientation were modified and the resultant flow distributions, characterized in terms of velocity, vorticity and pressure drop were analyzed. Increasing the throughput (velocity) and reducing backflow (vorticity) help reduce the regrinding of cutting, better cleaning while a lower pressure drop reduce the power requirement.

A series of computational simulations were performed to examine and characterize the drill bit performance. Computational models for the drill bit operating conditions were identified with the help of a highly simplified drill bit model. A statistical approach was undertaken to test various design parameters of the PDC drill bit. Significant factors were identified with the aid of factorial design simulations and the optimum levels of the selected significant factors were identified with response surface methodology. CFD simulations were than conducted for an optimized geometry for a Newtonian fluid model and a non Newtonian flow model. Predicted outcomes for the optimized geometry were then compared to those for the original drill bit.

The feasibility of CFD application on PDC drill was evaluated using preliminary simulations in which the boundary conditions and suitable computational models were identified using highly simplified drill bit geometry. The methodology for implementation was developed

by increasing complexity from a steady state single phase flow to a unsteady state two phase flow. From these preliminary simulations it was determined that a suitable CFD model can be represented by: the *k-ω* turbulence model for the viscous fluid, Volume of Fluid (VOF) model for multiphase flow, mud/clay inlet was provided form the downhole bottom surface, the drill bit inner wall and the downhole circumference surface are the no slip solid surfaces, water was assumed a drilling fluid that flows through the nozzle inlet and a constant ambient pressure outlet condition provided at the drill bit outlet or the annulus. A grid sensitivity study was performed with three different mesh sizes and an optimum grid size was selected based on (1) the sensitivity of the results to the grid, and (2) the simulation convergence with respect to the computing time. The optimal grid was determined to contain 650k-700k nodes.

The preliminary simulations results served as a representation of the flow pattern in the drill bit. The characteristics of an optimum flow pattern were identified as low recirculation velocity, high chip carry velocity, and minimum pressure drop across the drill bit. With the objective of improving the flow characteristics, the parameters of the bit geometry identified for the study were nozzle size (1 factor), location and inclination for each nozzle (7 factors each). The design of experiment (DOE) methodology was used to develop a simulation table for different design configurations by varying 15 factors. A factorial design approach has been used to identify the top five significant factors. Nozzle size is the top significant factor which is highly significant on pressure drop and influences velocity and vorticity in all flow paths. Location of nozzle#6, second most significant factor influences the average velocity and average vorticity across all flow paths. Location and inclination of nozzle#4 are significant as the nozzle#4 regulates velocity, vorticity and pressure drop. Similarly, inclination of nozzle#6

proved to be significant as it supports its location, which is one of the top significant factors. Hence, the above discussed top five significant factors were used for the further investigation.

The highlight of this study was the understanding of the influence of the nozzle size, location and inclination on the formation of recirculation and stagnation zones which would lead to bit balling across the PDC drill bit surface. Identification of the location and intensity of these zones allowed the modification of the design parameters to favor the removal or minimization of these zones (Akin et al., 1997; King et al., 1990). In addition, the statistical approach in this study encompassed different variations of the design of the PDC drill bit which led to understand the influence of the design parameters in a simplified manner. The response surface methodology (RSM) was used to establish the optimum levels for the selected five significant design parameters with the aid of central composite design (CCD) based simulations.

As there is limited study on the PDC drill bit hydraulic design and no literature is available for the specific design of the PDC drill bit considered in this research, it was not possible to validate the CFD simulations using experimental results. Hence, the results of optimization on the context of nozzle size, location and inclination were assessed by comparison with the respective geometry recommended for various PDC drill bits. In addition, the optimal design of the PDC drill bit was assessed by comparing the simulation results for the flow characteristics under Newtonian condition with that of the original PDC drill bit design. The optimal design favored over the original design in maximizing the average velocity and minimizing the pressure drop across the bit surface. The low recirculation velocity in the optimal design compared to the actual design helps to avoid the bit balling under Newtonian flow conditions. The selection of vorticity magnitude is not a bad choice for defining the recirculation,

but, it gives an idea about the boundary layer and the wall shear stress. Due to change in the nozzle size, the internal shear layer at the exit of the nozzle causes adverse effect on the vorticity magnitude. With the constant nozzle size, reducing the vorticity will reduce the dissipation losses. The optimal design was also compared to the original design for non-Newtonian flow condition by incorporating actual drilling fluid properties (NeoDrill fluid) instead of water. Compared to the actual design, the high average velocity in the optimal design favored faster chip removal by the prevention of chip regrinding. On the other hand, the high pressure drop and high recirculation velocity across the bit in the optimal design compared to the original design are not favorable due to the potential of formation of stagnation zones. However, the high average velocity would help to overcome the issues generated by the recirculation zone. In addition, the comparison of the optimal design with the original design for non-Newtonian flow reveals that a more detailed investigation of the influence of design parameters on the flow pattern across the PDC drill bit under non-Newtonian condition is required to reproduce and understand the real time scenario.

The methodology for the assessment of each of the design parameters of the drill bit simultaneously by combining the CFD simulations with the DOE application was developed. The evaluation of the bit hydraulics by changing the geometry of the drill bit encompasses the influence of large number of parameters. Using laboratory methods for studying the effect of the bit geometry on bit hydraulics is highly complex and difficult to observe the flow domain. On the other hand, CFD allows modifying the bit geometry with more detailed characterization of the flow domain. Yet, large number of CFD simulations and the related mesh development will be required to evaluate the effect of each of the design parameters on the drill bit hydraulics. The

application of DOE allows the evaluation of different combinations of the design parameters without compromising the importance of each of the parameters, along with reasonable number of simulations. Then, the following statistical analysis facilitates the estimation of the significance of the parameters. The application of response surface methodology results in the determination of the optimum limits for the significant parameters. Thus, the application of CFD with the DOE statistical tool allows simultaneous evaluation of the design parameters for improved bit hydraulics. The advantages of this methodology are: simple, logical, accuracy in the representation of the flow domain across the drill bit for various drill bit geometry.

6.2 Recommendations for Future Work

Based on the above research on PDC drill bit geometry for improvement in bit performance, the following recommendations have been made for future work.

- Validation of CFD simulations by experimental results of the actual PDC drill bit.
- Extending the above study to understand the influence of the other design parameters such as junk slot area, cutters location and the drill bit crown profile on bit hydraulics and to optimize the parameters for improved drilling performance.
- CFD simulation and flow pattern analyzes for design optimization with real time drilling fluid properties and mud properties by considering both as non-Newtonian fluids.
- Vorticity measurement should be carried out in terms of other parameters such as extent of recirculation.

- Study the drill bit performance by increasing or decreasing the number of nozzles.
- Including the cutter rock interaction with rock breaking simulation along with the fluid simulation will provide more realistic results.
- Development of computer codes for meta-modeling by incorporating both the CFD model and statistical model will reduce the multiple simulations.
- Validating the modified drill bit design with laboratory or field test.

References

Akin, J., Dove, N., Smith, S., Perrin, V. 1997. New nozzle hydraulics increase ROP for PDC and rock bits. *SPE/IADC drilling conference*. pp. 69-78.

Andersen, E., Azar, J. 1993. PDC-bit performance under simulated borehole conditions. *SPE Drilling & Completion*, **8**(3), 184-188.

Balkenbush, R., Onisko, J. 1985. Application of polycrystalline diamond compact bits in the Kuparuk River field, Alaska. *Journal of petroleum technology*, **37**(8), 1220-1224.

Bilgesu, H., Ali, M., Aminian, K., Ameri, S. 2002. Computational Fluid Dynamics (CFD) as a Tool to Study Cutting Transport in Wellbores. *SPE Eastern Regional Meeting*. Society of Petroleum Engineers.

Bourgoyne, A.T., Chenevert, M.E., Millheim, K.K., Young, F. 1991. *Applied drilling engineering*. Society of Petroleum Engineering of AIME.

Cerkovnik, J. 1982. Design Application and Future of Polycrystalline Diamond Compact Cutters in the Rocky Mountains. *SPE Rocky Mountain Regional Meeting*. Society of Petroleum Engineers.

Doiron, H.H., Deane, J.D. 1982. Effects of Hydraulic Parameter Cleaning Variations on Rate of Penetration of Soft Formation Insert Bits. *SPE Annual Technical Conference and Exhibition*. Society of Petroleum Engineers.

Eckel, J.R. 1968. Microbit studies of the effect of fluid properties and hydraulics on drilling rate. *Journal of Petroleum Technology*, **19**(04), 541-546.

FLUENT, A. 2012. 14.5, Theory Guide; ANSYS. *Inc., Canonsburg, PA*.

Garcia-Gavito, D., Azar, J. 1994. Proper Nozzle Location Bit Profile and Cutter Arrangement Affect PDC-Bit Performance Significantly. *SPE Drilling & Completion*, **9**(03), 167-175.

Glowka, D. 1983. Optimization of Bit Hydraulic Configurations. *Old SPE Journal*, **23**(1), 21-32.

Gueyffier, D., Li, J., Nadim, A., Scardovelli, R., Zaleski, S. 1999. Volume-of-fluid interface tracking with smoothed surface stress methods for three-dimensional flows. *Journal of computational physics*, **152**(2), 423-456.

Guo, B., Liu, G. 2011. *Applied Drilling Circulation Systems: Hydraulics, Calculations and Models*. Gulf Professional Publishing.

Hareland, G., Yan, W., Nygaard, R., Wise, J. 2009. Cutting efficiency of a single PDC cutter on hard rock. *Journal of Canadian Petroleum Technology*, **48**(6), 1-6.

Hargreaves, D., Wright, N. 2007. On the use of the< i> k</i>–ε model in commercial CFD software to model the neutral atmospheric boundary layer. *Journal of Wind Engineering and Industrial Aerodynamics*, **95**(5), 355-369.

Hariharan, P., Azar, J. 1996. PDC bit hydraulics design, profile are key to reducing balling. *Oil and Gas Journal*, **94**(50), 58-63.

Hatanaka, K., Saito, T. 2012. Influence of nozzle geometry on underexpanded axisymmetric free jet characteristics. *Shock Waves*, **22**(5), 427-434.

Henry, T.W., Sherif, M.M., Ragheb, A.M. 2011. New PDC Technologies Increases Durability and Enables Fast Drilling in Hard/Abrasive Formation. *SPE/IADC Middle East Drilling Technology Conference and Exhibition*. Society of Petroleum Engineers.

Hirt, C.W., Nichols, B.D. 1981. Volume of fluid (VOF) method for the dynamics of free boundaries. *Journal of computational physics*, **39**(1), 201-225.

Jie, K., Shasha, G., Wen, Y. 2011. Numerical simulation research on flow pattern of gas-water two-phase flow in horizontal pipeline. *Mechanic Automation and Control Engineering (MACE), 2011 Second International Conference on*, 15-17 July 2011. pp. 484-487.

Ju, P., Wang, Z., Zhai, Y., Su, D., Zhang, Y., Cao, Z. 2013. Numerical simulation study on the optimization design of the crown shape of PDC drill bit. *Journal of Petroleum Exploration and Production Technology*, 1-8.

Keller, W., Crow, M. 1983. Where and how not to run PDC bits. *IADC/SPE Drilling Conference*. Society of Petroleum Engineers.

Kendall, H., Goins Jr, W. 1960. Design and Operation of Jet-Bit Programs For Maximum Hydraulic Horsepower Impact Force or Jet Velocity.

Kerr, C.J. 1988. PDC drill bit design and field application evolution. *Journal of petroleum technology*, **40**(03), 327-332.

King, I., Bratu, C., Delbast, B., Besson, A., Chabard, J. 1990. Hydraulic Optimization of PDC bits. *European Petroleum Conference*. Society of Petroleum Engineers.

Kuru, E., Wojtanowsicz, A. 1988. A method for detecting in-situ PDC bit dull and lithology change. *SPE/IADC Drilling Conference*. Society of Petroleum Engineers.

Launder, B., Rodi, W. 1979. The turbulent wall jet. *Progress in Aerospace Sciences*, **19**, 81-128.

Lim, K.M., Chukwu, G. 1996. Bit hydraulics analysis for efficient hole cleaning. *Society of Petroleum Engineers. Annual Western regional meeting*. pp. 171-184.

McLean, R. 1964. Crossflow and impact under jet bits. *Journal of Petroleum Technology*, **16**(11), 1,299-1,306.

Mead, R. 1990. *The design of experiments: statistical principles for practical applications*. Cambridge University Press.

Mensa-Wilmot, G., Fear, M. 2002. Innovative Technology Improves Penetration Rates of PDC Bits in Shales Drilled at Great Depth With Weighted Water Based Mud Systems. *IADC/SPE Drilling Conference*. Society of Petroleum Engineers.

Menter, F. 1993. Zonal Two Equation k-w Turbulence Models for Aerodynamic Flows. *AIAA. paper-93-2906*.

Menter, F.R. 1992. Improved two-equation k-omega turbulence models for aerodynamic flows. *NASA STI/Recon Technical Report N*, **93**, 22809.

Menter, F.R. 2011. Turbulence Modeling for Engineering Flows. *Technical Paper, ANSYS inc*, 1-25.

Millheim, K.K. 1986. Advances in Drilling Technology and Where Drilling Technology Is Heading, Society of Petroleum Engineers.

Mortimer, L. 2010. Innovative Design Features On PDC Bit Result In Record Run In Orenburg Region Russia. *SPE Russian Oil and Gas Conference and Exhibition*. Society of Petroleum Engineers.

Moslemi, A., Ahmadi, G. 2014. Study of the Hydraulic Performance of Drill Bits Using a Computational Particle-Tracking Method. *SPE Drilling & Completion*(Preprint).

Motahhari, H.R., Hareland, G., James, J., Bartlomowicz, M. 2010. Improved drilling efficiency technique using integrated PDM and PDC bit parameters. *Journal of Canadian Petroleum Technology*, **49**(10), 45.

Myers, R.H. 1971. Response surface methodology, 1971. *Allyn-Bacon, Boston*.

Offenbacher, L.A., McDermaid, J., Patterson, C. 1983. PDC bits find applications in Oklahoma drilling. *IADC/SPE Drilling Conference*. Society of Petroleum Engineers.

Onwubolu, G.C., Kumar, S. 2006. Response surface methodology-based approach to CNC drilling operations. *Journal of Materials Processing Technology*, **171**(1), 41-47.

Prooyen, T., Gilbert, H., Juergens, R. 1982. Recent field results with new bits. *J. Pet. Technol.;(United States)*, **34**(9).

Qunfeng, L., Jin, C., Jiangtao, C., Ning, Q., Danao, L.A.M. 2011. Study of CFD simulation of a 3-D wind turbine. *Materials for Renewable Energy & Environment (ICMREE), 2011 International Conference on*. IEEE. pp. 596-600.

Rampersad, P., Hareland, G., Boonyapaluk, P. 1994. Drilling optimization using drilling data and available technology. *SPE Latin America/Caribbean Petroleum Engineering Conference*. Society of Petroleum Engineers.

Reeves, G.M., Sims, I., Cripps, J. 2006. Clay materials used in construction. Geological Society of London.

Schwarz, W., Cosart, W. 1961. The two-dimensional turbulent wall-jet. *Journal of Fluid Mechanics*, **10**(04), 481-495.

Simpson, T.W., Poplinski, J., Koch, P.N., Allen, J.K. 2001. Metamodels for computer-based engineering design: survey and recommendations. *Engineering with computers*, **17**(2), 129-150.

Speer, J.W. 1959. A method for determining optimum drilling techniques. *Gulf Coast Drilling and Production Meeting*. Society of Petroleum Engineers.

Stewart, P.J., Buttolo, P., Chen, Y. 2006. System and method for design of experiments using direct surface manipulation of a mesh model, Google Patents.

Striegler, J. 1979. Broader Use of Diamond Bits Cuts Cost. *Pet. Eng. IntI*, **51**, 24-27.

Warren, T. 1987. Penetration rate performance of roller cone bits. *SPE Drilling Engineering*, **2**(01), 9-18.

Warren, T., Armagost, W. 1988. Laboratory drilling performance of PDC bits. *SPE drilling engineering*, **3**(02), 125-135.

Warren, T., Winters, W. 1984. The effect of nozzle diameter on jet impact for a tricone bit. *SPEJ, Soc. Pet. Eng. J.;(United States)*, **24**(1).

Warren, T.M., Sinor, A. 1986. Drag Bit Performance Modeling, Society of Petroleum Engineers.

Watson, G., Barton, N., Hargrave, G. 1997. Using new computational fluid dynamics techniques to improve PDC bit performance. *SPE/IADC Drilling Conference*. Society of Petroleum Engineers.

Wells, M., Marvel, T., Beuershausen, C. 2008. Bit Balling Mitigation in PDC Bit Design. *IADC/SPE Asia Pacific Drilling Technology Conference and Exhibition*. Society of Petroleum Engineers.

White, F.M. 1999. *Fluid mechanics*. WCB/McGraw-Hill.

Wilcox, D.C. 1998. *Turbulence modeling for CFD*. DCW industries La Canada, CA.

Wu, A., Hareland, G., Rashidi, B., Gao, X., Yang, Y. 2011. Geometrical Modeling of Rock Breakage Craters to Improve the Performance of a ROP Simulator. *45th US Rock Mechanics/Geomechanics Symposium*. American Rock Mechanics Association.

APPENDIX A: Numerical Optimization and desirability function

Each of the design parameters (X) of the PDC drill bit were chosen for optimization. The performance of the drill bit is characterized by five responses (Y), mean velocity at Ψ=10 mm and 20 mm; mean vorticity at Ψ=10 mm and 20 mm, and pressure drop. The desirable characteristics are maximum mean velocity and minimum mean vorticity and minimum pressure drop. For each response, the desired characteristic is either at the maximum or minimum point. In order to obtain the combined desirable characteristics of all the responses, it is necessary to determine the optimum point. The optimum point is located at the closest distance to the peaks of each response. Numerical optimization was used to determine the optimum point.

A.1 Numerical Optimization procedure

The exact optimization procedure is given as follows: Numerical optimization reduces to a general non-linear algorithm with constraints.

1. Let X, a vector of x_i for i=1 to n represent design variables over the optimization space which is a subset of the design space.

2. Let y_j, U_j, L_j for j=1 to m be responses with upper and/or lower bounds serving as constraints.

3. Let y(X) be the response to be optimized. Then f(X) = y(X) for minimization, f(X)=-y(X) for maximization. Define the constraints as a series of discontinuous functions:

$$g_j(X) = y_j(X) - U_j \qquad \text{for } y_j > U_j \qquad \text{...(A-1)}$$

$$g_j(X) = 0 \qquad \text{for } L_j \le y_j \le U_j \qquad \text{...(A-2)}$$

$$g_j(X) = L_j - y_j(X) \qquad \text{for } y_j < L_j \qquad \text{...(A-3)}$$

This produces a system of m constraints that can be solved as an unconstrained problem via a penalty function approach:

$$\text{Minimize} \left\{ f(X) + p \sum_i g_j(X) \right\} \qquad \text{...(A-4)}$$

where p is a penalty parameter>0 for j = 1 to m. (The penalty parameter p starts at 1 and increases with each iteration by a factor of 100. The number of iterations is limited to 15, which gives a penalty factor of 1030 maximum.)

The initial guess is started with a small value of a penalty function in a downhill simplex multi-dimensional pattern search which converges at either a stationary point or a design space boundary. Limits of the design space are maintained by evaluating the f(X) to +1010 at the design boundaries. The search around the initial convergence point is restarted using a larger penalty function. Convergence is achieved when the distance moved or objective function change is less than a 10-6 ratio.

The starting N+1 simplex points are constructed by adding or subtracting a fraction of each of the N factor ranges to the initial starting point. The decision to add or subtract is made to maintain a maximum distance from the factor limits.

A.1.1 Desirability Details

Myers and Montgomery [Myers, R. H., Montgomery, D. C., Anderson-Cook, C. M., (2002) Response Surface Methodology, John Wiley & Sons, Inc.,, USA.] describe a multiple response method called desirability. The method makes use of an objective function, D(X), called the desirability function. It reflects the desirable ranges for each response (d_i). The numerical optimization finds a point that maximizes the desirability function. The desirable ranges are from zero to one (least to most desirable, respectively). The simultaneous objective function is a geometric mean of all transformed responses:

$$D = (d1 \times d2 \times \ldots \times dn)(1/n) = \left(\prod_{i=1}^{n} d_i\right)^{\frac{1}{n}} \quad \ldots(A\text{-}5)$$

where n is the number of responses in the measure. If any of the responses or factors fall outside their desirability range, the overall function becomes zero.